NAVAL POSTGRADUATE SCHOOL

MONTEREY, CALIFORNIA

THESIS

EFFICIENT RECTENNA DESIGN FOR WIRELESS POWER TRANSMISSION FOR MAV APPLICATIONS

by

Tan, Lee Meng Mark

December 2005

Thesis Advisor:	David C Jenn
Thesis Co-Advisor:	Richard Harkins

Approved for public release; distribution is unlimited

THIS PAGE INTENTIONALLY LEFT BLANK

REPORT DOCUMENTATION PAGE			Form Approved OMB No. 0704-0188
Public reporting burden for this collection of information is estimated to average 1 hour per response, including the time for reviewing instruction, searching existing data sources, gathering and maintaining the data needed, and completing and reviewing the collection of information. Send comments regarding this burden estimate or any other aspect of this collection of information, including suggestions for reducing this burden, to Washington headquarters Services, Directorate for Information Operations and Reports, 1215 Jefferson Davis Highway, Suite 1204, Arlington, VA 22202-4302, and to the Office of Management and Budget, Paperwork Reduction Project (0704-0188) Washington DC 20503.			
1. AGENCY USE ONLY ***(Leave blank)***	**2. REPORT DATE** December 2005	**3. REPORT TYPE AND DATES COVERED** Master's Thesis	
4. TITLE AND SUBTITLE Efficient Rectenna Design for Wireless Power Transmission for MAV Applications.			**5. FUNDING NUMBERS**
6. AUTHOR(S) Tan, Lee Meng Mark			
7. PERFORMING ORGANIZATION NAME(S) AND ADDRESS(ES) Naval Postgraduate School Monterey, CA 93943-5000			**8. PERFORMING ORGANIZATION REPORT NUMBER**
9. SPONSORING /MONITORING AGENCY NAME(S) AND ADDRESS(ES) N/A			**10. SPONSORING/MONITORING AGENCY REPORT NUMBER**
11. SUPPLEMENTARY NOTES The views expressed in this thesis are those of the author and do not reflect the official policy or position of the Department of Defense or the U.S. Government.			
12a. DISTRIBUTION / AVAILABILITY STATEMENT Approved for public release; distribution is unlimited			**12b. DISTRIBUTION CODE**

13. ABSTRACT (maximum 200 words)

This thesis is a continuation in part of a NPS project relating to wireless transmission of power to a MAV. The conversion of rf power into usable dc power is done by a rectifying antenna or rectenna. The emphasis of this thesis is an in-depth study of all components of the rectenna to determine the limitations of an existing design which has low efficiency, and to determine improvements to the design, specifically for MAV applications.

Studies relating to each rectenna subsystem were conducted, highlighting improvements and design trade-offs. The analysis of the rectenna is broken into four subsystem, namely, (1) the receiving antenna, (2) the pre-rectification filtering, (3) the rectification and lastly, (4) post-rectification filtering. From the findings of this thesis, the final rectenna design implemented a capacitive probe fed circular patch that exhibits relatively wide bandwidth, high tolerance to manufacturing variances, and a radiation efficiency of 95%. The pre-rectification filter was re-designed to increase its transmittance characteristics to 94%. The Schottky diode was re-analyzed and its conversion efficiency and trade-offs for MAV applications were documented. The post-rectification filter was reconstructed taking into consideration the positioning of the Schottky diode, and impedance matching for both antenna and Schottky diode was explained. The issue of microstrip discontinuities and probe feed connection was subsequently addressed.

The final design has a dimension of approximately 112.5 mm^2 which is only 15% of the existing design, and has an estimated weight of less than a gram. The estimated rf-to-dc conversion efficiency is approximately 50%.

14. SUBJECT TERMS rectenna, wireless power transmission, patch antenna, MAV			**15. NUMBER OF PAGES** 144
			16. PRICE CODE
17. SECURITY CLASSIFICATION OF REPORT Unclassified	**18. SECURITY CLASSIFICATION OF THIS PAGE** Unclassified	**19. SECURITY CLASSIFICATION OF ABSTRACT** Unclassified	**20. LIMITATION OF ABSTRACT** UL

NSN 7540-01-280-5500 Standard Form 298 (Rev. 2-89)
Prescribed by ANSI Std. 239-18

THIS PAGE INTENTIONALLY LEFT BLANK

Approved for public release; distribution is unlimited

EFFICIENT RECTENNA DESIGN FOR WIRELESS POWER TRANSMISSION FOR MAV APPLICATION

Lee Meng Mark Tan
Captain, Singapore Army
B.E. (Electrical & Electronic Engineering), Nanyang Technological University, 2001

Submitted in partial fulfillment of the
requirements for the degree of

MASTER OF SCIENCE IN COMBAT SYSTEMS AND TECHNOLOGIES

from the

NAVAL POSTGRADUATE SCHOOL
December 2005

Author: Lee Meng Mark Tan

Approved by: David C. Jenn
Thesis Advisor

Richard Harkins
Co-Advisor

James Luscombe
Chairman, Department of Physics

THIS PAGE INTENTIONALLY LEFT BLANK

ABSTRACT

This thesis is a continuation in part of a NPS project relating to wireless transmission of power to a MAV. The conversion of rf power into usable dc power is done by a rectifying antenna or rectenna. The emphasis of this thesis is an in-depth study of all components of the rectenna to determine the limitations of an existing design which has low efficiency, and to determine improvements to the design, specifically for MAV applications.

Studies relating to each rectenna subsystem were conducted, highlighting improvements and design trade-offs. The analysis of the rectenna is broken into four subsystem, namely, (1) the receiving antenna, (2) the pre-rectification filtering, (3) the rectification and lastly, (4) post-rectification filtering. From the findings of this thesis, the final rectenna design implemented a capacitive probe fed circular patch that exhibits relatively wide bandwidth, high tolerance to manufacturing variances, and a radiation efficiency of 95%. The pre-rectification filter was re-designed to increase its transmittance characteristics to 94%. The Schottky diode was re-analyzed and its conversion efficiency and trade-offs for MAV applications were documented. The post-rectification filter was reconstructed taking into consideration the positioning of the Schottky diode, and impedance matching for both antenna and Schottky diode was explained. The issue of microstrip discontinuities and probe feed connection was subsequently addressed.

The final design has a dimension of approximately 112.5 mm^2 which is only 15% of the existing design, and has an estimated weight of less than a gram. The estimated rf-to-dc conversion efficiency is approximately 50%.

THIS PAGE INTENTIONALLY LEFT BLANK

TABLE OF CONTENTS

THIS PAGE INTENTIONALLY LEFT BLANK

LIST OF FIGURES

THIS PAGE INTENTIONALLY LEFT BLANK

LIST OF TABLES

THIS PAGE INTENTIONALLY LEFT BLANK

ACKNOWLEDGMENTS

I would like to express my sincerely thank to my advisor Professor David C. Jenn for his insights, guidance, and encouragement in this thesis topic throughout the six months that I was working with him. He made the conscious effort to put aside his precious time to discuss project matters and was always able to bring a new perspective to the problem. This topic proved to be extremely challenging, with the requirement to master the use of Microwave Studio and being able to critically investigate each subsystem while keeping the overall system requirements in consideration.

I would like to thank Professor Dick Harkins for his enthusiasm in being part of this thesis; his advice, comments and instructions helped in the understanding of the patch antenna.

Lastly I would like to thank my wife, Wai Ling, for her love, support, and understanding, not forgetting the numerous late night coffees that she lovingly brewed, so that I would be able to complete this thesis.

THIS PAGE INTENTIONALLY LEFT BLANK

I. INTRODUCTION

A. WIRELESS POWER TRANSMISSION

The sustenance of flight is mainly restricted to the amount of fuel or power that an aircraft or air vehicle is able to carry. Therefore, in order to lengthen flight time, a logical assumption is the requirement to put more fuel on the platform. This is assuming that the plane's efficiency in other aerodynamic aspects have already been maximized. However, the increase of fuel would increase the laden weight of the platform which hinders its flight performance. For that reason determining the maximum flight duration of any plane requires a careful balance of all considerations.

Now consider the implications if it was possible to remove the need for an on board fuel system in an air platform. This would mean that air platforms could theoretically be airborne for an unlimited amount of time. Where then is the power going to come from? This is the motivation that has lead to the concept of wireless power transmission. One application that would employ a small ground station remotely powering a small unmanned air vehicle (UAV) is depicted in Figure 1.

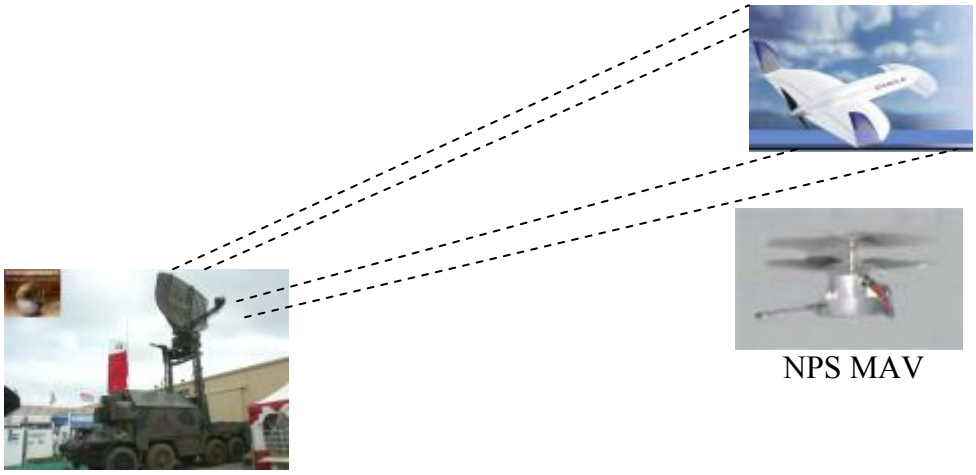

Figure 1. Conceptual powering of UAV by mobile ground station

The concept of wireless power transmission (WPT) dates back to the days of Hertz and Tesla, when it was discovered that energy could be transported in electromagnetic waves in free space. Nikola Tesla was the first to seriously consider the

use of wireless power transmission on a global scale employing low frequency transmission sustained by the earth's natural electromagnetic resonance. A detailed account of the growth of WPT can be found in Reference [1].

With the development of a series of supporting technological innovations, WPT has seen further progress, especially within the last two decades. In the last 5 years, there have been two projects in the Naval Postgraduate School that have related to this field of work, of which the most recent was the implementation of a rectenna array to power a micro air vehicle (MAV).

The definition of a MAV according to the Defense Advanced Research Project Agency (DARPA) program is a fully functional Unmanned Air Vehicle no larger than 15 cm in length, width or height. Due to the restriction in size of the MAV, a crucial aspect of the design was in achieving a light weight rectenna array while supplying adequate power for the MAV. Therefore, implementation options for the rectenna design were rather constrained.

The measured level of efficiency of the most recent NPS rectenna was only 7% compared to other reported designs of over 70%. This thesis follows up on determining the probable causes of low efficiency and to determine a better overall design. These recommended design changes may yield higher manufacturing tolerances and lighter weight.

B. OBJECTIVE

The efficiency of the previous rectenna design was approximately 7% which was insufficient to power an existing lightweight MAV. The purpose of this thesis is to understand the functionality of a rectenna element and analyze the shortcomings of the previous design. The possible areas that might have contributed to the low conversion efficiency in the previous design are presented and further explorations into these areas give direction for this research.

In addition, the robustness of the rectenna design will be investigated to determine whether other types of patch configurations, filter systems or diodes could be used to attain better rectenna performance while achieving the requirement of being lightweight.

C. THESIS ORGANISATION

This thesis is divided into seven chapters, organized as follows:

Chapter II covers the background of WPT, highlighting its growth from the early 1950s through today. Worth mentioning are the advances that make WPT a possible reality in our time. References to WPT feasibility studies and applications of WPT are also covered in this chapter. Finally, an overview of the two related thesis projects that were conducted in the Naval Postgraduate School are presented.

Chapter III proceeds to explain the architecture of a rectenna element and how a rectenna is able to convert rf energy into usable dc power. A detailed account of each subsystem is given.

Chapter IV focuses on the design considerations pertaining to employing patch antennas as well as taking into consideration weight and size restrictions imposed by the nature of the project. The analysis on the choice of patch, feed method, dielectric material and antenna dimensions are covered in this chapter.

Chapter V examines the rectification of rf energy by employing the GaAs Schottky diode. A study of the diode's ac performance is done, which allows for the calculation of the impedance at resonance. With the known impedance, it is possible to match all components to this particular impedance to maximize power transfer and conversion efficiency.

Chapter VI discusses on the pre- and post-rectification filtering process, the effect of common microstrip discontinuities and the connection of the probe feed. The analysis for designing a filter system on a microstrip circuit board is documented followed by a comparative performance study of the pre- and post-rectification filter designs. The effect of the common 90° microstrip discontinuity is then analyzed, ending with the proper connection of the probe feed.

Lastly, Chapter VII summarizes the findings of this research and subsequently presents conclusions and recommendations for an overall better rectenna design.

THIS PAGE INTENTIONALLY LEFT BLANK

II. BACKGROUND

A. HISTORY OF WIRELESS POWER TRANSMISSION

The concept of WPT is simply to transmit electrical power from one point to another through the atmosphere without the physical need of transmission lines or cables. This process usually entails dc-to-ac power conversion, followed by the transmission of this electromagnetic (EM) energy through the radiation of either rf, microwave, laser or light. At the designated target, the reverse process occurs where the ac energy is rectified and converted into dc energy which is then used for power. The power can be used directly, but is most often used to charge a battery.

Brown [1] wrote a descriptive paper on the history of WPT and its progress through the years. In it, he gives detailed accounts of the milestone advances in the work of WPT and the problems that it faced along the way. His references date back to Hertz [2] who was the first to discover that electrical energy could be transmitted through electromagnetic fields in the air. His work was further explored by Tesla [3, 4] who noted that the earth had its own resonance that could be used to sustain low frequency power transmissions for a virtually endless amount of time. However, Tesla's work was hampered by funding issues and the requirement of extremely large plots of land to conduct his experiments.

B. EARLY EXPERIMENTATIONS

A number of advances in different areas came together around the late 1950s which enabled WPT to become a reality. The first advance was the ability to focus electromagnetic power into a beam and achieve high efficiencies [5], and the second was the amplifier tube, which created the required amount of transmitting power [6, 7] to power the electromagnetic beam. With these two advances, the efficient transmission of microwave power was satisfied and the next step was then to look at the reception and conversion of the microwave power.

The first completed microwave power transmission system was conducted in May 1963, where 100 W of dc power was converted from a 400 W transmitter, was used to drive a motor attached to a fan (Figure 2).

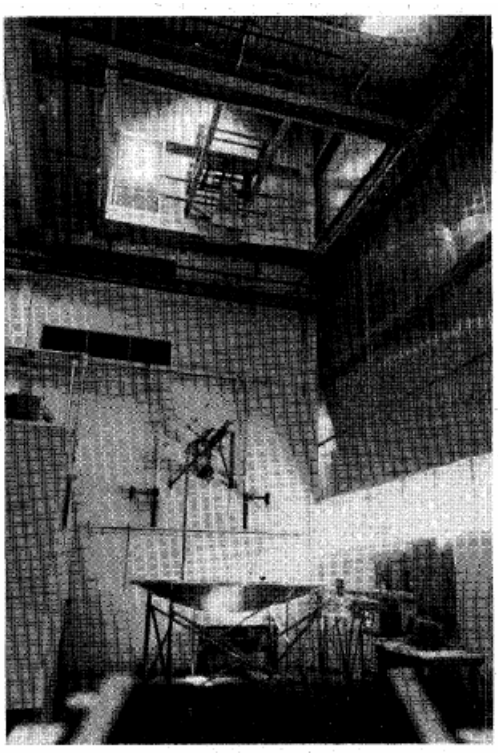

Dc-to-dc efficiency is defined as the percentage of the dc power converted after the WPT process, over the initial dc power used. Rectenna efficiency on the other hand is calculated as the output dc power over the input rf power of each rectenna element.

Figure 2. First known microwave power transmission system, conducted in Raytheon's Spencer Lab in May 1963. Overall dc-to-dc efficiency was about 13 percent (From [1])

The advancement of WPT was, however, hampered by the short lifespan and unreliability of the thermionic diode used in the rectification process. Soon thereafter solid state semiconductor diodes were developed and the concept of a rectenna, consisting of a half-wave dipole antenna connected to the rectifying diode with a ground plate behind it, was conceived. Although the power handling capability of the diode in each rectenna was relatively small, these rectenna elements were then configured in an array to generate sufficient power required for the application.

On Oct. 28, 1964, the concept and demonstration of a microwave power helicopter was presented to the mass media. Following the build up of interest, a non-stop 10 hour hovering of a helicopter was conducted in November of that year (Figure 3).

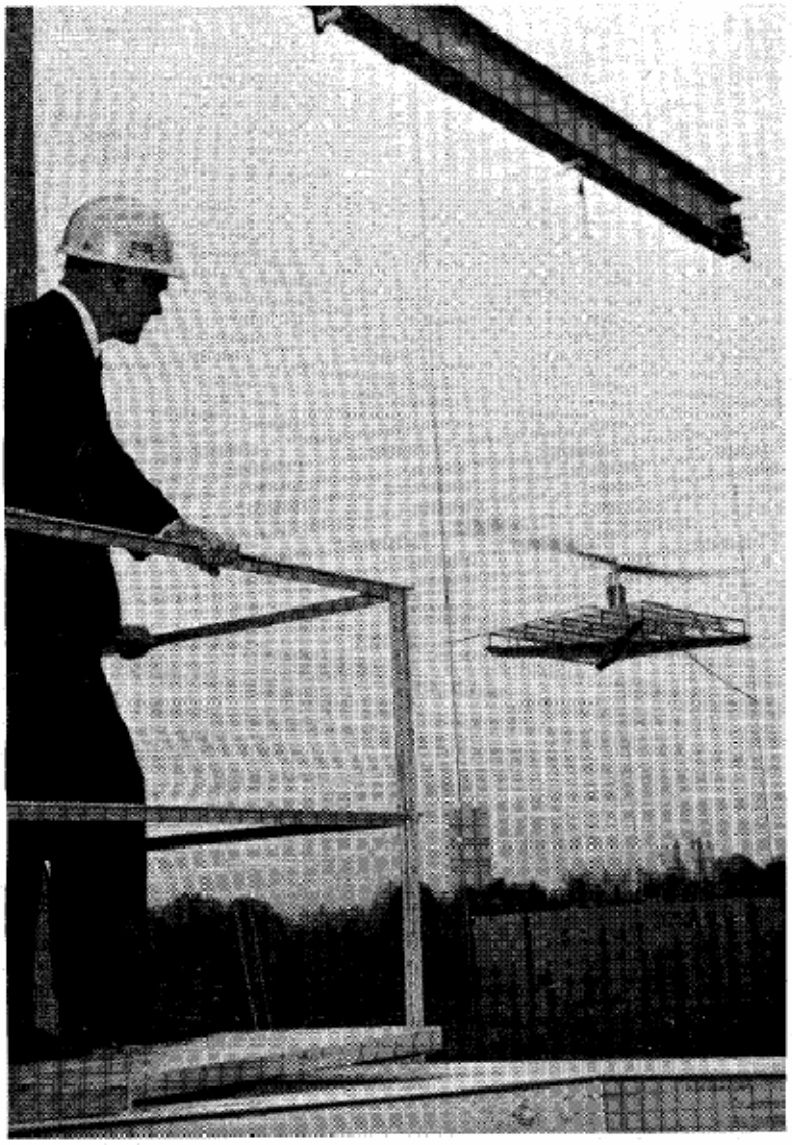

Figure 3. Sustained flight powered solely from WPT technology (From [1])

More experiments were conducted following the successful endurance flight of the microwave powered helicopter with the intent of improving the design. Subsequent milestones of WPT worth highlighting are mentioned in the following paragraphs.

C. MILESTONES OF WPT

1. Ability to Work at Higher Frequencies

Working at the lower end of the frequency spectrum, as in Tesla's case, had its drawbacks. Because wavelength is in the tens of kilometers, large antennas require long

stretches of land to lay the antennas. As rf transmission technology improved, transmissions at higher frequencies became possible. With this technology the move towards high frequency power transmission became prominent. The main advantage of using high frequencies is that the dimensions of the antennas could be reduced due to the reduction in wavelength. As the dimension of antenna is reduced, its application on mobile platforms or other places where space was limited became more feasible.

2. Better Rectification Diodes

One of the most important milestones in the advancement of WPT is related to the diode used in the rectification process. Many papers have shown that the efficiency of the rectenna is mainly attributed to the efficiency of the diode. This is supported by several references, Brown [1] and McSpadden [8] to name a few. A good rectenna diode would have characteristics such as low turn-on voltage, high reverse bias voltage, linear response to minimize harmonic generation and low power loss. Advances in this area began with the use of solid state silicon based PN junction diodes, which have a high turn on voltage of 0.7 V, and new fast switching GaAs Schottky diodes that exhibit very fast switching capabilities suitable for high frequency rectification processes. The advances in the design of Schottky diodes which were capable of achieving good rectification efficiencies rejuvenated the interest in wireless power transmission to where we are today.

D. RECENT FEASIBLITY STUDIES

Within the last decade a number of feasibility studies were carried out for WPT through the use of rectennas. In 1999, a joint experimental study on a large rectenna array was conducted by the Radio Atmospheric Science Centre of Kyoto University and Kansai Electric Power Company [9]. In their field experiment, they were able to attain rf-to-dc conversion efficiencies of 64% at 2.5 W.

In 1999, the Korea Electrotechnology Research Institute conducted a study on the wireless power transmission system [10], where they were able to achieve single rectenna conversion efficiency of 75.6% and an overall system efficiency of 33%.

Another feasibility study into the application of WPT, was whether ambient microwave energies could be recycled using rectennas. This concept utilized broadband antenna arrays instead of narrowband ones in order to convert as much microwave power into dc power. In the study done by Hagerty [11], an array of 64 circularly polarized spiral elements was designed, where rectification efficiencies of 20% for 0.1 mW/cm^2 radiation was achieved.

E. POWER SYSTEM IMPLEMENTATION

Of all the studies concerning the use of WPT, the one invention thought of by Peter Glaser in 1968, was directed towards Earth's growing need for an alternate source of energy on a global scale.

In March of 2002, the *IEEE Microwave Magazine* published an article by Lin [12], spanning 3 pages, on the concept of solar power satellites (SPS) and wireless power transmission. The concept was to build satellites with a sole function of gathering solar power and converting it into rf or microwave energy. This energy would then be transmitted through the vacuum of space using WPT technology back to Earth for use. The article highlighted supporting theory and present advances in technology that have made the possibility of SPS-WPT very real. In addition the concerns relating to both environmental and safety-related issues were mentioned.

In December of 2002, another article was published in the *IEEE Microwave Magazine* written by McSpadden [13]. In the article, McSpadden gave a detailed account of NASA's efforts of achieving a realizable space solar power (SSP) program, and explained the different components required in the SSP system which entailed the use of WPT technology. The main components were the transmitter, beam control, and state-of-the-art rectennas. Although it was mentioned that present technology has not achieved the state of maturity for successful implementation, the strategic roadmap highlights the incremental steps required for its assured growth. These point towards a day where its implementation will be the source of power for future generations.

Another variant of similar intent is being explored by the TEXAS SPACE GRANT CONSORTIUM [14]. Lunar bases are used in place of geo-synchronous satellites. Figure 4 shows the concept of such a system.

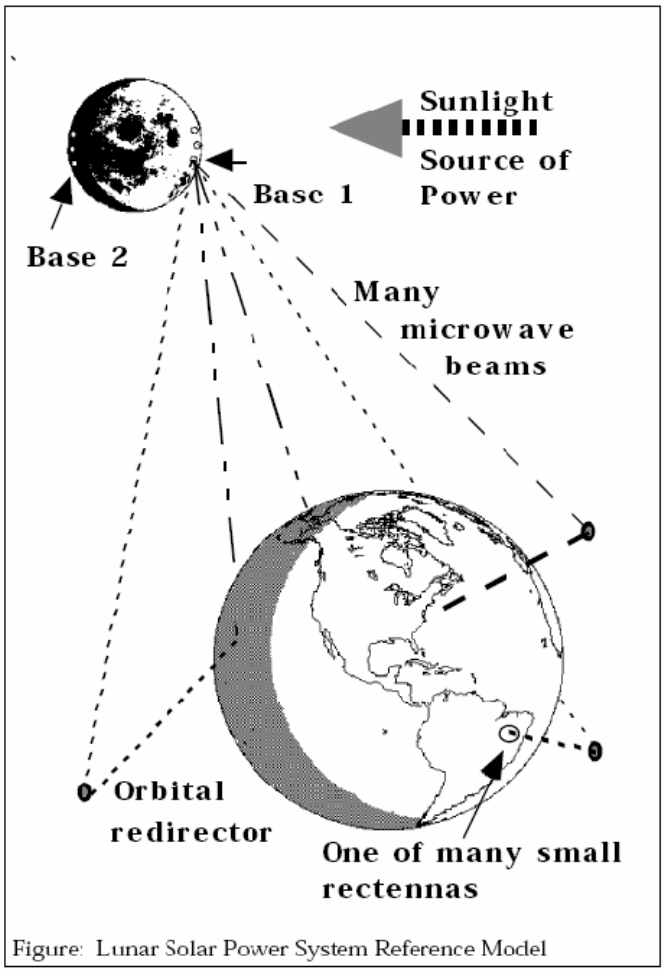

Figure 4. Lunar solar power system reference model (From [14])

F. SMALL SCALE IMPLEMETATION

The idea of WPT is, however, not limited to large scale implementations. In fact miniaturized applications have had their own fair share of interest, especially in the area of warfare. The concept of micro unmanned aerial vehicles, high altitude high endurance reconnaissance crafts, helicopters, and similar platforms, which utilize WPT technology, could possibly attain unlimited flight time, resulting in continuous availability.

In fact the world's first untethered microwave powered flight was conducted on September 17, 1987 [15]. As shown in Figure 5, the plane flew in a circular path above the grid of antennas which directed the microwave beam onto the plane. The recorded flight duration was 20 minutes.

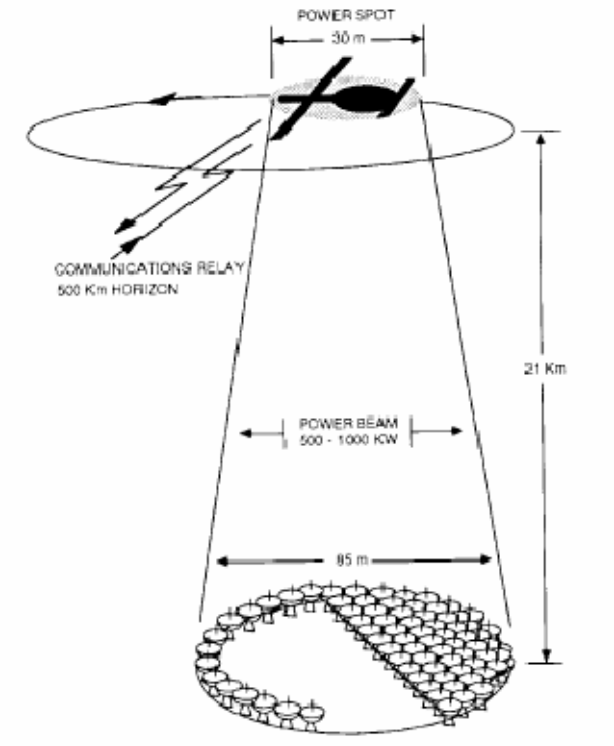

Figure 5. The SHARP SYSTEM (From [14])

There are other possible applications of WPT other than the attainment of unlimited sustenance of flight. Within the last decade, another area of science which has great potential for exploiting WPT is that of nanotechnology. Due to the miniaturization of both mechanical and electrical components, the energy requirements of such devices would generally be small and the physical size of the power source is very limited. In line with these requirements, WPT could very well be the ideal technology for powering these elements on a microscopic scale.

In the *NASA Tech Brief*, Siegel [16] proposed integrated-circuit modules called "nanoconverters" that will be able to generate dc power from electromagnetic beams in the terahertz range. Each nanoconverter will be composed of microscopic antennas and diodes which resemble conventional rectennas used in the gigahertz range (Figure 6).

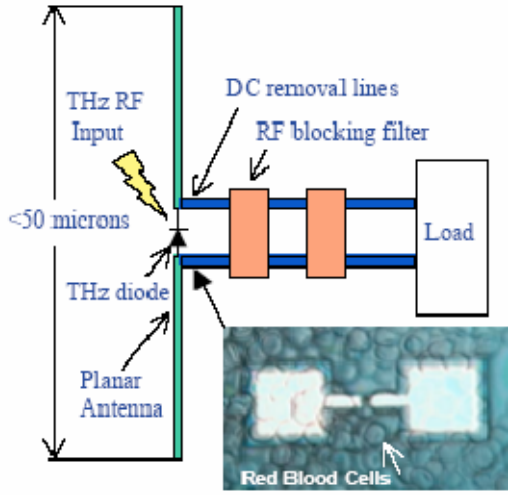

Figure 6. Schematic of a nanoconverter and the physical size with respect to red blood cells. (From [16])

These nanoconverters will supply sufficient power to nanodevices. The range of applications that could utilize such nanodevices would be extremely large ranging from medical, biological and, of course, military in nature. A recent article [17] described a working model of a micro-UAV that was observed flying and believed to be remotely powered by an off-board source (Figure 7). The report said it was equipped with nano-sensory capabilities.

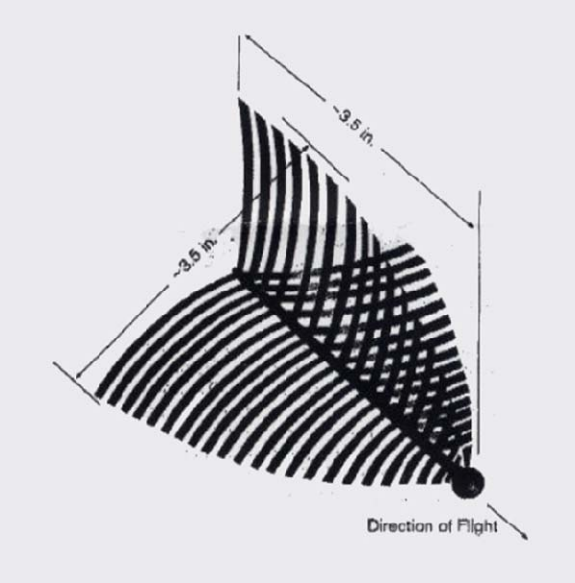

Figure 7. Drawing of a remotely powered Micro UAV, including dimensions (From [17])

The article stated that the technology used in the remote powering of such devices with microwave beams was an established technology and could provide propulsive power for a micro-UAV without carrying the power source on board. Quoting the article,

> A couple of months ago, Darpa [the Defense Advanced Research Projects Agency] showed Pentagon officials about 15 very small UAV designs. Of these, five were flying. − a senior Defense Department official

With such vehicles already being developed and paving the way of future warfare, it will not be surprising to see the proliferation of WPT in other areas as well.

G. NPS RESEARCH

Students at the Naval Postgraduate School have looked into aspects of WPT for MAV propulsion (Vitale [18] and Tsolis [19]).

Vitale designed a rectification circuit using a metal semi-conductor diode and was able to experimentally determine the S parameters of the diode, which lead to it being modeled analytically. He then utilized a dipole antenna in his design, and from experimentations determined his rectification conversion efficiency was approximately 30%. He recommended that future research could be done in the areas of employing GaAs Schottky diodes, the use of better rectification configurations and high power sources, and lastly, to examine improvements into the MAV antenna design.

Tsolis extended Vitale's work by utilizing Schottky diodes and the microstrip patch antenna in the effort to maximize the power-to-weight ratio. However, the patch antenna design could only gain efficiencies of around 7%. He highlighted that further analysis into preventing mismatches was necessary (to minimize reflection losses) as was the use of higher power rectification diodes (to enable higher power handling capabilities).

H. SUMMARY

The history of WPT was briefly covered and the major milestones in the development of WPT were highlighted. Much interest and research has been conducted

to determine the feasibility of implementing WPT and its applications, which range from futuristic large scale power systems to miniaturized versions of remotely powered vehicles.

III. RECTENNA DESIGN

A. BASIC RECTENNA DESIGN

The design of a rectenna system can take many forms, however, as varied as they can be, they tend to have four subsystems. These four subsystems are: (1) the receiving antenna, (2) the pre-rectification filtering, (3) rectification and (4) post-rectification filtering. The basic configuration of a rectenna is shown in the Figure 8.

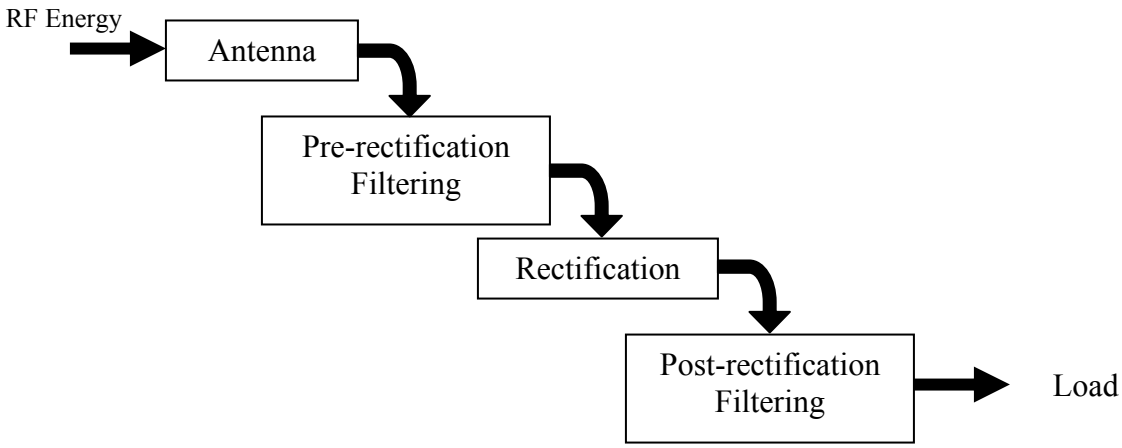

Figure 8. Basic configuration of a rectenna system

1. Antenna

The main function of the antenna is to collect as much rf radiation as possible and transfer this energy to the pre-rectification filter stage. The main factors considered in antenna design are its power handling capabilities, size and weight of the antenna, efficiency, broadband filter response, frequency of operation, and gain.

Antennas come in different designs ranging from simple half-wave dipoles, parabolic dishes, horns, helixes to thin microstrip patch antennas. The choice of antenna design is influenced mainly by the specific needs of the application. In the case of a MAV, a principal consideration is to keep the power-to-weight ratio as high as possible. This requires that the rectenna element should be kept as lightweight as possible. Also a low profile aerodynamic antenna structure is desirable. Therefore the utilization of microstrip patch antennas was selected as the best option for our applications.

The efficiency of the antenna is critical, as it affects the overall performance of the remaining stages of the rectenna. Rectenna designs may also employ a small array of antennas, summing up the incoming rf energy before feeding it into the subsequent subsystem for rectification.

2. Pre-rectification Filtering

The pre-rectification filter has two main functions. Primarily it limits the frequency of the incoming rf signals, to ensure that the incoming signal is resonating below the operation frequency of the rectifier. The second function is to prevent the re-radiation of higher order harmonics produced by the non-linear *I-V* characteristics of the rectifying diode.

Depending on the frequency response of the antenna, it is possible for the patch antenna design to have inherent characteristics that enhance the second function of the pre-rectification filter. For example, with square or rectangle patches, the resonant frequencies are usually integer multiples of the lowest resonating mode frequency. Such a patch will re-radiate higher order harmonics if they were present. However, in the case of a circular patch antenna, the resonant frequencies are a function of the Bessel function, which are not multiple integers of the mode frequency, therefore suppressing the re-radiation of high order harmonic frequencies.

The minimization of higher order harmonic radiation is critical on two accounts. The first is to minimize the interference caused to other equipment or apparatus working at the same higher order harmonic frequencies. The other is to minimize loss of energy in the rectenna, which increases its conversion efficiency.

3. Rectification

The heart of a rectenna is essentially the rectifier, which is usually a diode of some nature. The selection of the diode is usually based on considerations such as its power handling capabilities, maximum switching speed, weight, cost, *I-V* characteristics, operating frequency impedance, forward bias voltage, maximum reverse breakdown voltage, saturation current, and efficiency, among others.

An ideal diode for our rectenna application would be one which has a small turn-on voltage or zero-bias is preferable, large reverse breakdown voltage, and low capacitance (less than 1 pF in order to work at 10 GHz). It should also have a high power handling capacity.

As mentioned in the previous section, the non-linear characteristics of the diode will create a dc component followed by harmonic components, and it is the extracted dc component that will be fed to the load (motor or battery).

4. Post-rectification Filtering

After the incoming rf wave is rectified by the diode, the signal is fed to the post rectification filter whose function is to extract the dc component and reflect the rest of the frequencies back to the rectifier. Because it is not possible to achieve an ideal cut-off low pass filter response, some low frequency components may still be present at the output end of the rectenna. They will show up as ripples in the dc voltage.

The post-rectification filter is usually implemented either as microstrip filter similar to the pre-rectification filter, or with a capacitor and resistive load, or possibly a combination of both.

B. DISCUSSION OF PREVIOUS DESIGN AND AREAS OF CURRENT RESEARCH

The overall efficiency of the rectenna element is a function of cascading the efficiency of each subsystem. As such it is critical to analyze each of these subsystems carefully to understand its function, and to minimize possible causes of inefficiency in each subsystem. This section of the chapter will discuss the rectenna that was used in the previous MAV design. It will summarize the details and findings of each rectenna subsystem, and will serve as the basis for determining possible cases of low efficiency. It will also state criteria that must be fulfilled by the new rectenna design.

This section will cover areas of the original rectenna design such as the frequency used, the patch antenna design, choice of feeding method, analysis of the schottky diode, the filter design, motor selection, and lastly, the effect of microstrip discontinuities.

1. Use of 10 GHz Operating Frequency

Although the primary reason stated for using 10 GHz was to reduce the size of the antenna patch, because antenna dimensions are a function of the wavelength of transmission, the factor of antenna size is but one of many considerations that must be taken in totality. Another factor is interference; who are the other shareholders or common users to the frequency, and is the frequency heavily used in the vicinity of operation? Since the transmission of energy is involved, the next consideration would be to determine the atmospheric attenuation at the operating frequency. Safety issues will also need to be considered when operating at high power levels.

In the case of supplying dc power to a MAV, the requirement for a lightweight and small antenna superseeded other considerations. Another supporting factor was the fact that a transmitter of sufficient power at 10 GHz was available in the laboratory, which aided in the practical experimentation of the rectenna design. Other frequencies could be chosen for future designs. The design and analysis resulting from this research will be applicable to all operating frequencies.

2. Patch Antenna Design

Although there are many different configurations of microstrip patch antennas, common ones are the square, rectangle, circular disc, and annular rings as shown in Figure 9. The circular patch was chosen because of its inherent advantages of being smaller than the square or rectangle patches for a given resonant frequency. It has no preferred axis and the feed can be placed anywhere around the circumference. However it has a smaller bandwidth, lower efficiency and higher input resistance than the rectangular patch. Given that the principal consideration is to minimize weight, the choice of the circular patch seems appropriate. The details of the previous design by Tsolis are given in Table 1.

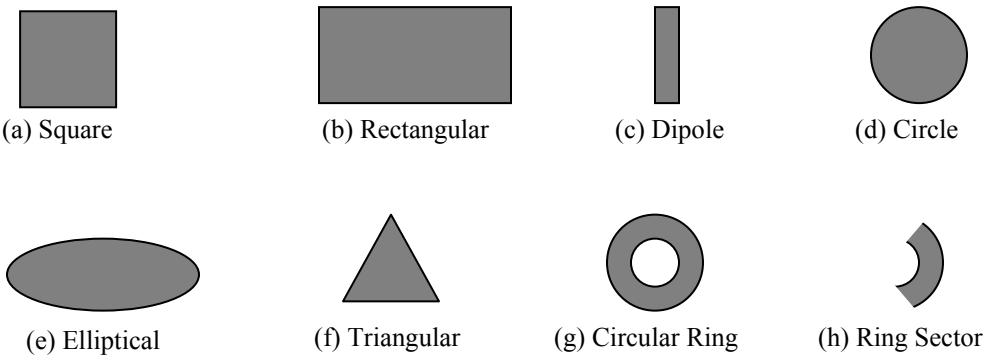

Figure 9. Representative shapes of microstrip patch elements

PARAMETER	**VALUE**
Dielectric Material	RO 3003 from Rogers Corporation
ε_r	3
Loss tangent, $\tan\delta$	0.0012 @ 10 GHz
Substrate height, h	0.127 mm
Copper thickness	½ oz or 17.5 μm
Patch radius	5.03 mm
Feed point	1.15 mm to achieve 30 Ω impedance

Table 1. Circular patch parameters for the previous design (From [19])

Another reason supporting the choice of a circular patch was that it resonated in harmonics governed by the Bessel function of the order n. The equation of resonance is [20]

$$J_n'\left(\sqrt{\varepsilon_r}k_0 a\right) = 0 \tag{3.1}$$

where $k_0 = 2\pi/\lambda_0$ (λ_0 is the wavelength in free space). The prime denotes a derivative with respect to the argument.

This implies that the circular patch's resonant frequencies are not synchronized with the harmonics generated by the rectification diode. It was the intent of minimizing

energy lost from the retransmission of the higher order harmonics and the minimization of interference at the higher harmonics frequencies that the circular patch was finally chosen. This consideration however, was not emphasized in other patch designs, and yet were still able to achieve good conversion rates. In addition, before any higher order harmonics are re-radiated, they must pass through the pre-rectification low pass filter, which is designed to minimize the transmission of such harmonics. If the minimization of higher order harmonics can be achieved through the pre-rectification low pass filter, then could other patch designs be used? This question is investigated in Chapter VI.

As seen in Figure 10, the original patch's performance is not optimized to the frequency of 10 GHz, which is exceptionally critically for such a low bandwidth antenna. The return loss, $20\log_{10}\left(S_{11}\right)$, is a measure of the reflected power at the antenna. Ideally it should be as low as possible in order to transfer as much rf energy into the subsequent rectenna systems. From the figure the return loss of the previous design was approximately -7 dB at 10 GHz. That is, 20% of the energy is being reflected back out of the antenna.

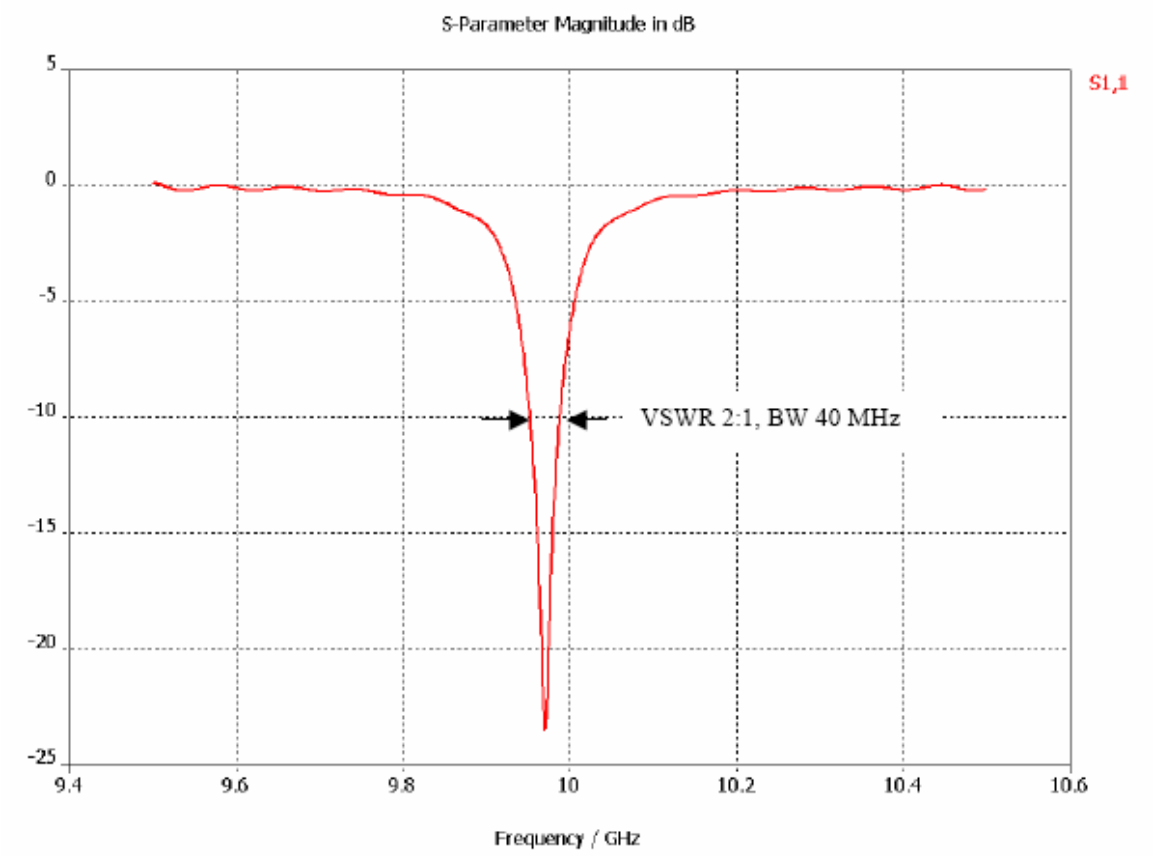

Figure 10. Return loss S_{11} in dB as a function of frequency for the original circular disc design (From [19])

In addition, the use of the circular patch antenna together with a thin substrate of only 0.127 mm, resulted in a narrow bandwidth of 0.4% for a voltage standing wave ratio (VSWR) of 2:1. This requires that the transmitter be capable of transmitting with little deviation from center frequency, which increases the overall system cost. Therefore in order to reduce the issue of variance in patch manufacturing and stringent transmitter requirements, the investigation of more broadband patch antennas will be conducted.

3. Choice of Feeding Method

There are number of feeding methods for microstrip antennas, as shown in Figure 11. They are the direct feed, probe feed, aperture feed, and lastly the electromagnetic coupled feed.

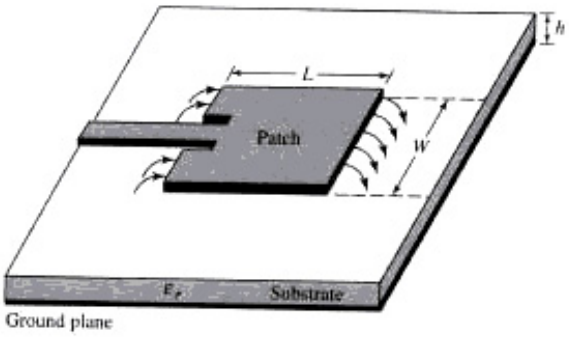

(a) Microstrip line feed

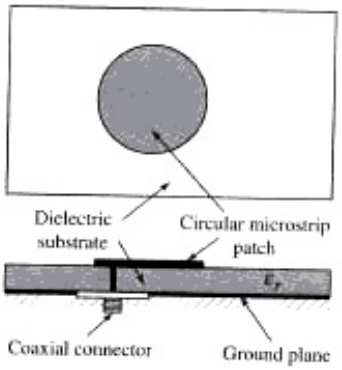

(b) Probe feed

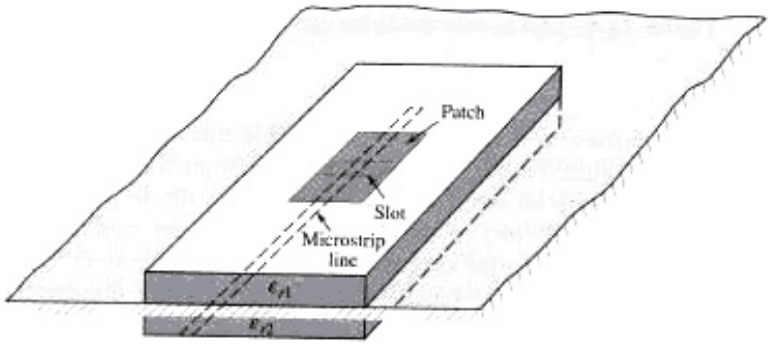

(a) Aperture-coupled feed

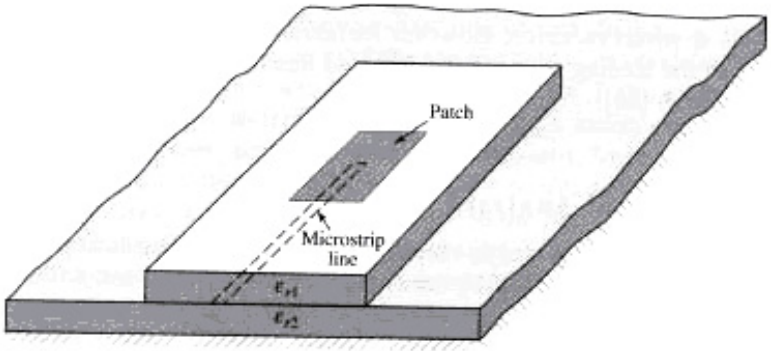

(a) Proximity-coupled feed

Figure 11. Different types of microstrip feeding methods (From [21])

The probe feed was used in the last design, and it serves to electrically connect the patch antenna with the microstrip filters on the opposite side of the ground plane. The position of the probe on the antenna is critical in achieving good impedance matching, which is desired for maximum power transfer. In his thesis, Tsolis [19] recommended that the issues of impedance mismatches should be investigated. Could the low efficiency

performance of the previous design be caused by impedance mismatches occurring through manufacturing variances in the probe feed position? Do other feeding methods have better tolerances to manufacturing variances? This issue will be investigated in Chapter IV.

The procedures used in the manufacturing of the probe feed were not documented in the previous thesis and there was no mention regarding the dimension of the relief hole drilled into the ground plate to accommodate the probe. These issues will be examined so that the limitations of the probe feed are determined, should it be chosen for the current design.

The decision to use the ground plane to isolate the microstrip filters from spurious radiation from the antenna and minimize space has its advantages. However, it does require two layers of dielectric which has substantial weight. Is this the ideal approach, or would a single layer dielectric configuration be more efficient? In addition, the use of balsa wood (Figure 12) to separate the two layers was not examined, and perhaps the space and weight could be used more effectively.

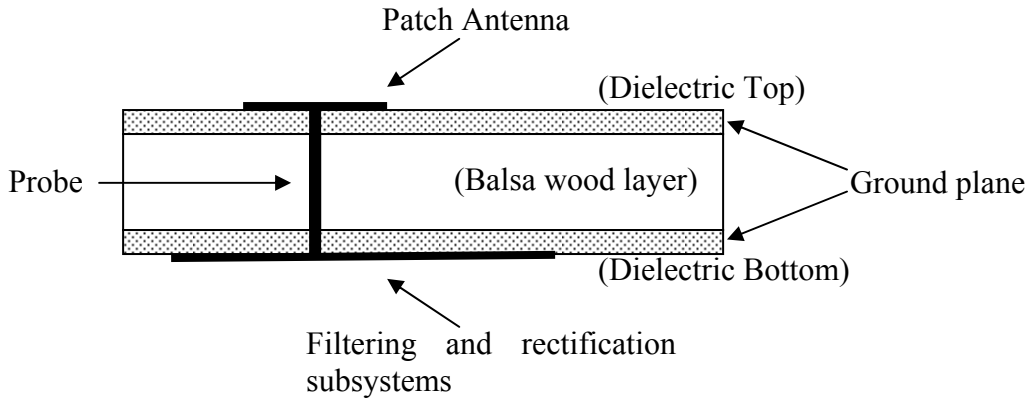

Figure 12. Balsa wood buffer layer used in original design

4. Schottky Diode Operation

The Schottky diode is the heart of the rectenna element. Therefore it is critical to understand the operation of the diode in order to obtain better rf-to-dc conversion efficiency. The physical performance of the Agilent HSMS-8101 Schottky diode was experimentally determined in [19] and was found to operate within the manufacturer's

specification, except for its power handling capability. Although the diode's power handling capacity was rated at 75 mW, it was found that it could operate at a maximum power of 242 mW, with a voltage of 1.8 V and current of 140 mA. From the required power of approximately 1.2 W to sustain the MAV flight, and taking 80% of the maximum measured power handing capacity of each diode, at least six diodes will be required to power the MAV. The diode's rf impedance was subsequently calculated at $30 - j340\ \Omega$ at the operating frequency of 10 GHz. Employing the real value of 30 Ω, the rest of the circuit was designed to match this resistance.

Upon careful inspection of the findings it was noticed that there was a miscalculation in the power of the diode. The previous calculation used 100 mW of input rf power and expected 65 mW of output dc power, when in fact 650 mW should have been calculated. This is definitely not possible and further analysis on determining the cause of this miscalculation will be explored. In addition, the calculation of the junction resistance of the diode was not clearly specified and will be examined in detail.

5. Filtering Aspects

In order to minimize the size and weight of the filters, they were implemented using a series of microstrip stubs. The main performance measure was the S_{12} parameter which is the voltage transmission coefficient of the filter across the spectral range. In [19], the goal of the pre- and post-rectification filter was to attain an attenuation of 15 dB at 20 GHz, and 25 dB at 10 GHz. The pre-rectification filter was a fourth order low pass microstrip filter, with a cutoff frequency of 12 GHz, while the post-rectification filter was a second order low pass microstrip filter with a cutoff frequency of 2 GHz.

Although the low pass filter designs were previously simulated using the Agilent ADS software, the filters characteristics will be re-verified in Microwave Studio. Other possible configurations for the microstrip filter will be investigated to determine if these are better filtering solutions.

6. Motor Selection

Based on the previous design, a small pager motor was chosen to drive the prop shaft of the MAV. The measured impedance of the motor at the rpm required to hover the

MAV was in the vicinity of 50 Ω and the power requirement of this motor is given in Table 2.

Weight (g)	**Vehicle Only**	**Rectenna system weight**					
		5	10	15	20	25	30
Voltage (V)	5.5	7	8.1	9.9	11.5	14	16
Current (mA)	0.1	0.136	0.17	0.22	0.264	0.319	0.357
Resistance (Ω)	54.9	51.4	47.4	45	43.5	43.8	44.8
Power (W)	0.55	0.952	1.3817	2.1780	3.036	4.466	5.712
RPM	1200	1440	1620	1740	1770	1800	2100

Table 2. Power requirement of MAV motor for different weights (After [19])

With a rectenna array weight of 5 and 10 grams, the power requirement is 0.95 W and 1.4 W respectively. The new rectenna design must achieve these power requirements, while trying to minimize weight, in order to attain flight.

7. Microstrip Discontinuities

In the effort of minimizing space for each rectenna element, microstrip discontinuities in the form of 90° bends were used in the design. As seen in Figure 13 there are two bends in the previous design. However from [20], such microstrip discontinuities results in added inductance and should be minimized. The consideration for the placement of the bends was not stated in [19] and gives no explanation on why they were situated in such critical locations; namely, the point of rectification, and in the middle of the output low pass filter. The effects of the 90° bend in the microstrip design will be evaluated in the following chapters.

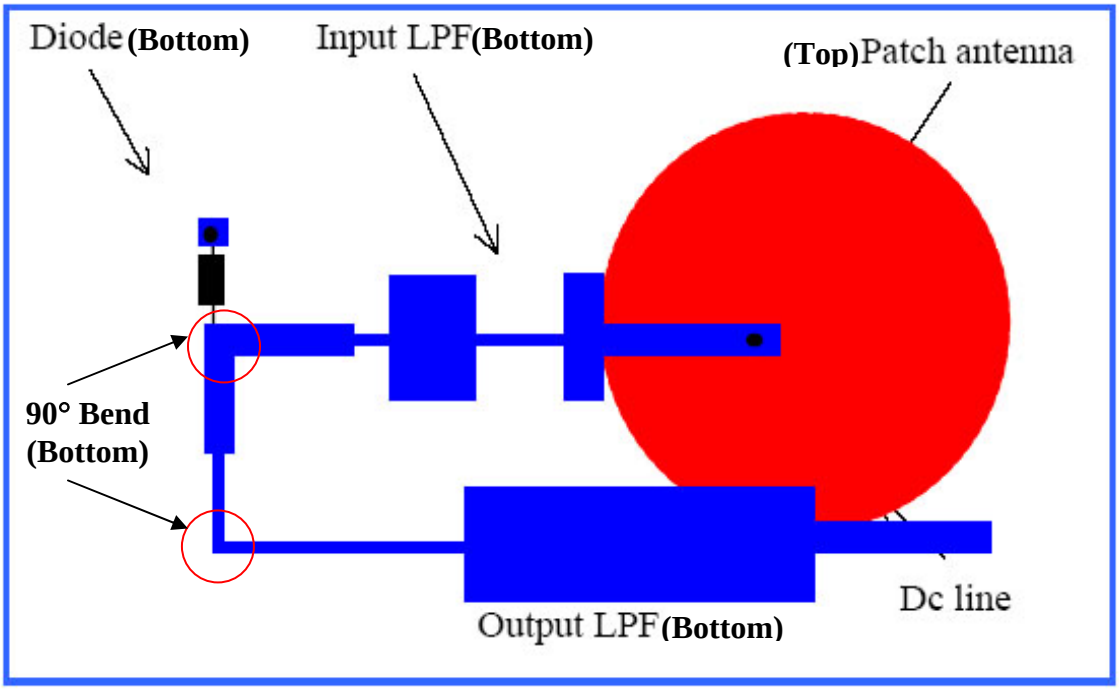

Figure 13. Presence of microstrip 90° bends in the original design (From [19])

IV. PATCH ANTENNA

There are three objectives to this chapter. The first is to analyze the performance of the original patch antenna and determine its limitations. The second objective is to determine the effect of manufacturing and assembly errors, such as variations in patch radius and probe location that might be the cause of reduced patch performance. And lastly, to determine an improved patch antenna that suits our application, validated with simulation results.

A. PARAMETERS FOR DESIGNING A CIRCULAR PATCH

A circular patch can be designed by choosing the appropriate values for four variables; namely, the height of the dielectric substrate, the dielectric constant of the substrate, the radius of the patch, and the feed location. The Tsolis design used a substrate height of 0.127 mm and a relative dielectric constant of 3. The resonant frequency of the circular patch antenna is determined by the radius of the patch. The relationship between patch radius and resonant frequency is a Bessel function [20], where for the dominant mode TM_{110}^{z}

$$(f_r)_{110} = \frac{1.8412c}{2\pi r_{patch}\sqrt{\varepsilon_r}} \tag{4.1}$$

where c is the speed of light, and ε_r is the relative dielectric of the substrate. However Equation (4.1) does not account for the fringing E-fields experienced at the edge of the patch. This fringing makes the patch look electrically larger and a corrective factor must be introduced to the patch radius to compensate for the fringing. An effective radius can be calculated from

$$r_{patch\_eff} = r_{patch}\left\{1+\frac{2h}{\pi r_{patch}\varepsilon_r}\left[\ln\left(\frac{\pi r_{patch}}{2h}\right)+1.7726\right]\right\}^{1/2} \tag{4.2}$$

Substituting the effective patch radius into Equation (4.1) the resonance frequency is now

$$(f_r)_{110} = \frac{1.8412c}{2\pi r_{patch\_eff}\sqrt{\varepsilon_r}} \tag{4.3}$$

With this equation, the patch radius can be calculated for any frequency provided that the substrate height satisfies, $h < 0.05\lambda$ [21]. Based on the required resonant frequency of 10 GHz, the patch radius of the old design was theoretically calculated at 5.1 mm for a resonant frequency of 9.952 GHz, and the PatchD program [20], calculated the patch radius of 5.03 mm for a resonant frequency of 9.9992 GHz.

The required patch impedance is determined by the location of the feed point with respect to the center of the circular patch. The closer the probe is to the center of the patch, the lower the impedance. The location of the feed probe calculated using the PatchD program was 1.15 mm from the center of the patch. Derivations towards the calculation of the probe location can be found in [21]. Since the substrate used was relatively thin, the issue of inductance introduced by the probe can be neglected. However for thicker substrates, the probe's inductance does matter and will be discussed subsequently in this chapter.

B. VERIFICATION OF PREVIOUS DESIGN AND ITS LIMITATIONS

The program Microwave Studio (MWS) Version 5 was used extensively in this thesis as a tool to determine the performance of different patch antennas. Other insights were gained from its results and will be discussed subsequently. The Tsolis circular patch was re-validated in MWS, using the data from [19]. However as there was no mention on the relief hole dimension drilled into the ground plate, it is assumed that Tsolis took this into consideration in his design. From [20], it was found that the ratio of the relief hole to probe radius should satisfy

$$Z_0 = \frac{60}{\sqrt{\varepsilon_r}} \ln\left(\frac{r_h}{r_p}\right) \tag{4.4}$$

where r_h and r_p are the radii of the relief hole and probe respectively, in order for the traveling rf wave to view the relief hole as a coaxial cable with impedance Z_0.

Since an impedance of 30 Ω is required, given that r_p is 0.125 mm, r_h was calculated as 0.3 mm. With these dimensions, the previous patch antenna design was re-verified on MWS and the results obtained were close to those in [19]. Although there were variations in the resonant frequency, it can not be determined if the dimension of the relief hole was the cause of the differences.

There are multiple measures of performance for an antenna, such as gain, directivity, insertion loss, VSWR and bandwidth, to name a few. The reflection loss, S_{11}, which is related to impedance matching, is the ratio of the reflected wave power to that of the incident wave, is the main attribute used in the performance evaluation. This is because the gain and pattern are primarily determined by the antenna configuration (size and shape). Therefore, if the impedance is matched then the other antenna parameters are likely to be well behaved.

1. Patch Tuning

Figure 14 shows the return loss of the original antenna design by Tsolis using the relief dimension of 0.3 mm. As seen in Figure 14, the insertion loss of the patch at 10 GHz is approximately -2 dB, which means that 63% of incoming rf energy is reflected back. The mismatch loss is $-10\log\left(1-\left|S_{11}\right|^2\right)=4.3$ dB. This could explain the low efficiency of the rectenna, and why so little rf power is being transmitted through the first subsystem. The main cause is due to the notch of the response being off the required resonant frequency of 10 GHz by 0.11 GHz. If the antenna can be retuned so that the notch is at the 10 GHz then the mismatch loss will be reduced significantly.

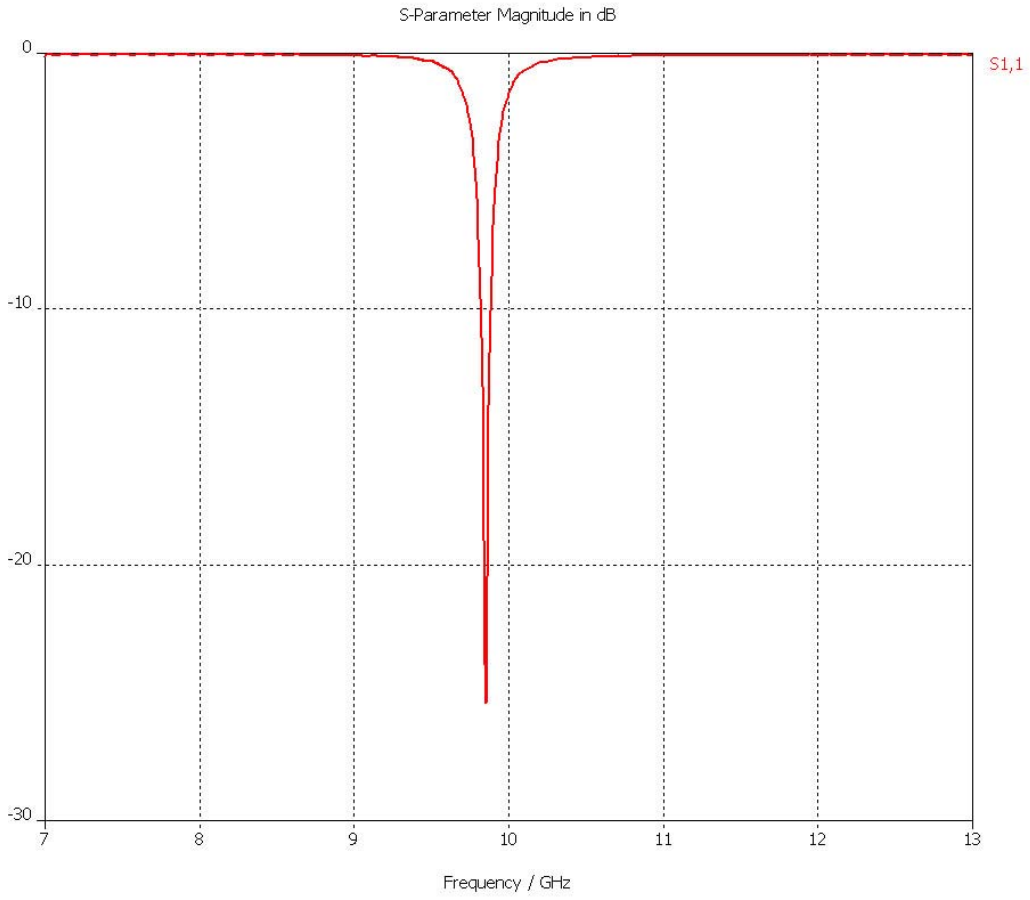

Figure 14. Return loss of Tsolis design

As mentioned in [20], the patchD program over-estimates the patch radius by around 2% for thin substrates and, therefore, since a higher resonant frequency is required, the new patch radius was subsequently reduced by 4% to 4.83 mm. Using the new radius, the notch of S_{11} is centered over the required 10 GHz, as seen in Figure 15.

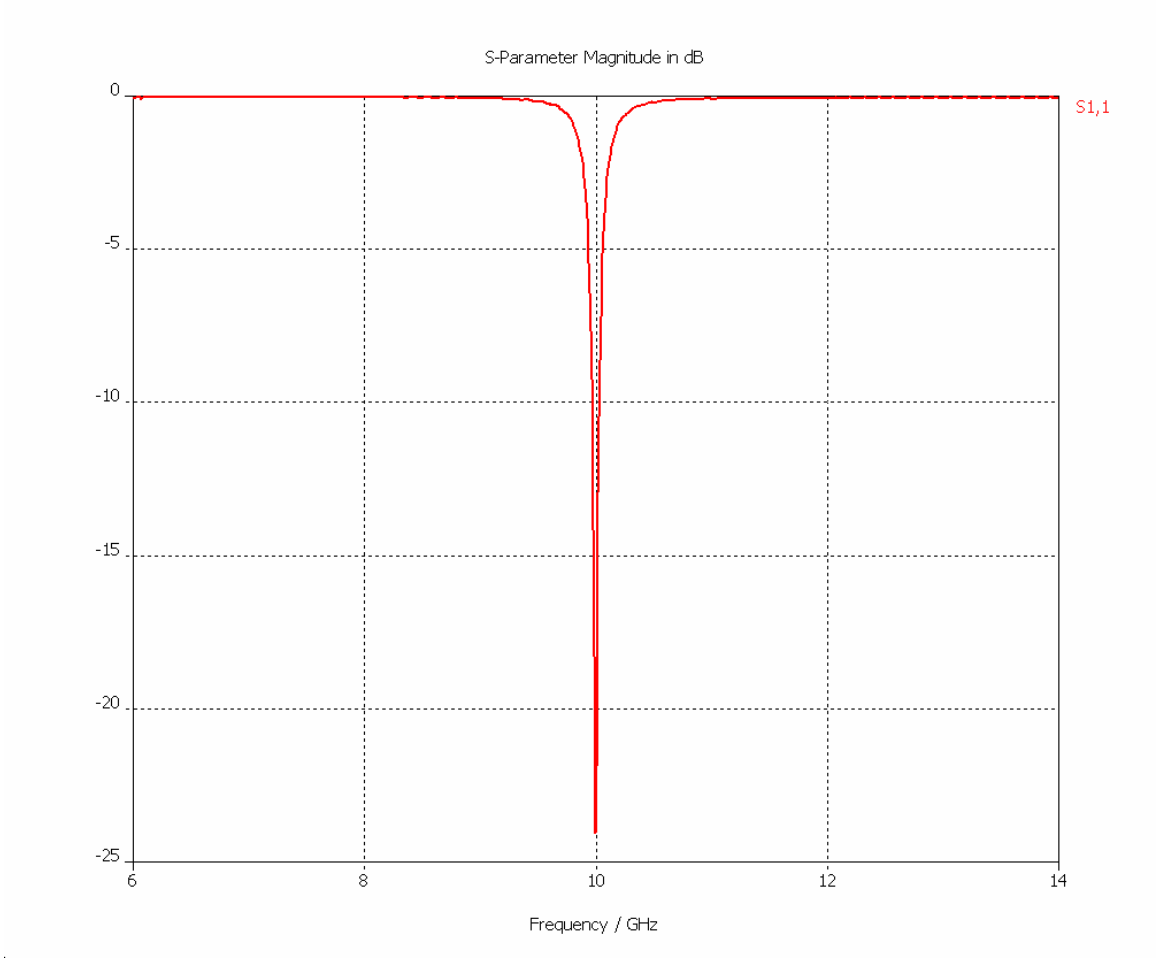

Figure 15. Return loss of the improved design

2. Probe Position

Since the impedance of the probe is dependent on the patch radius, the original design with a feed offset of 1.15 mm had an input resistance of $2.8 - j0.67\ \Omega$ at 10 GHz as seen on the Smith chart in Figure 16.

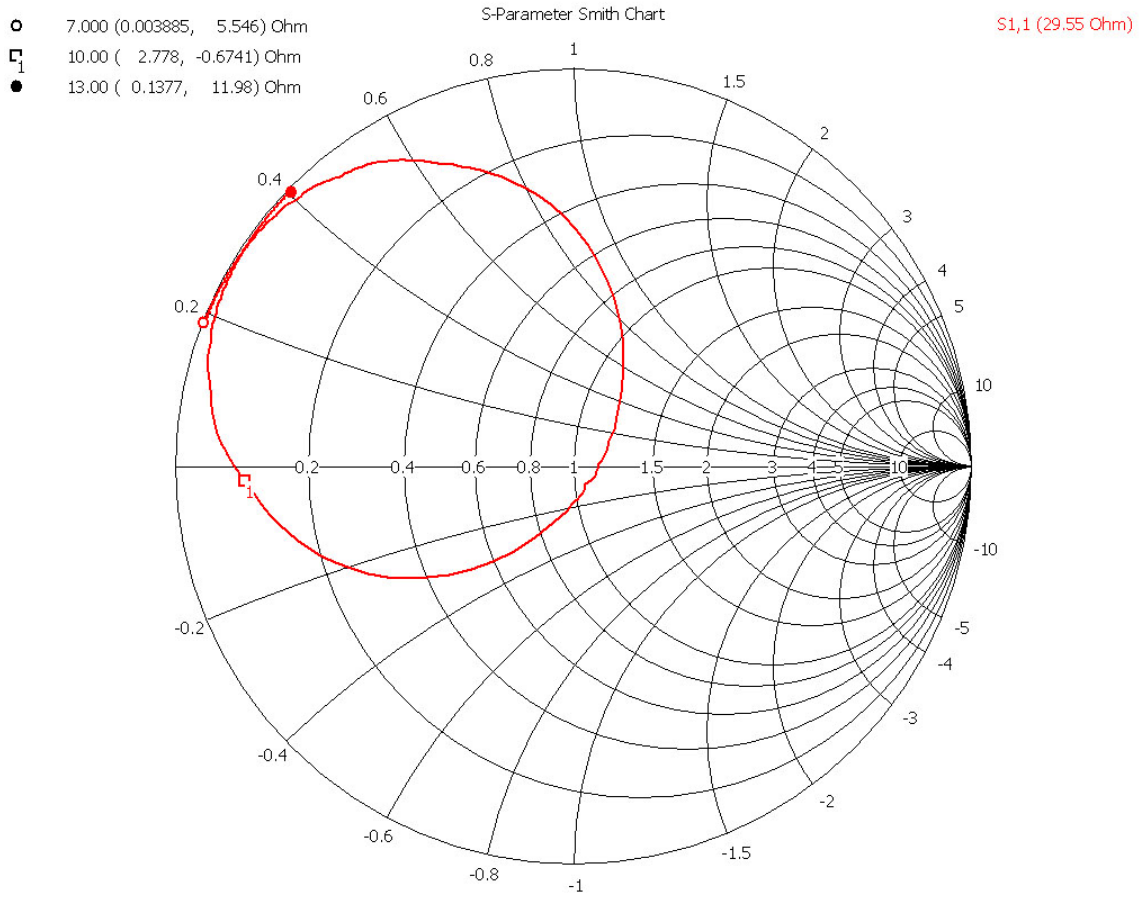

Figure 16. Smith Chart of the original design

After changing the patch radius to match the resonant frequency, the location of the feed was subsequently varied to 1.02 mm, to achieve the best match of 33.4 Ω. This can be seen from the Smith chart of the improved design in Figure 17.

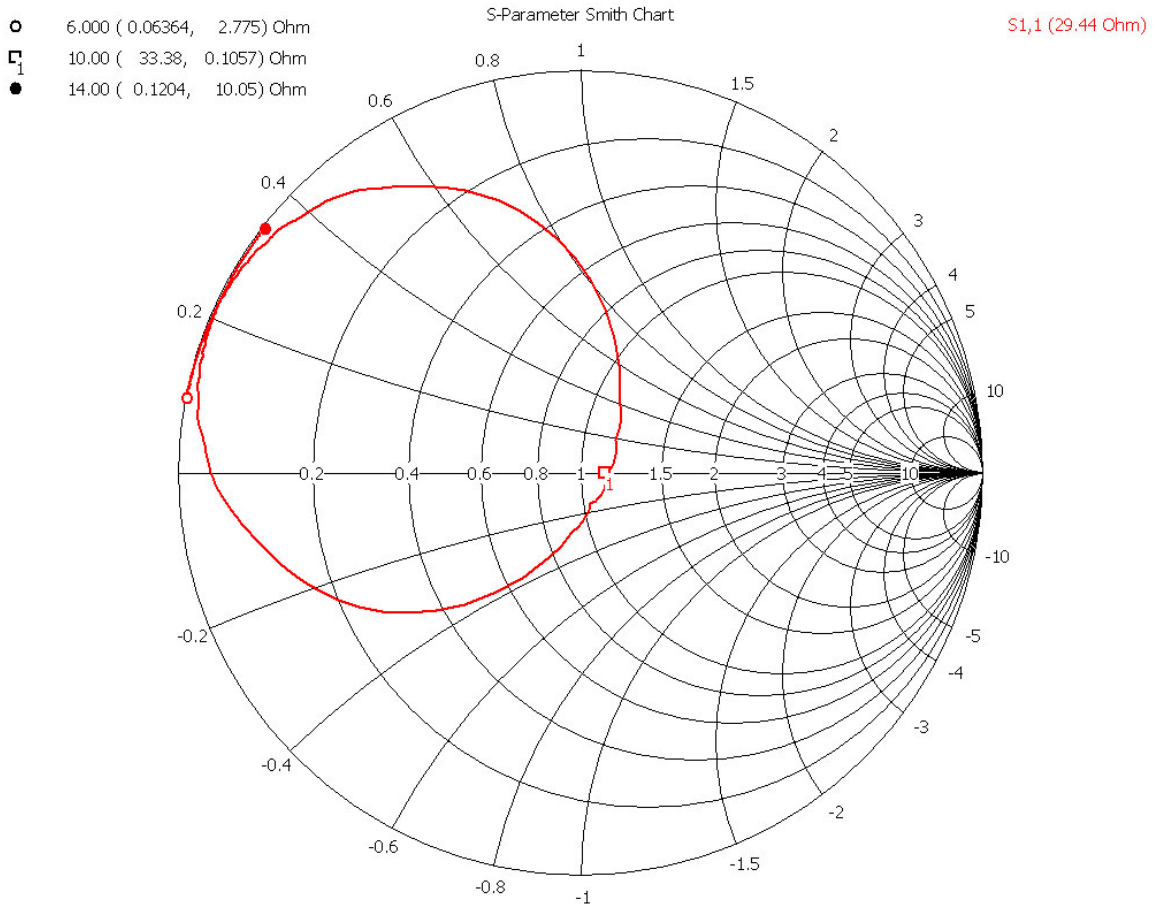

Figure 17. Smith Chart of the improved design

Lastly the far-field radiation pattern of the patch is shown in Figure 18. The radiation efficiency of the patch is 60% with a gain of 7.7 dB.

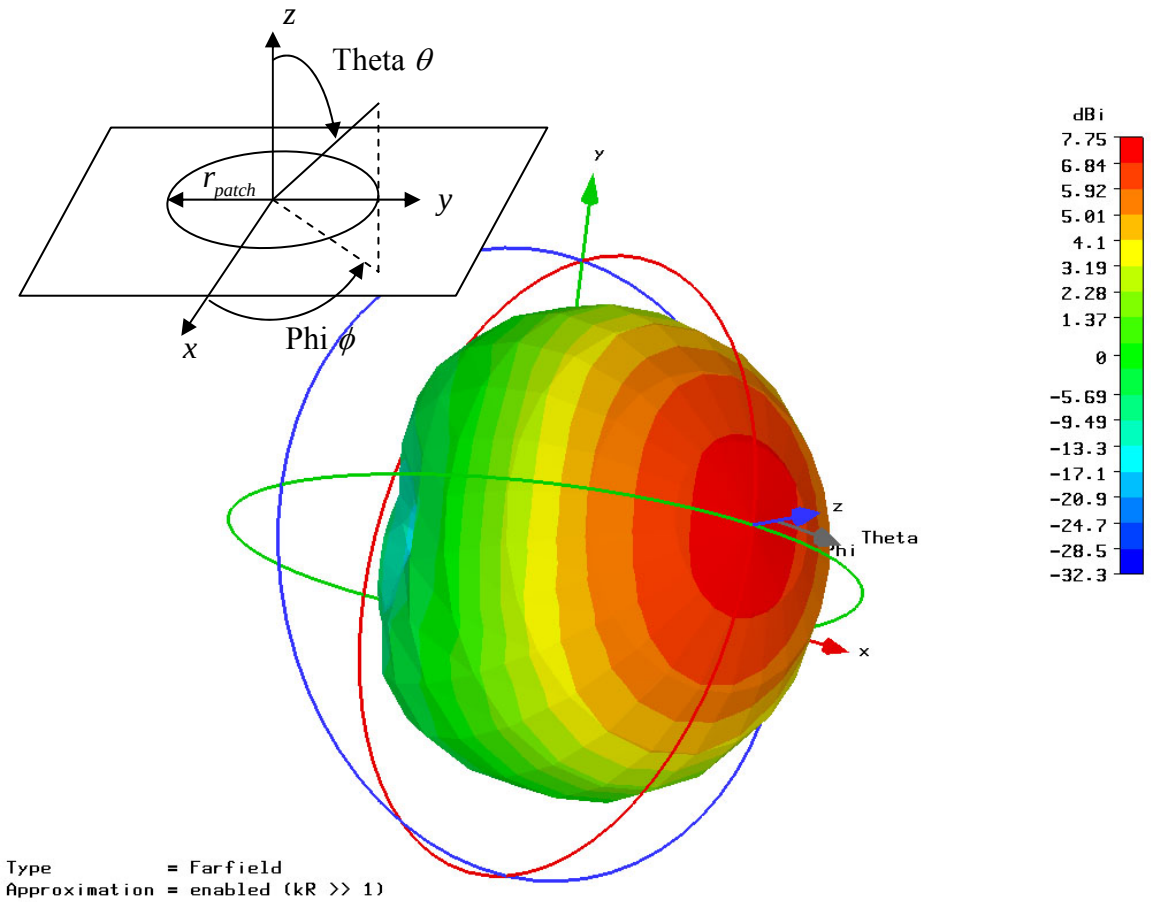

Figure 18. Radiation pattern of the improved circular patch design

3. Effect of Variance in Patch Radius and Probe Feed Location on S_{11}

Because of the small bandwidth of the antenna, 0.8% for -12 dB return loss, a study was done to determine the variance of the circular patch's S_{11} performance with a change in patch radius and probe feed location. In Table 3 data is shown for the patch radius varied from 4.79 to 4.89 mm while keeping the feed probe position constant. The data is plotted in Figure 19.

Patch Radius (mm)	S_{11} (dB)	Resonant Frequency (GHz)
4.79	-1.1	10.184
4.81	-1.3	10.144
4.83 (optimal)	-22	10.008
4.85	-11.4	9.976
4.87	-5	9.936
4.89	-2.48	9.904

Table 3. Variance of S_{11} and resonant frequency with patch radius

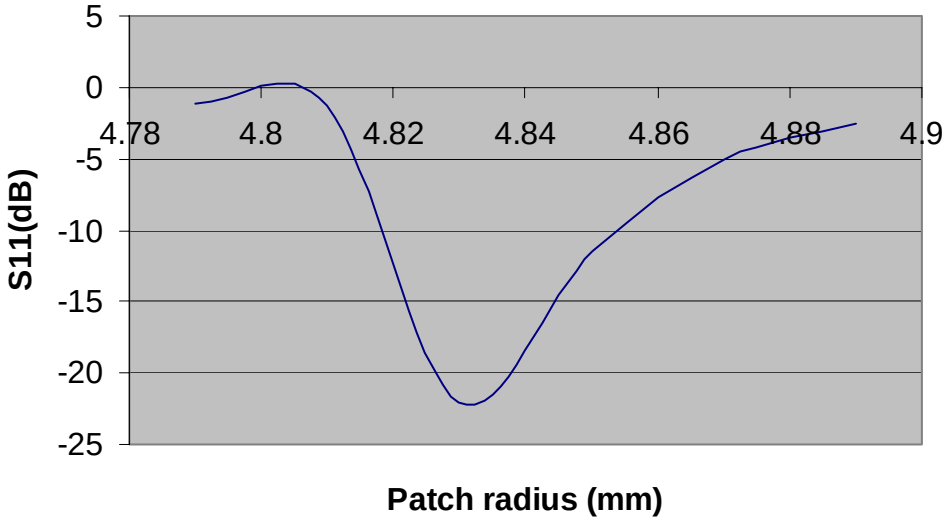

Figure 19. Variance of S_{11} with patch radius

From the Figure 19 it is noticed that only a ±0.015 mm tolerance in patch radius is allowed to achieve the target S_{11} value of -12 dB. This highlights the very tight manufacturing tolerances for the patch radius. Since the patch radius directly influences the resonant frequency, this problem would be alleviated if the patch could be designed with a wider bandwidth.

Next the probe feed is varied with an offset ranging from 0.86 mm to 1.18 mm, and the results for S_{11} and impedance are tabulated in Table 4.

Feed Position (mm)	**S_{11} (dB)**	**Impedance (Ω)**
0.86	-10	$21.74 + j15.89$
0.90	-13	$26.62 + j12.72$
0.94	-16	$29.91 + j9.395$
0.98	-20	$32.22 + j4.98$
1.02 (optimal)	-24	$33.38 + j0.1$
1.06	-20	$33.16 - j4.8$
1.10	-15	$31.72 - j9.28$
1.14	-13	$29.38 - j12.92$
1.18	-11	$26.59 - j15.62$

Table 4. Variance of S_{11} and impedance with probe feed location

A probe variance of approximately ± 0.15 mm can be tolerated to achieve a minimum S_{11} of -12 dB.

4. Findings

From the simulation results, it was determined that the original design presented in [19] was not tuned sufficiently to achieve the desired antenna performance. New values of patch radius and feed location were presented in order to achieve the required patch performance. In addition, a study on the effect of variances in patch radius and probe feed location on S_{11} was conducted. It was found that the patch was very susceptible to variances in patch radius and probe feed location, which points to the need for tight manufacturing tolerances.

A limiting factor was the circular patch's inherent characteristic of small bandwidth of approximately 0.8%. Any minute variance in patch radius shifts the resonant frequency, which results in the degradation of patch antenna performance.

Next, a study into determining a better patch design with better tolerance for manufacturing variances was performed.

C. WAYS OF IMPROVING BANDWIDTH AND DIFFERENT FEEDING METHODS

There are numerous ways to improve the bandwidth of a probe fed patch antenna, ranging from the use of wide-band impedance matching networks, edge couple patches, stacked patches and shaped probes. A good document summarizing the range of techniques to increase probe-fed patch antenna bandwidth is reference [22]. However, the simplest way is to increase the substrate height and use materials with a low dielectric constant, which aids in the radiation of rf energy. The relationship of between substrate height, ε_r, bandwidth and efficiency is given in Figure 20.

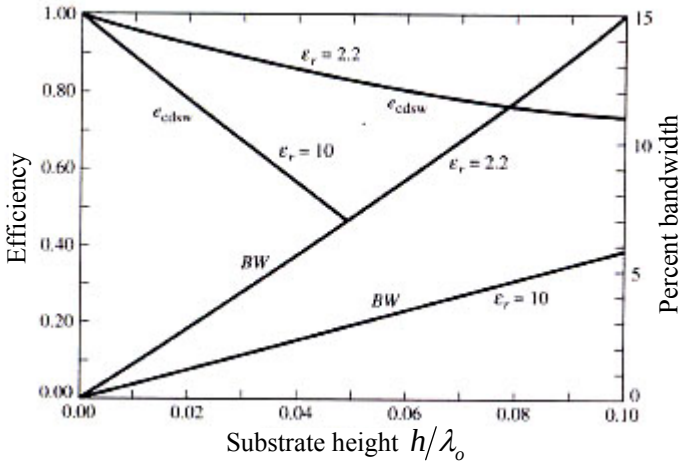

Figure 20. General relationship between ε_r, bandwidth, efficiency and substrate height (From [21])

The choice between increasing the substrate height versus other methods is mainly motivated by its simplicity. Although increasing the substrate height may increase the overall weight of each rectenna element, the removal of the balsa wood spacer between the antenna board and the rectifier circuit board that was presented in the original design of 2 mm, should counter this added weight.

In addition, different feed methods can be used that result in better manufacturing tolerances, especially the electromagnetic coupling feed method, which has been reported to attain large bandwidth [20]. To evaluate the tolerances related to different feed methods and large bandwidth patch designs, two other patch configurations were designed and simulated in MWS. The comparison of results from these two designs versus the improved patch antenna is discussed next.

D. COMPARISON OF DIFFERENT DESIGNS

Two other patch antennas were designed. One is a corner-fed electromagnetic coupled square patch antenna, and the second is a single dielectric layer insert feed rectangular patch. Simulations were performed on both patches to determine the feeding method's tolerance performance compared to the probe feed line. In addition, since both patches used relatively thick substrates, wider bandwidths were naturally expected. The details of both designs are described in the following sections,

1. Corner-fed Electromagnetic Square Coupled Patch

Details regarding the design of the corner-fed electromagnetic square patch can be found in [23]. The layout of the design is shown in Figure 21, where the resonant frequency is determined by the dimensions of the square patch, L, and the matching of impedance between line and patch is done by varying the distance D. The ratio of h_1/h is 0.2, in order to achieved the best possible VSWR performance for this patch. The width W of the feed line is calculated to match an impedance of 50 Ω. In order to minimize the weight of the patch, the superstrate of the feed line on the design in [23] was removed. The dimension *h* remained at 2 mm as in [23] and W was calculated. The values of *L* and *D* however were determined experimentally through simulations.

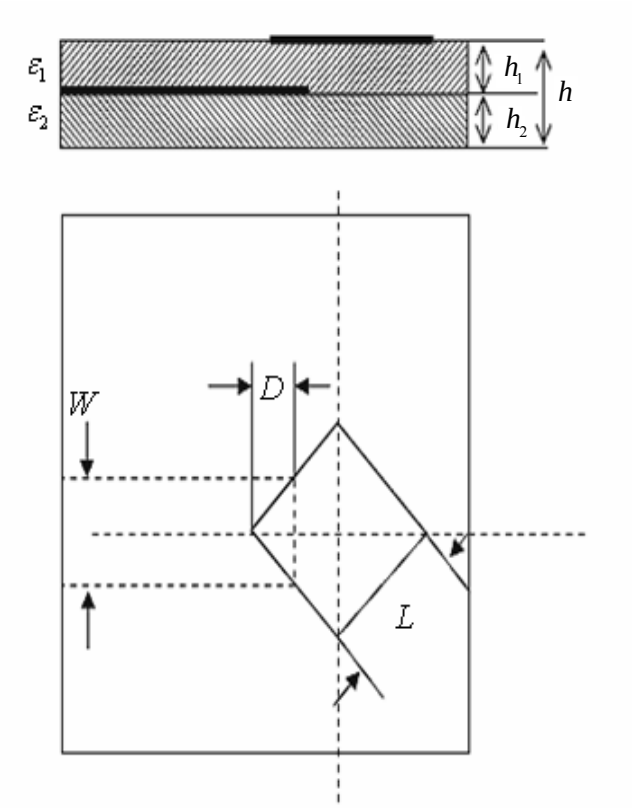

Figure 21. Layout of corner-fed square patch with electromagnetic coupled feed (From [23])

a. Calculation of W

The width of the microstrip feed line is determined from the following equations taken from [24]. They were used over the ones given by IPC-2141 [25], due to a comparison done in [26], where it was found that these equations have the best accuracy. The impedance is

$$Z_0 = \frac{377}{2.0\sqrt{2.0}\pi\left(\varepsilon_r + 1\right)^{1/2}} \ln\left[1 + \frac{4.0h}{w'}\left(A + B\right)^{1/2}\right] \tag{4.5}$$

where

$$A = \frac{14.0 + 8.0/\varepsilon_r}{11.0} \times \frac{4.0h}{w'}$$

$$B = \left(A^2 + \frac{1.0 + 1.0/\varepsilon_r}{2.0} \times \pi^{1/2}\right)^{1/2}$$

$$w' = w + \Delta w'$$

The parameter w' is the equivalent width of a track of zero thickness due to a track of rectangular profile, width w and thickness h. Reference [24] gives additional equations to determine the incremental value $\Delta w'$. A software program implementing these calculations can be found in [27].

With the total substrate height, h, of 2 mm and ratio, h_1/h, of 0.2, the height of the microstrip substrate, h_2, is 0.16 mm. For a copper track height of ½ oz thickness, i.e. 17 μm, the estimated width W was found to be 3.7 mm to achieve an impedance of 50 Ω.

b. Optimum Design Parameters and Feed Tolerance Performance

The optimum design parameters for the corner-fed electromagnetic coupled square patch were found through simulation and are tabulated in Table 5. The MWS model of the patch is shown in Figure 22.

Parameter	**Symbol**	**Unit**	**Value**
Relative dielectric constant	ε_r		3
Loss tangent	$\tan\delta$		0.0012 @ 10 GHz
Length	L	mm	6.6
Superstrate length	$L_{\text{superstrate}}$	mm	7.5
Feed width	W	mm	3.7
Top dielectric height	h_1	mm	0.4
Bottom dielectric height	h_2	mm	1.6
Total dielectric height	h	mm	2
Overlap distance	D	mm	0.797
Copper track height		μm	17

Table 5. Optimum parameters for corner-fed electromagnetic coupled square patch antenna

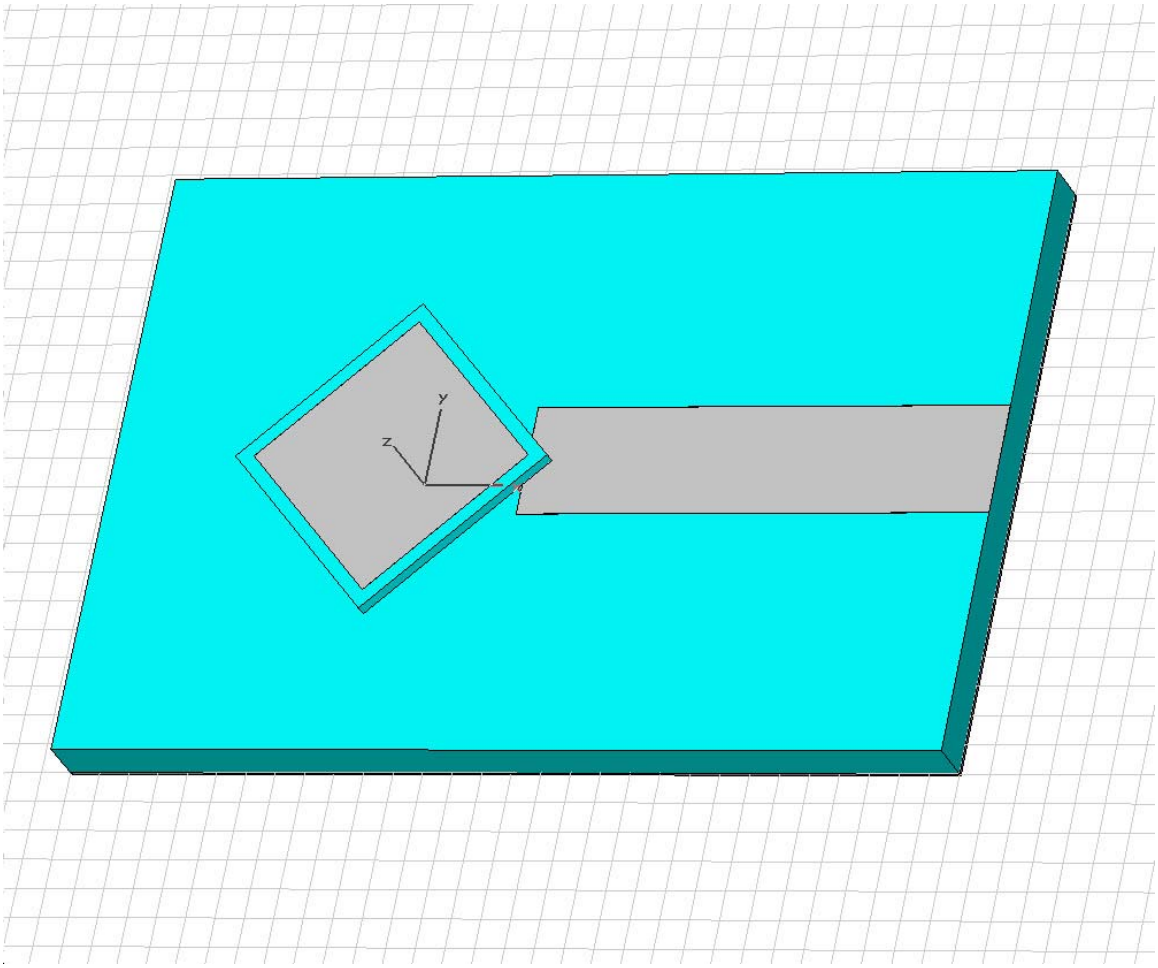

Figure 22. Layout of corner-fed electromagnetic square patch

The return loss of this patch was computed at -40 dB as shown in Figure 23. The bandwidth based on a return loss of -12 dB was 5%, which is a marked improvement over the 0.8% achieved by the improved circular patch.

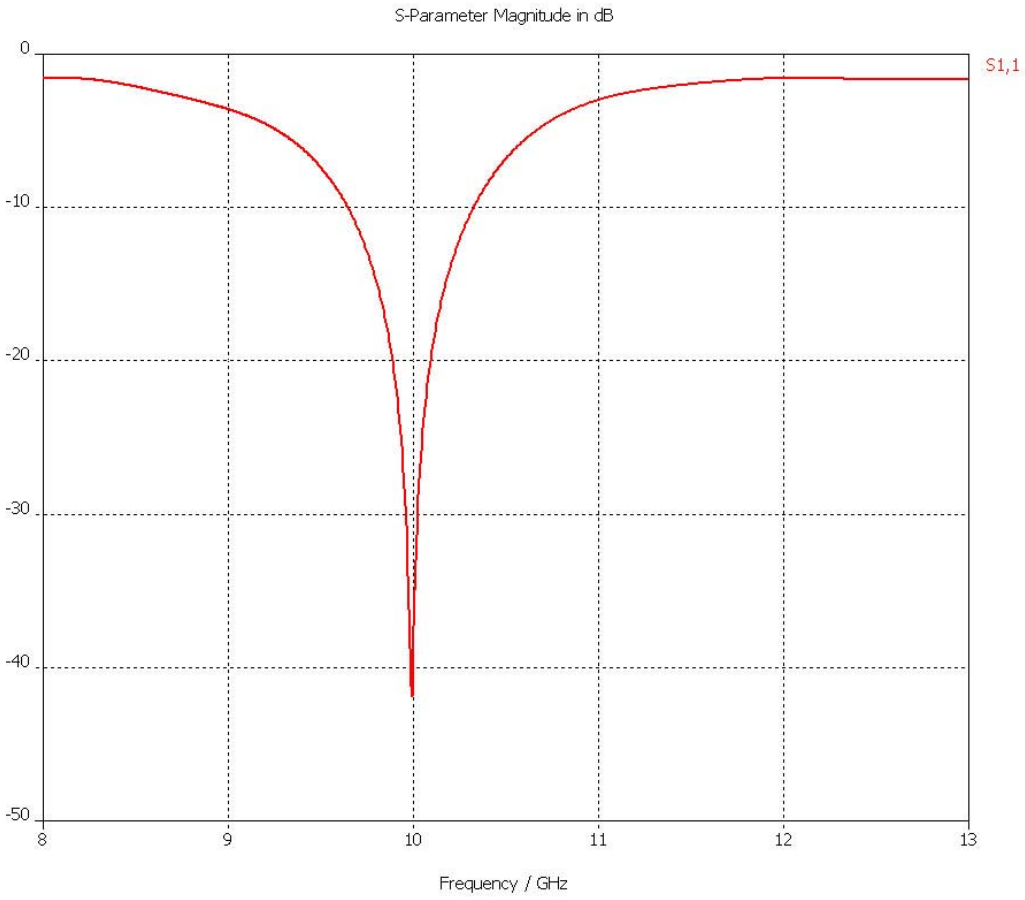

Figure 23. Return loss of the corner-fed electromagnetic square patch

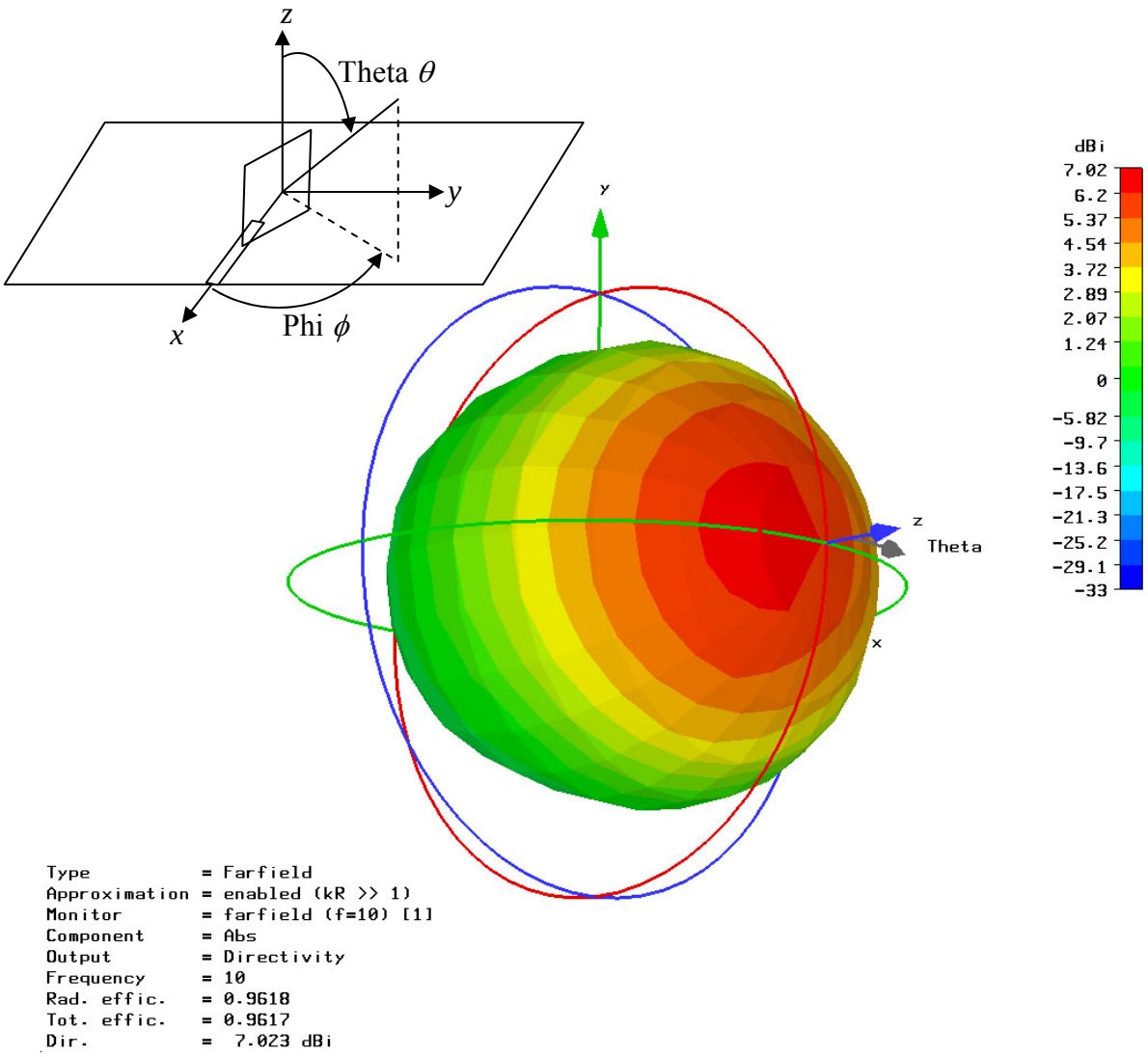

Figure 24. Far-field radiation pattern of corner-fed electromagnetic coupled square patch

The maximum radiation efficiency of the square patch was found to be 96% with a gain of 7 dB as seen in Figure 24. Since the top patch needs to be aligned with the microstrip feed line, the tolerance in variance of D was simulated and tabulated in Table 6.

D (mm)	S_{11} (dB)	Impedance (Ω)
0.557	-10.4	$68.11 + j33.88$
0.597	-14.3	$60.98 + j19.8$
0.637	-15.6	$59 + j16.84$
0.677	-16.5	$60.38 + j14.38$
0.717	-24.6	$52.91 + j6.02$
0.757	-30	$52.36 + j3.33$
0.797 (optimal)	-40	$51.44 + j1$
0.837	-35	$50.32 - j1.21$
0.877	-29.5	$51.28 - j3.36$
0.917	-26.5	$51.83 - j4.99$
0.957	-19.5	$56.86 - j10.31$
0.997	-19	$55.91 - j11.46$
1.037	-18.5	$54.66 - j12.49$
1.077	-16.3	$55.76 - j16.15$
1.117	-15.5	$53.82 - j17.74$

Table 6. Variance of S_{11} and impedance with change in D

Table 6 highlights that the feed has a tolerance range of 0.5 mm which is 166% more than the improved probe feed design. The possible increase of feed tolerance might be due to the increase in bandwidth and the use the electromagnetic coupling feed.

2. Rectangular Insert Feed Patch

Another possible design is a rectangular insert fed patch (see Figure 25) that uses a single substrate layer. Employing a substrate with $\varepsilon_r = 3$, to attain an equivalent

bandwidth of 5%, the dielectric height-to-wavelength ratio of 0.04 is required in Figure 20 and the substrate height of 1 mm was chosen.

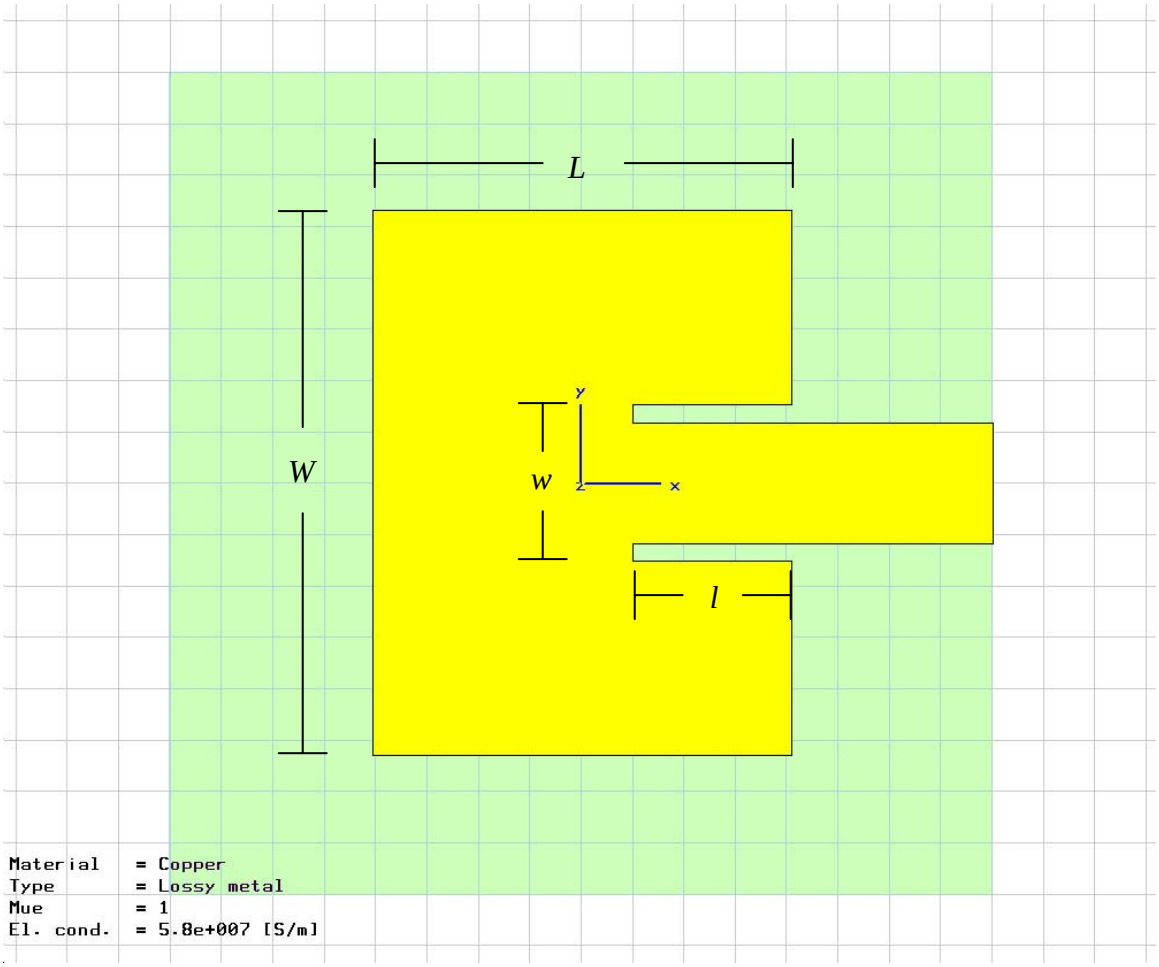

Figure 25. Layout and dimension of insert fed rectangular patch

The design steps of this patch can be found in [20, 21] and many other electromagnetic textbooks. The aim is to determine this patch's feed tolerances and its performance. The procedure for designing such a patch is summarized in the following section.

a. Determine Width of Patch, W

From [21], for an efficient radiator, a practical width that leads to good radiation efficiencies is given as

$$W = \frac{1}{2 f_r \sqrt{\mu_0 \varepsilon_0}} \sqrt{\frac{2}{\varepsilon_r + 1}} \tag{4.6}$$

Substituting f_r = 10 GHz and ε_r = 3, W equals to 10.6 mm.

b. Determine Effective Dielectric Constant of Patch

Because of the fringing electric fields that make the patch seem electrically longer, the effective dielectric constant is found using

$$\varepsilon_{reff} = \frac{\varepsilon_r + 1}{2} + \frac{\varepsilon_r - 1}{2}\left[1 + 12\frac{h}{W}\right]^{-1/2}, \qquad \text{for } W/h > 1 \tag{4.7}$$

where h is the height of the substrate. Subsequently ε_{reff} was calculated at 2.865.

c. Determine Extended Incremental Length of Patch, ΔL

Since the electrical length of the patch is of concern, the extended length ΔL must be calculated and subsequently used to find the physical patch length

$$\Delta L = 0.412h\frac{\left(\varepsilon_{reff} + 0.3\right)\left(\frac{W}{h} + 0.264\right)}{\left(\varepsilon_{reff} - 0.258\right)\left(\frac{W}{h} + 0.8\right)} \tag{4.8}$$

which gives ΔL of 0.483 mm.

d. Calculate Physical Length of Patch

The physical length of the patch is determined from

$$L = \frac{\lambda_0}{2\sqrt{\varepsilon_{reff}}} - 2\Delta L \tag{4.9}$$

The length of the patch was calculated to be 8.19 mm. Now that the patch dimensions have been determined, the insert length must be specified.

e. Determine Patch Conductance, G_1

The patch conductance, G_1, is found using the following equations,

$$G_1 = \frac{I_1}{120\pi^2} \tag{4.10}$$

where

$$I_1 = \int_0^{\pi} \left[\frac{\sin\left(\frac{k_0 W}{2} \cos\theta \right)}{\cos\theta} \right]^2 \sin^3\theta d\theta \qquad (4.11)$$

$$= -2 + \cos(X) + XS_i(X) + \frac{\sin(X)}{X}$$

and $X = k_0 W$. Subsequently G_1 was found as 0.0013 S.

f. Calculate Insert Length, l

Assuming that the mutual conductance between the radiating edges of the patch is small, and ignoring its contribution to the overall patch conductance, the insert length is

$$l = \frac{L \cos^{-1}\left(\sqrt{2 Z_0 G_1} \right)}{\pi} \qquad (4.12)$$

where Z_0 is the characteristic impedance of the feed line. The insert length was found to be 3.14 mm, with $Z_0 = 50\ \Omega$.

g. Effect of Width of Feed Inset, w

The width of the feed insert determines the capacitance of the feed. As such, it is selected so that it will cancel out any feed inductance to achieve a purely resistive impedance. No equation could be found that determines this width and therefore must be determined experimentally.

h. Optimum Patch Parameters and Feed Tolerance Performance

Based on the above calculations, the design was simulated in Microwave Studio and found to be optimized with the parameters in Table 7. The S_{11} performance of the insert-fed rectangular patch at 10 GHz is shown in the Figure 26.

Parameter	**Symbol**	**Unit**	**Value**
Relative dielectric constant	ε_r		3
Loss tangent	$\tan\delta$		0.0012 @ 10 GHz
Patch Length	L	mm	8.15
Patch width	W	mm	10.6
substrate height	h	mm	1
Insert length	l	mm	3.1
Insert width	w	mm	3.04
Feed width		mm	2.36
Copper track height		μm	17

Table 7. Optimum parameters for insert fed rectangular patch antenna

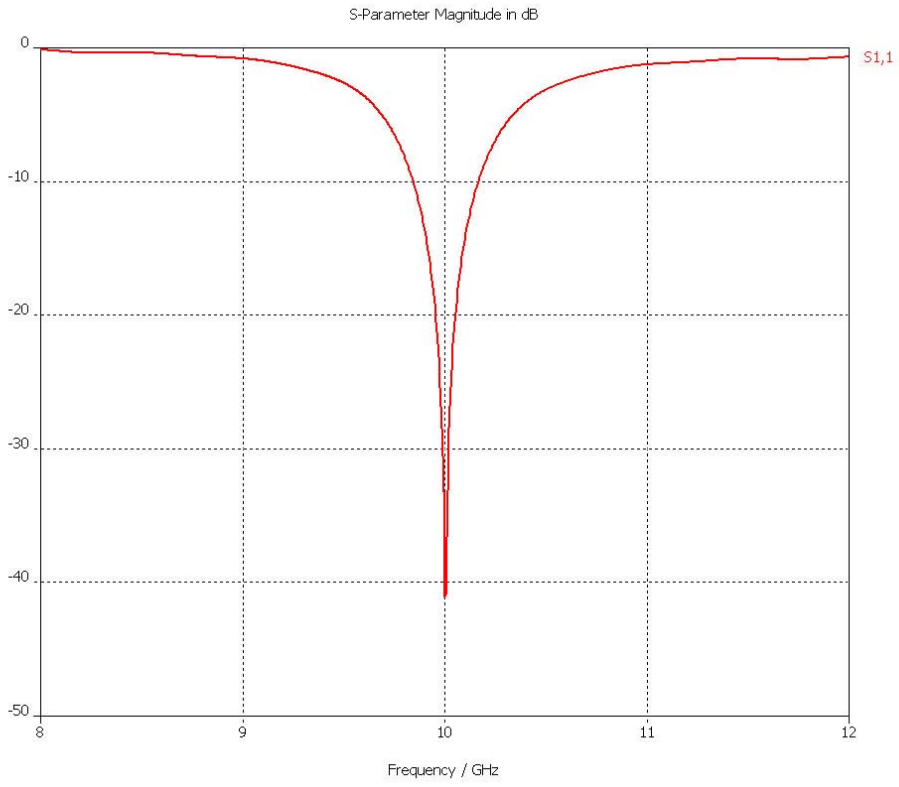

Figure 26. Return loss of the insert-fed rectangular patch

From Figure 26 it is seen that the maximum insertion loss is approximately −37 dB with a bandwidth of 2.4%. With a thickness of only 1 mm, which is half that used in the corner-fed electromagnetic coupled square patch, it demonstrates that the bandwidth is mainly affected by the height of the substrate.

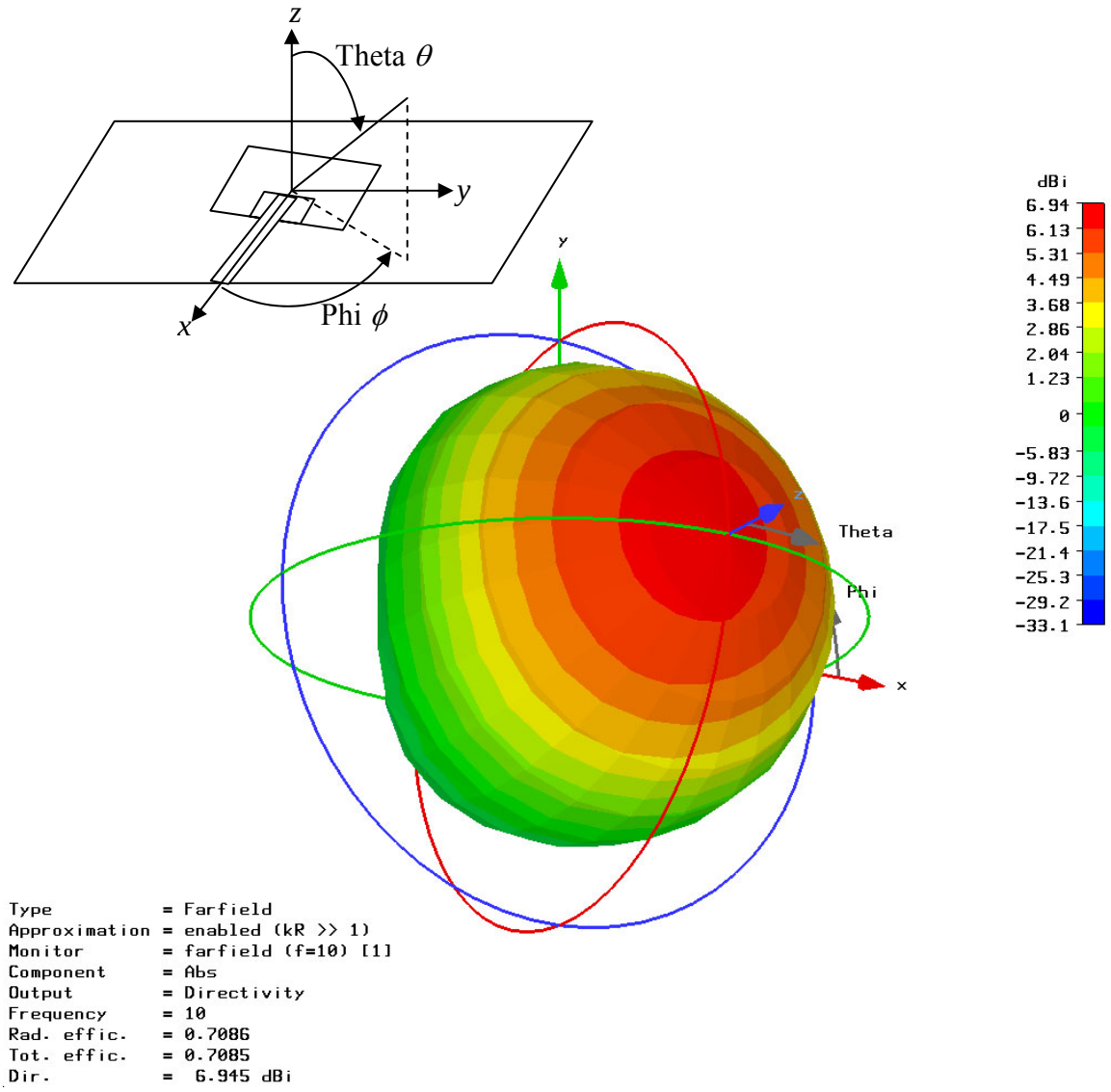

Figure 27. Far-field radiation pattern of insert feed rectangular patch

The radiation pattern is shown in Figure 27. The maximum radiation efficiency of the rectangle patch was found to be 70% with a gain of 6.945 dB. Although it is unlikely for single layer printed circuit elements to suffer from severe printing misalignments, the tolerance of such misalignment is summarized in Table 8. It was

determined that the feed has a tolerance of approximately 0.5 mm, similar to the corner-fed electromagnetic coupled square patch design.

Feed location along y axis (mm)	**S_{11} (dB)**	**Impedance (Ω)**
+0.24 mm	-11.8	$31.23 + j9.667$
+0.20 mm	-15	$37.17 + j8.531$
+0.16 mm	-19	$42.05 + j6.57$
+0.12 mm	-23.4	$45.63 + j4.39$
+0.08 mm	-28.5	$47.96 + j2.57$
+0.04 mm	-34	$49.21 + j1.27$
+0.00 mm (optimal)	-37	$49.56 + j0.84$
-0.04 mm	-34	$49.21 + j1.27$
-0.08 mm	-28.5	$47.92 + j2.5$
-0.12 mm	-23.4	$45.62 + j4.387$
-0.16 mm	-18.8	$42.05 + j6.567$
-0.20 mm	-15	$37.17 + j8.53$
-0.24 mm	-11.8	$31.23 + j9.665$

Table 8. Variance of S_{11} and impedance with feed misalignment

3. Design Comparison Conclusion

Both new patch designs that were analyzed and simulated exhibited wider bandwidths of 2.5 to 5%, which is 3 to 6.5 times larger than the improved circular patch design. The main contributing factor to the increase in bandwidth is the increase in substrate height. The use of a low dielectric constant aids in the efficiency of the patch. However with the increase in substrate thickness, the weight of each rectenna element

increases. There are available methods to reduce the overall weight. For example, removal of the balsa wood layer, or the removal of unnecessary dielectric material away from the radiating patch.

In addition both alternative patches exhibit better radiation efficiency compared to the original design, especially the corner-fed electromagnetic coupled patch. Lastly, with regard to tolerances in feed position, both patches were able to accept variances of approximately 0.5 mm.

E. FILTER IMPLEMENTATION AND PATCH ISOLATION WITH GROUND

As pointed out the Section C, a thick substrate with a low dielectric constant is desired to increase the overall performance of the patch antenna. The use of thick low dielectric substrates aids in the fringing of the E-fields, which is necessary for good antenna radiation.

However, this type of substrate is not ideal for the implementation of microstrip filters. This problem arises because of the overlapping fringing E-fields from the stubs, which affects the calculated electrical dimensions. It would be very difficult to design an efficient patch and filter on a common substrate because of the conflicting requirements.

Therefore, a method of using a ground plane to isolate the radiating element from the filter and other subsystems was desired. Since it is the height of the substrate that mainly determines the overall performance of the patch antenna and not the feeding method, the probe feed method should still be used in conjunction with the ground plate.

A modified circular patch utilizing thicker substrates is presented next, along with a solution which tackles the issue of probe reactance associated with the use thicker substrates.

F. CIRCULAR PATCH WITH THICK SUBSTRATE

A circular patch was designed for an impedance of 50 Ω using the same procedures outlined in Section A, but with a thicker substrate height of 0.75 mm. With the use of a thick substrate the probe inductance now contributes to the overall resonance of the patch. This inductance is estimated using the following equation from [21]

$$X_f \approx -\frac{\eta kh}{2\pi}\left[\ln\left(\frac{kd}{4}\right)+0.577\right] \tag{4.13}$$

where η is the intrinsic impedance of the dielectric, h is the substrate thickness, and d is the diameter of the probe feed. This inductance must be cancelled out in order to achieve optimal resonance. This is done by introducing some capacitance in the form of a small ring etched out of the patch antenna surrounding the probe. Figure 28 shows an example of the new circular patch. By varying the dimension of this ring, the probe inductance can be cancelled out.

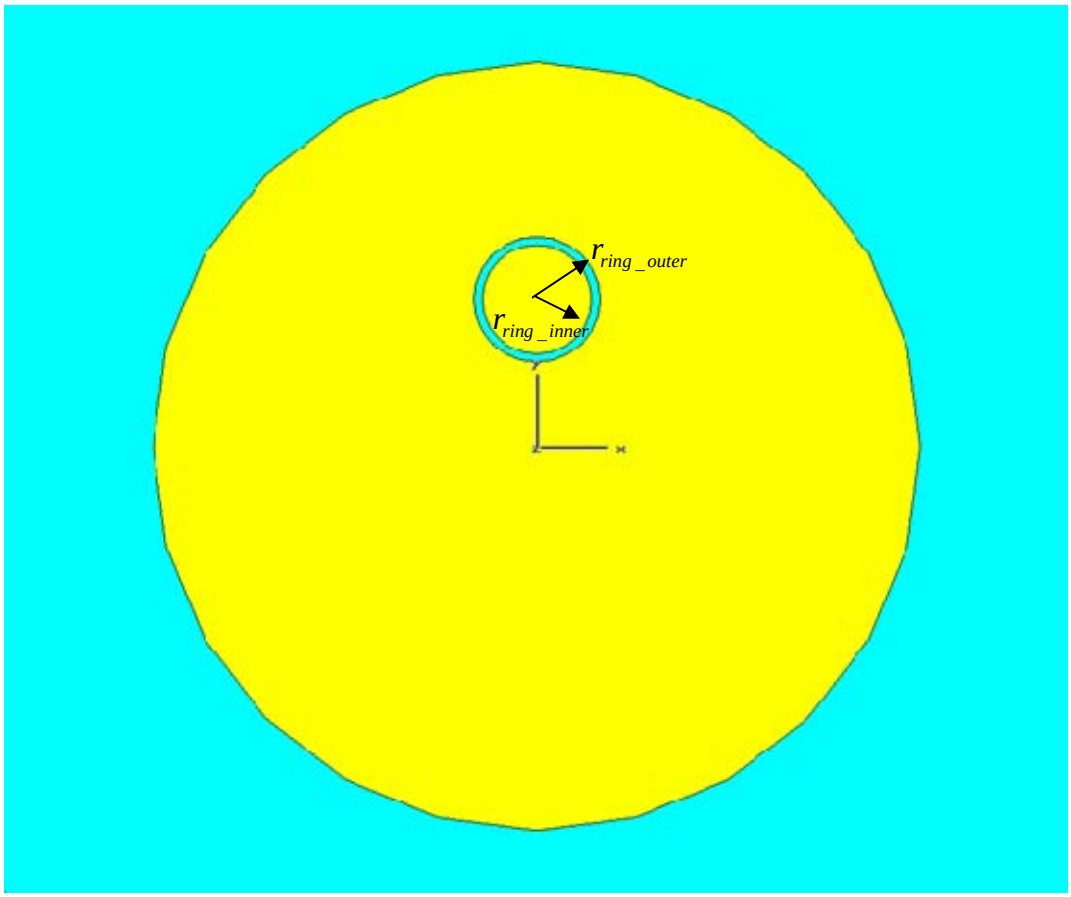

Figure 28. Layout of capacitive probe circular patch antenna

The relationship between the inner radius, r_{ring_inner}, and outer radius, r_{ring_outer}, controls the capacitance ($r_{ring\_outer} - r_{ring\_inner} \propto$ capacitance). The minimum value of r_{ring_inner} should at least be equal to the radius of the relief hole, in order to ensure that the impedance of the relief hole is not adversely affected by the probe capacitance. In order to attain the required patch resistance, the probe location is varied with respect to the center of the patch just like an ordinary circular antenna. The new patch dimensions are given in Table 9 and its performance is presented in Figure 29 through 31.

Parameter	**Symbol**	**Unit**	**Value**
Relative dielectric constant	ε_r		3
Loss tangent	$\tan\delta$		0.0012 @ 10 GHz
substrate height	h	mm	0.75
Patch radius	r	mm	4.57
Ring inner radius	r_{ring_inner}	mm	0.65
Ring outer radius	r_{ring_outer}		0.75
Probe offset	x	mm	1.75
Probe radius	r_{probe}	mm	0.125
Relief hole radius	r_{relief}	mm	0.55
Copper track height		μm	17

Table 9. Optimum parameters of capacitive probe circular patch antenna

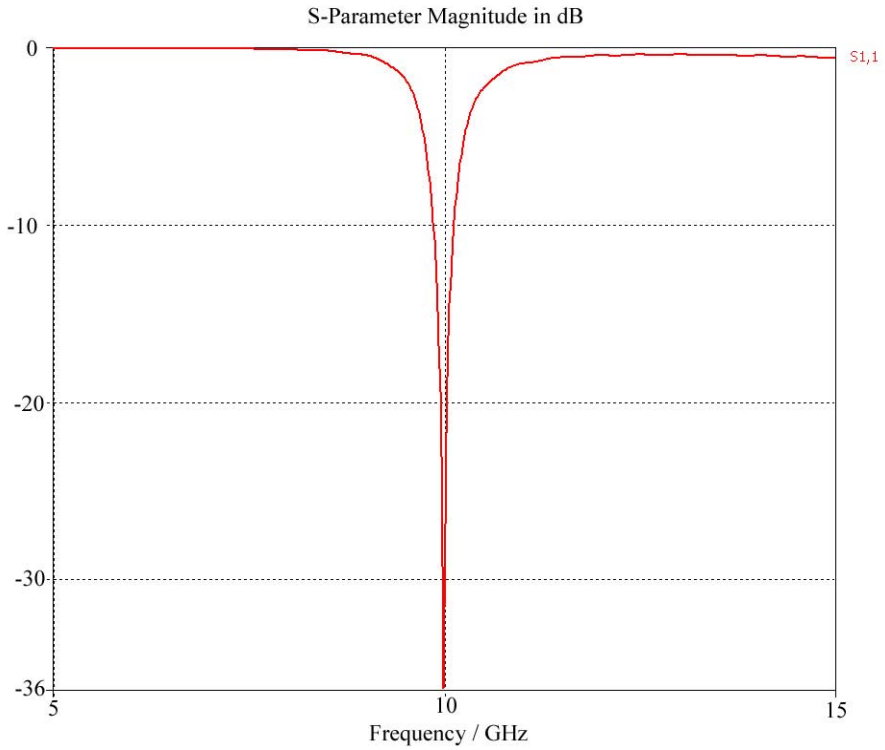

Figure 29. Return loss of capacitive probe fed circular patch antenna

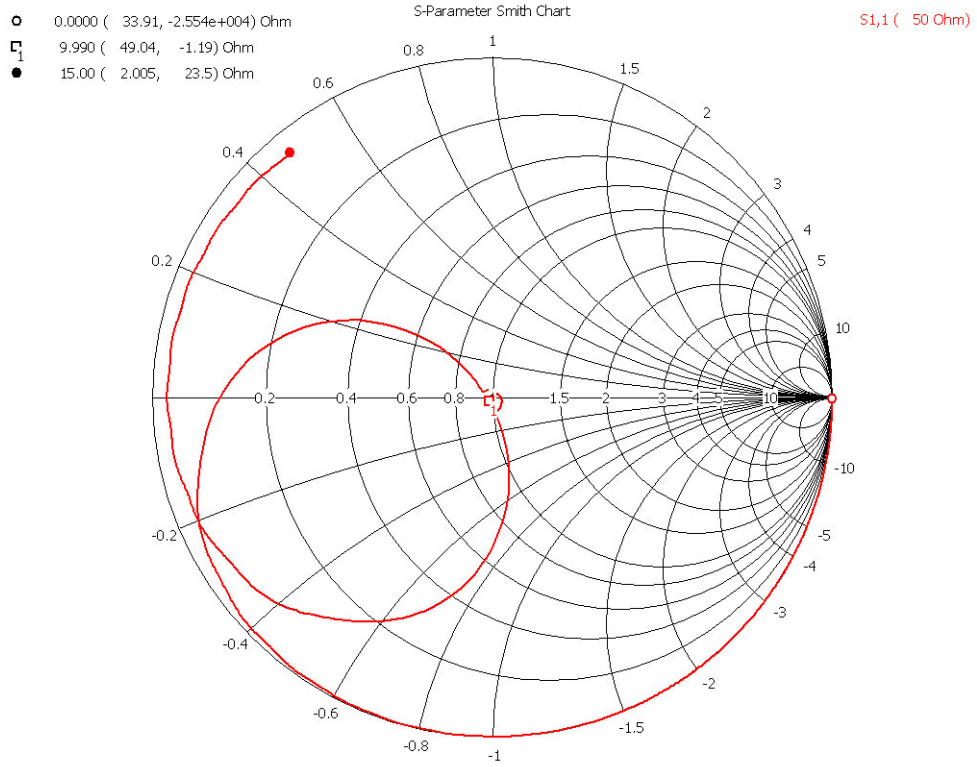

Figure 30. Smith chart plot of impedance for the capacitive probe fed circular patch antenna

The new probe design has an impedance of $49 + j1.2\ \Omega$ at 10 GHz and its return loss is -30 dB. The bandwidth at -12 dB is 2%, slightly lower than that of the rectangular patch, which has a 0.75 mm thick substrate. The radiation efficiency of the new patch is at 95%, with a gain of 7.61 dB. The efficiency of this patch is almost as good as the corner-fed electromagnetic coupled square patch, and has 0.61 dB higher gain.

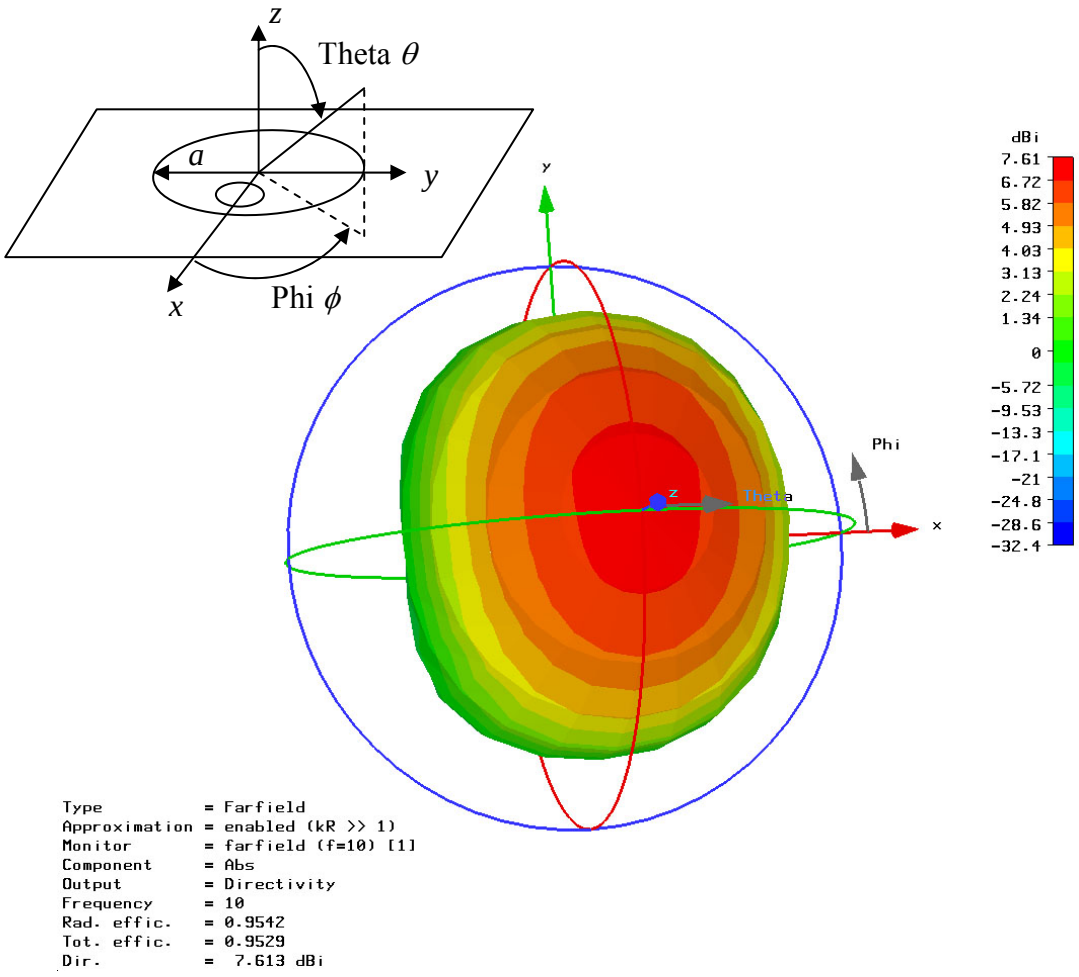

Figure 31. Far-field radiation pattern of capacitive probe fed circular patch antenna

Since there will be variances in the probe feed location as well as radius, the patch's tolerances to changes in probe feed location and patch radius were computed and are shown in Tables 10 and 11.

Patch Radius (mm)	**S_{11} (dB)**
4.50	-10.7
4.53	-16
4.55	-24.5
4.57 (optimal)	-30
4.59	-18
4.61	-13
4.63	-9.8

Table 10. Change in return loss with patch radius

With the circular patch fed with the capacitive probe, the antenna exhibits a higher patch radius tolerance of ±0.05 mm relative to the standard circular patch antenna of ±0.015 mm. This is a direct result of the increased bandwidth (wider notch) that allows for more shifts in the resonant frequency.

Feed location from centre (mm)	**S_{11} (dB)**	**Impedance (Ω)**
2.05	-12.8	64.4 - *j*19.33
1.95	-16.5	62.03 - *j*8.45
1.87	-20	55.98 - *j*5.93
1.79	-27	51.95 - *j*1.54
1.75 (optimal)	-30	49.04 - *j*1.2
1.71	-28	46.85 - *j*0.83
1.63	-19	40.12 - *j*3
1.55	-15.3	35.15 - *j*2.884
1.55	-11.3	28.5 - *j*5.44

Table 11. Change in return loss with probe feed location

The tolerance to probe feed variance is similar to that of the corner-fed electromagnetic coupled square patch and the insert-fed rectangular patch, being able to obtain a return loss of -12 dB with a ± 0.3 mm variance in probe location. This means that the probe feed method has similar, if not slightly better, performance over the electromagnetic coupled and direct feed method.

Based on the new patch design, the inductance associated with the probe feed for thick substrates can be eliminated. With the use of thicker substrates, larger bandwidths can be achieved, resulting in better radiation efficiency and wider tolerances to changes in patch radius and probe feed location.

It is a good practice however to minimize the length of the probe and it is highly likely that the original patch suffered more from probe reactance due to the extension of the probe through the balsa wood center (See Figure 12).

G. CONCULSION

In order to determine the possibility of employing other feeding methods and patches that exhibit better tolerances to manufacturing variances, a study was done on two alternative patch designs. It was concluded that increasing the substrate thickness contributed most to the increase in bandwidth, radiation efficiency and robustness to manufacturing errors, rather than the use of different feeding methods and patch antenna configurations.

The use of thick low dielectric substrates is favorable for efficient radiation of antennas. However, they are not favorable for microstrip filter applications. As such the need for the isolating ground plane was confirmed.

A new circular patch antenna employing a thicker substrate was simulated, and the effect of the probe inductance was negated by etching a ring off the patch around the probe. The performance of the capacitive probe feed circular patch antenna was superior to the initial design, having a larger bandwidth of 2%, higher tolerances to manufacturing errors, and better radiation efficiency.

THIS PAGE INTENTIONALLY LEFT BLANK

V. SCHOTTKY DIODE PERFORMANCE

The essence of a rectenna is the rectification performed by the diode. Therefore it is critical to understand the operation and performance of the diode, taking all things into consideration, in order to achieve maximum operational efficiency of the rectenna. The diode used in the rectification of rf energy for the rectenna is a Schottky diode. The Schottky diode is used mainly because of its low turn on voltage and low junction capacitance characteristics, which enables it to work at the high frequencies required.

A. DIODE CHARACTERISTICS

All diodes are related to the Shockley equation, where the current and voltage through the diode is defined as

$$I = I_s \left(e^{\frac{q(V - IR_S)}{nk_bT}} - 1 \right) \tag{5.1}$$

where k_b is Boltzmann's constant, q is electron charge (C), T is the diode temperature ($^\circ K$), I_S is the saturation current, R_S is the series resistance and n is the ideality factor. The values of these diode parameters can be found in the manufacturer's specification sheets. The temperature dependent *I-V* curve of a typical Schottky diode is shown in Figure 32.

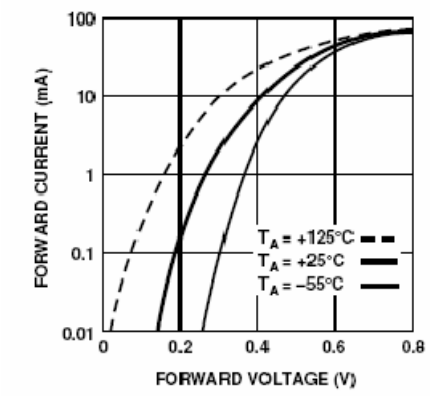

Figure 32. Typical forward current from forward voltage at three temperatures (From [28])

There are two linear equivalent models of a diode (Figure 33) which consist of the series resistance, R_S and the current dependent junction resistance and capacitance, R_j and C_j of the diode. The lead and bond wire inductance and package capacitance associated with the diode's packaging are represented as L_L, L_B and C_P respectively. Generally at operating frequencies above 6 GHz the bond wire inductance should be taken into consideration.

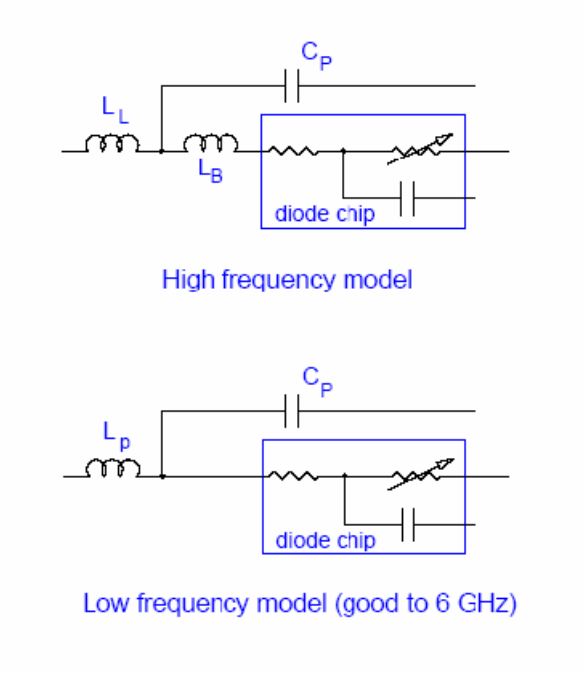

Figure 33. Linear Equivalent circuit model of a diode

B. PREVIOUS WORK DONE AND ITS LIMITATIONS

In [19], the Schottky diode used was the Agilent HSMS-8101. It was selected because it was designed to work around 10 GHz and had characteristics that suited rectenna operations. The electrical characteristics of the diode are reiterated in Table 12.

In [19] the output dc voltage to input rf power calculations were carried out according to references [29, 30] without the need to determine the current dependent junction resistance R_j. However the Ritz-Galerkin technique was used, and it tends to overestimate the output voltages at the higher end of the power scale. This is because the technique assumes that the no energy is lost in the generation of harmonics. The

generation of harmonics is usually not critical in the low power region, but since the diode in a rectenna is driven at much higher power levels, the harmonic contribution is significant and thus leads to wrong results.

A Matlab program (Appendix A) was created which employs the Ritz-Galerkin technique and modeling with the HSMS-8101 diode specifications, the $P_{out(dc)}$ versus $P_{in(rf)}$ graph is plotted in Figure 34.

Electrical characteristics of the HSMS-8101 Schottky diode			
Symbol	**Parameter**	**Unit**	**Value**
P_T	Total Power Dissipation	mW	75
T_J	Junction Temperature	°C	+150
T_{OP}	Operating Temperature	°C	-65, +150
V_{BR} (I_R=10 uA)	Breakdown Voltage	V	4 (min)
C_T V_R=0 V, f=1 MHz	Total Capacitance	pF	0.26
I_S	Saturation Current	A	4.6×10^{-8}
n	Ideality Factor		1.09
R_S	Parasitic Series Resistance	Ω	6
C_J	Zero-bias junction capacitance	pF	0.18

Table 12. HSMS-8101 electrical characteristics (From [28])

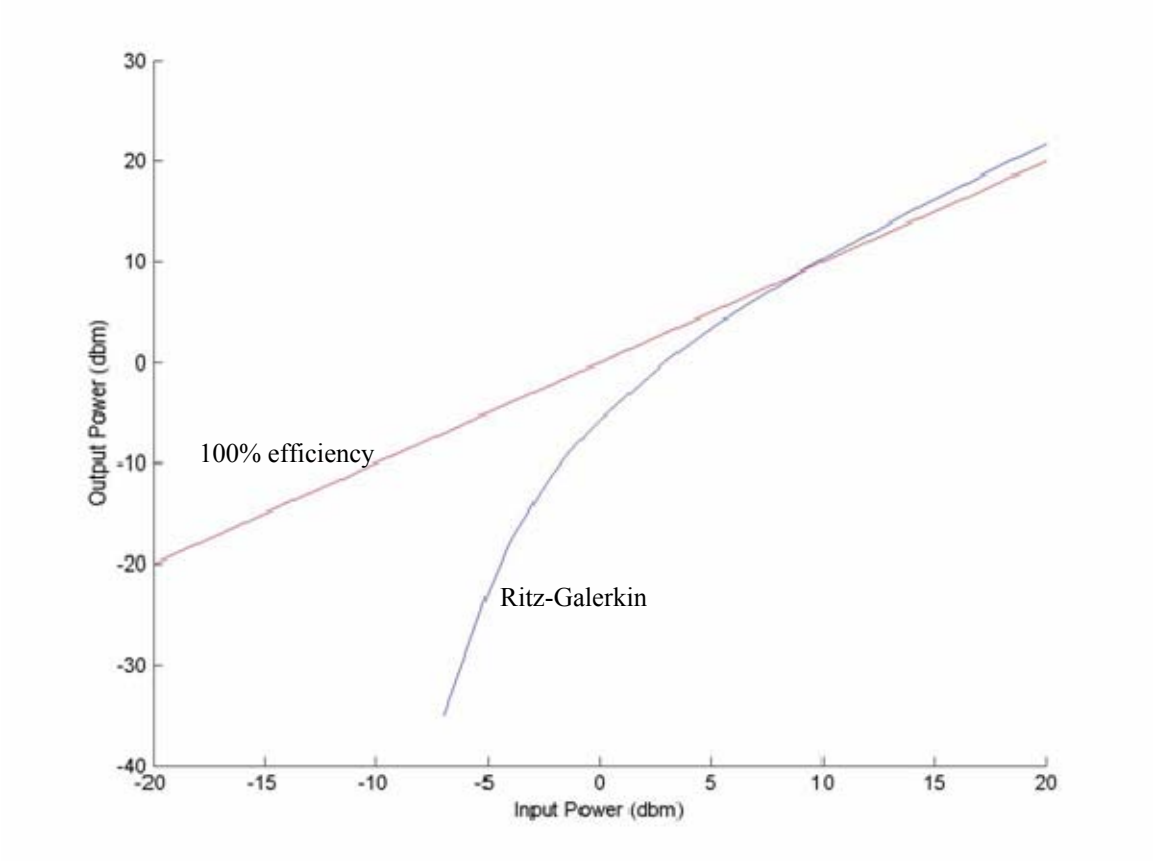

Figure 34. Output dc power vs input rf power of a diode using the Ritz-Galerkin technique

The lines in Figure 34 compare the results employing the Ritz-Galerkin technique and the response of a diode with 100% conversion efficiency. For input rf power above 9 dBm, the Ritz-Galerkin technique returns results that are not valid; the output dc power is more than the input rf power. Since the diode in the rectenna is operating at powers above 20 dBm, there is a need to use another method to determine the diode's conversion performance.

C. CALCULATING DIODE EFFICIENCY AND IMPEDANCE

Two papers [31, 32] from McSpadden and Yoo gives good analytical detail on the performance of the diode used in a rectenna system. In the paper, the derivation of a closed form equation for the conversion efficiency of the diode and its operating

impedance is given. Although the paper uses the linear unpackaged model of the diode, and assumes a constant series resistance, R_S , the model yields theoretical results that were relatively close to measured ones.

The equivalent circuit model of the rectifying circuit used in the derivation of the closed form equation consists of the diode's series resistance, junction resistance and capacitance, and lastly the load resistance. The diode in this configuration is placed in reverse bias with respect to the feed line and the ground plane as shown in Figure 35.

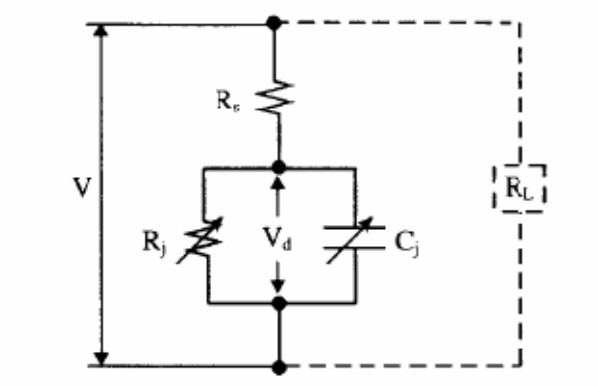

Figure 35. Equivalent circuit model of diode and load resistor (From [32])

As the oscillating rf signal creates voltages across the diode, the diode will create voltage waveforms in the form of Figure 36.

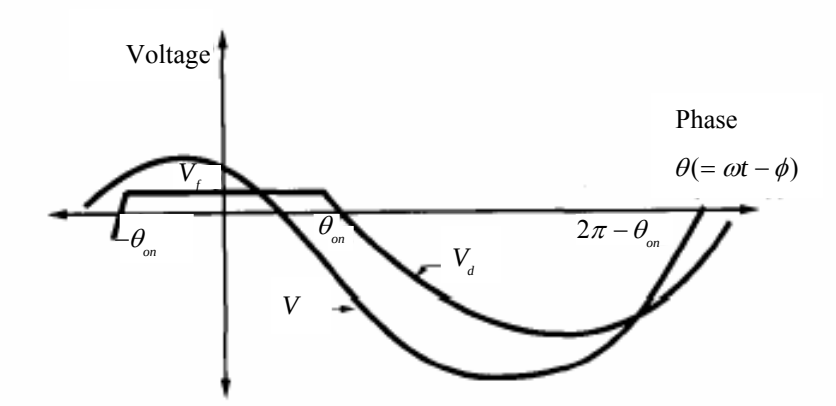

Figure 36. Time domain signal across diode (After [32])

The power conversion efficiency of the diode is dependent on the operating rf input power. Because there is a finite forward voltage for the diode, the efficiency is

small in low power because the voltage swing across the diode in forward bias is small compared to the forward voltage required to turn on the diode. As such, choosing a diode with low turn on voltage characteristics is favorable for our application. The general relationship between diode conversion efficiency, reverse breakdown voltage and load resistance is shown in Figure 37.

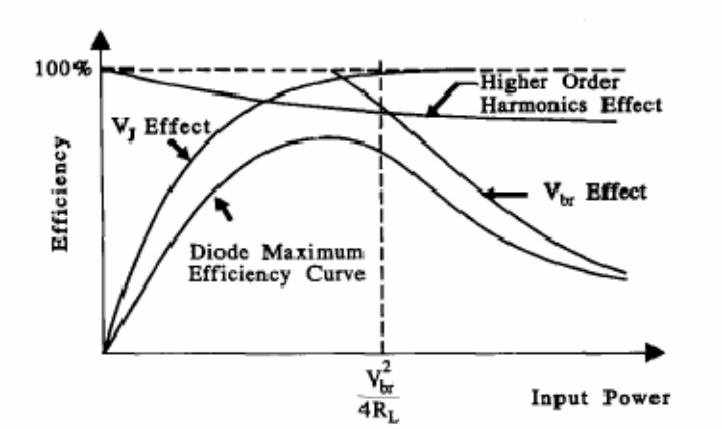

Figure 37. General relationship between rf-to-dc power conversion efficiency and input power (From [32])

Therefore employing the same diode from the original design, HSMS-8101, with the motor's load resistance of 50 Ω and an estimated V_{br} of 7 V, the maximum output power is estimated to be 245 mW. With the known diode parameters from the manufacturer's specification sheets, the following steps from [31] can be taken to determine the efficiency of the diode.

1. Determine Output Power and Output Voltage

First the output voltage is determined as a function of the diode reverse bias breakdown voltage. Then, based on the load resistance, P_{OUT} is determined

$$V_O = V_{BR} / 2 \tag{5.2}$$

$$P_{OUT} = \frac{V_O^2}{R_L} \tag{5.3}$$

In [31], the factor of 2.2 is recommended over 2 in Equation (5.2), to prevent the situation of overdriving the diode in reverse bias, which could lead to its failure. However for this study the ideal case will be analyzed.

2. Determine Forward Bias Turn-on Angles

With V_O found in Equation (5.2), the forward bias voltage, V_f, is determined

$$V_f = n\left(25.852\times10^{-3}\right)\ln\left(\frac{I}{I_s}+1\right) \tag{5.4}$$

where n is the ideality factor and $I = \frac{V_O}{R_L}$. Followed by the forward bias turn on angle, θ_{on}

$$\tan\theta_{on} - \theta_{on} = \frac{\pi R_S}{R_L\left(1+\frac{V_f}{V_O}\right)} \tag{5.5}$$

3. Determine Diode Efficiency

The diode rf-to-dc conversion efficiency is then expressed as

$$\eta_d = \frac{1}{1+A+B+C} \tag{5.6}$$

where

$$A = \frac{R_L}{\pi R_S}\left(1+\frac{V_f}{V_O}\right)^2\left[\theta_{on}\left(1+\frac{1}{2\cos^2\theta_{on}}\right)-\frac{3}{2}\tan\theta_{on}\right]$$

$$B = \frac{R_S R_L C_j^2 w^2}{2\pi}\left(1+\frac{V_f}{V_O}\right)\left(\frac{\pi-\theta_{on}}{\cos^2\theta_{on}}+\tan\theta_{on}\right)$$

$$C = \frac{R_L}{\pi R_S}\left(1+\frac{V_f}{V_O}\right)\frac{V_f}{V_O}\left(\tan\theta_{on}-\theta_{on}\right)$$

ω is the angular frequency ($2\pi f$) and the junction capacitance, C_j is defined as

$$C_j = C_{jo}\sqrt{\frac{V_f}{V_f+|V_O|}} \tag{5.7}$$

where C_{jo} is the diode's zero bias junction capacitance. With the known load (motor) resistance of 50 Ω, a plot of diode efficiency to V_O is depicted in Figure 38. The

relationship between diode maximum efficiency and power is clearly demonstrated. At higher power levels, the highest obtainable efficiency is approximately 60%.

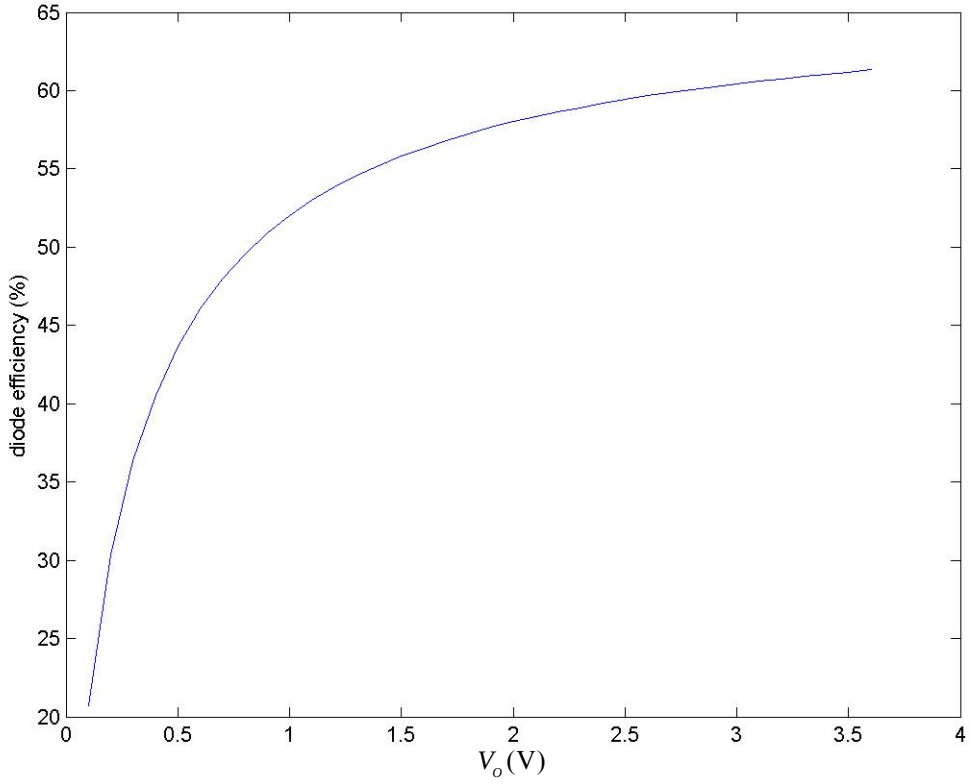

Figure 38. Diode efficiency versus output voltage for load of 50 Ω

4. Calculate Impedance of Diode

The input impedance of the diode is expressed as follows:

$$Z_{diode} = \frac{\pi R_S}{\cos\theta_{on}\left(\frac{\theta_{on}}{\theta_{on}} - \sin\theta_{on}\right) + j\omega R_S C_j\left(\frac{\pi - \theta_{on}}{\cos\theta_{on}} + \sin\theta_{on}\right)} \tag{5.8}$$

The impedance of the same diode for the same range of V_O was calculated and is shown in the Figure 39.

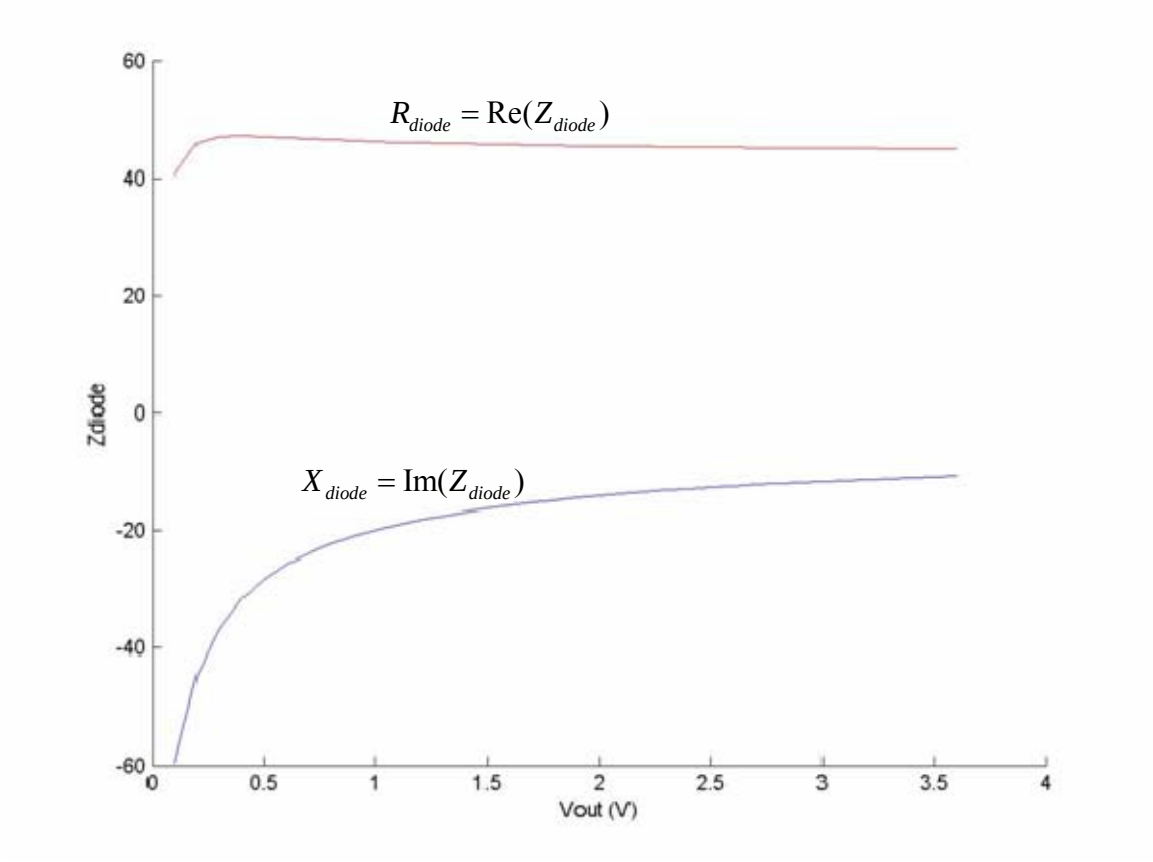

Figure 39. Resistance and reactance of the diode as a function of V_O

It can be seen that at higher power levels, the impedance of the diode remains fairly constant, which is desirable for our rectenna design. This means that any matching networks should work reasonably well for slight differences in power variations. The diode impedance at its maximum operating power level is $45.5 - j13.9\ \Omega$.

Appendix B contains a Matlab program that was used in the calculation of the diode rf-to-dc conversion efficiency and its impedance with respect to the operating power level.

D. IMPROVING DIODE EFFICIENCY AND ITS EFFECTS ON RECTENNA PERFORMANCE

The maximum diode efficiency is presently limited to around 60%, however, it has been reported that this can be increased by varying the load resistance. The effect of

changing the load resistance on diode efficiency and its implications on rectenna design will now be discussed.

Since it is known that the diode efficiency is proportional to the operating power level, it is presumed that the diode is operating at the maximum output power level. Then employing Equations (5.2) to (5.8) for a range of R_L from 10 Ω to 10 kΩ, the plot of diode efficiency is shown in Figure 40. Appendix C contains the codes to the Matlab program that calculates the maximum diode efficiency versus load resistance.

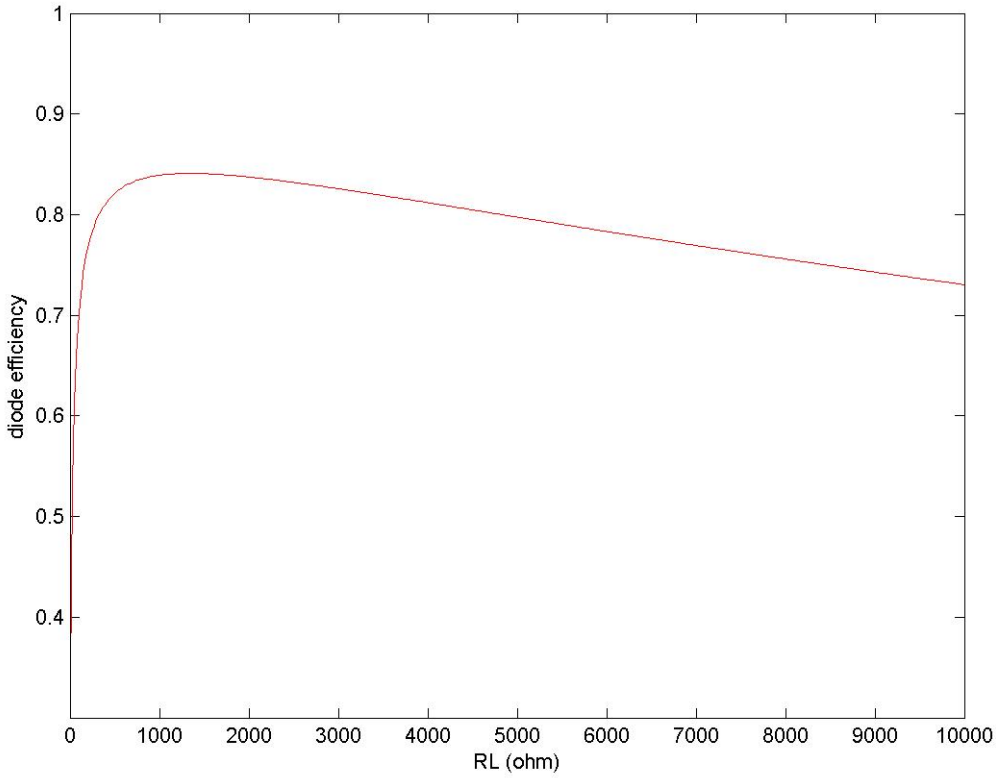

Figure 40. Diode efficiency versus load resistance

Figure 40 depicts that a maximum diode efficiency of 84% is obtainable when a load resistance of around 1.4 kΩ is used. However, because the maximum output power of a rectenna element is inversely proportional to the load resistance, the diode's maximum power handling capacity is reduced. This results in a need for more diode elements to achieve the operating power requirements of the MAV. Figure 41 shows the number of required diodes needed to achieve 1.2 W with respect to load resistance.

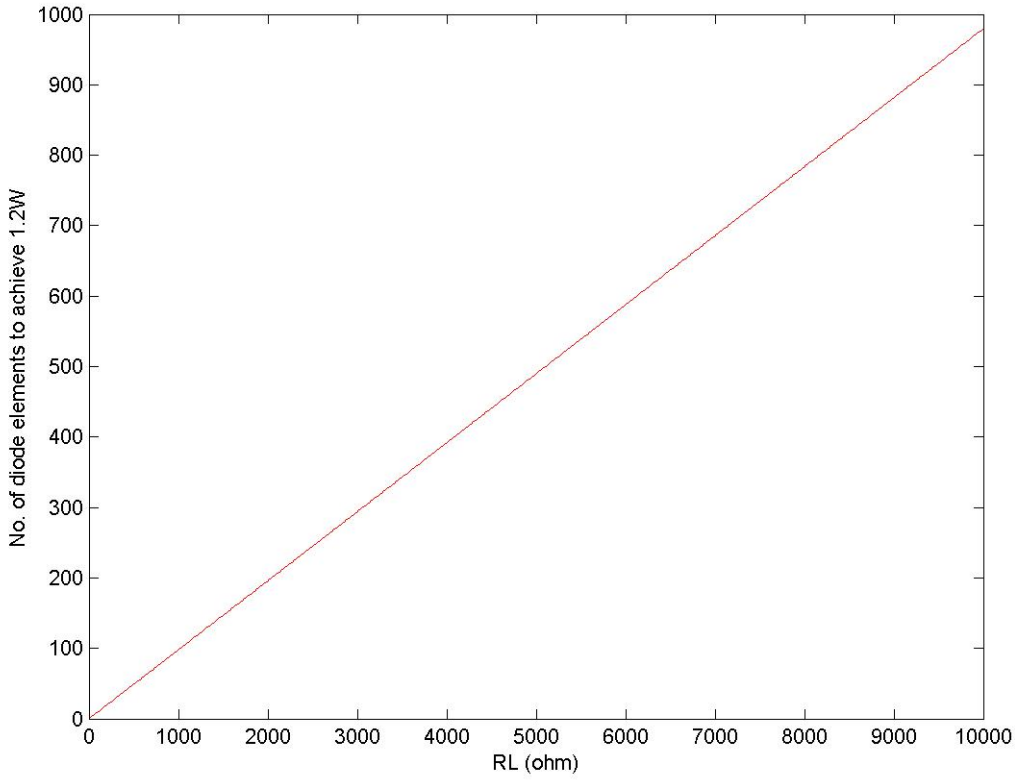

Figure 41. Number of diodes required to achieve 1.2 W versus load resistance

As seen in Figure 41, the number of diodes increases linearly with the increase in load resistance. Therefore, in order to achieve maximum diode efficiency with a load resistance of 1.4 kΩ, 137 diodes must be used, which is not possible given the weight and size constraints of its application.

In addition, Figure 42 shows the variance of the diode impedance with a load resistance of 1.4 kΩ with respect to operating power levels.

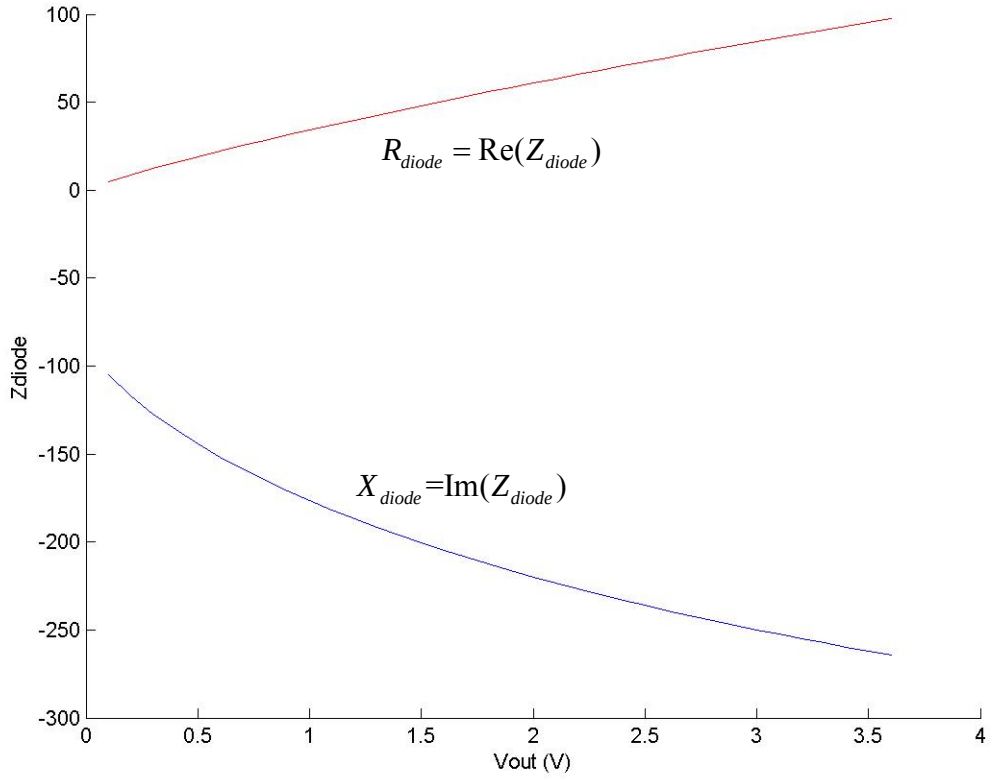

Figure 42. Variance of diode impedance with $R_L = 1\mathrm{K}\Omega$

With the use of higher load resistance, the impedance of the diode varies significantly compared to Figure 39. This means that the matching network must be adaptable to changes in diode impedance. If not, the transmitter or operating range must be to maintain the diode's operating power level.

A higher load resistance may increase the diode conversion efficiency, however, it creates two critical problems: (1) decreasing maximum output power and therefore requiring more rectenna elements, and (2) increasing the range of the diode impedance, which creates impedance mismatches with varying power levels. Therefore the decision of choosing load resistance is highly dependent on constraints of the intended application, the issue of efficiency trade-off versus number of diode elements, and the availability of good matching networks to minimize impedance mismatches.

E. CONCLUSION

The limitations of employing the Ritz-Galerkin technique in determining the diode's output voltage at higher operating power levels was discussed. The Agilent HSMS-8101 Schottky diode was used in the efficiency analysis similar to [31, 32] for the rectenna application. Design curves were generated to determine the rf-to-dc conversion efficiency and the impedance of the diode as a function of several operating parameters.

The possibility of changing the load resistance to achieve a higher rf-to-dc conversion efficiency was discussed, and it was noted that a trade-off between maximum conversion efficiency and the size and weight constraints of this application must be made. This involves an evaluation of load resistance, the application operating constraints, diode efficiency, and rectenna impedance matching.

Overall, the present motor's load resistance of 50 Ω fits very well with this application. It minimizes the number of rectenna elements in the array and reflection losses due to variances in the diode impedance.

THIS PAGE INTENTIONALLY LEFT BLANK

VI. RECTIFICATION FILTERS AND TUNING THE PROBE FEED

This chapter is broken into three parts. Part one will explain how filters are implemented on microstrip lines. It then proceeds to describe the performance of the original filter, and then suggests improved filter designs. Part two covers the implications of microstrip discontinuities that will be present in the rectenna system. Part three briefly covers the considerations for connecting the probe feed to the antenna and filter.

A. THEORETICAL CALCULATION OF FILTER SUBSYSTEMS

1. Introduction

In days before the printed circuit board, filters were implemented using a series of inductors and capacitors connected together to obtain the required filter response. This method had disadvantages of inaccuracy, due to the difficulty of tuning inductors, large in size, and the issue of coupling effects from neighboring inductor coils. The only advantage of employing physical components was its ability to handle large levels of power.

The next advancement in filter implementation was the printed circuit board which was thin and lightweight. Through simply altering the width and length of an open or short-circuit microstrip stub, accurate implementations of capacitance and inductance can be achieved. This proved to be an attractive option as it required less space, was lightweight, and simple. So long as the power level was within the microstrip line's capability, microstrip line filters became the de-facto option, inline with the industries' drive towards miniaturization of electronic equipment.

Chapter III highlighted the role of the pre-rectification filter, which was two fold: (1) to limit the frequency of incoming microwave signals being rectified, and (2) to prevent the retransmission of harmonics generated from the non-linear *I-V* characteristics of the diode. The post-rectification filter's role is to select the dc from the frequency components and deliver it to the load.

Numerous publications on microstrip filter implementation can be found. Some particularly worth noting are from Pozar [33] and Collin [34]. The two methods

commonly used to calculate microstrip filter dimensions are the image-parameter method and the insertion loss method.

The older image-parameter method has limitations in that it is only able to specify the required passband and stopband responses, but it fails to provide accurate frequency characteristics over each of the two regions. The insertion loss method, however, gives very accurate control over the filter's passband and stopband performance and the calculation of dimensions is done in a very systematic manner. Therefore the insertion loss method is employed for this application.

2. Insertion Loss Method

The insertion loss process of calculating the dimensions of a microstrip filter is summarized in the following steps:

a. Determine type of filter (low pass, band pass or high pass)

b. Determine the type of filter response (Butterworth or Chebyshev)

c. Determine the order of the microstrip filter, N, that would satisfy the required filter response.

d. Develop the prototype filter with a cutoff frequency of 1 Hz with an impedance of 1 Ω.

e. Determine the capacitance (C) and inductance (L) values necessary for filter performance.

f. Lastly, convert the C and L values into real microstrip dimensions, based on cut-off frequency, dielectric attributes, and microstrip line width.

The method of calculating the pre- and post-rectification filters is identical, thus only the pre-rectification filter is explained in detail.

Step a. Determine Type of Filter

Based on our present application, both pre- and post-rectification filters are low pass filters.

Step b. Determine the Type of Filter Response

Butterworth filters are also known as maximally flat filters, where the filter band pass response is flat but the cut off response is fairly limited. The Chebyshev filter on the other hand has slight variation in the band pass response, but has a higher cut off response. The Butterworth implementation is chosen, in order to make comparisons with the last design. It should be noted that the Chebyshev filter could be used as well, because constant phase and gain performance is not critical for rectenna applications. Figure 43 shows the filter insertion loss (IL) of the Butterworth and Chebyshev low pass filters, where IL = $-20\log_{10}|S_{21}|$.

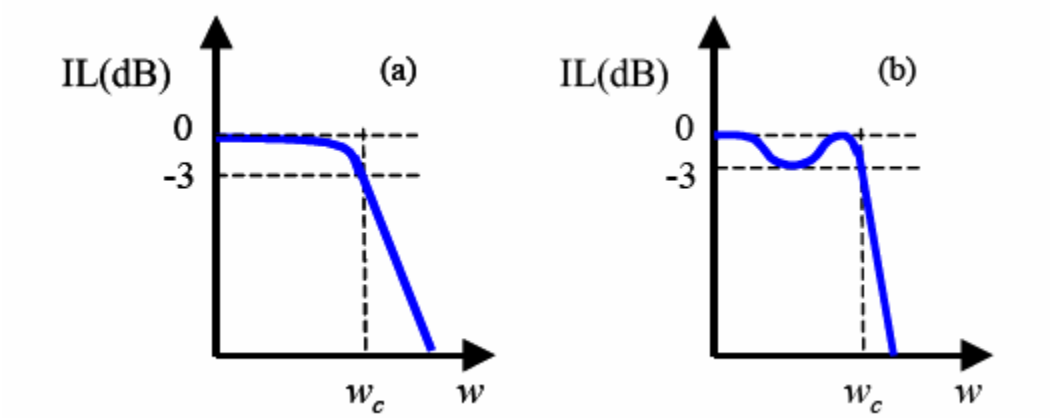

Figure 43. Insertion loss (S_{21} , dB) of (a) maximally flat Butterworth filter and (b) Chebyshev filter (From [35])

Step c. Determine the Order of the Microstrip Filter

The generic Butterworth low pass filter has a power loss ratio given as

$$P_{LR} = 1 + k^2 \left(\frac{\omega}{\omega_c} \right)^{2N} \tag{6.1}$$

where N is the order of the filter, with the cutoff frequency, $\omega_c = 2\pi f_c$. The power loss ratio (P_{LR}) is equal to the ratio of the power available from the source (P_{in}) to the power that is delivered to the load (P_{load})

$$P_{LR} = \frac{P_{in}}{P_{load}} = \frac{1}{1 - \left| \Gamma(\omega) \right|^2} \tag{6.2}$$

where $\Gamma(\omega)$ is the reflection coefficient at the input port of the filter assuming that the output port is matched. From P_{LR}, the insertion loss for frequencies higher than the 3 dB point, can be approximately represented as

$$IL = -20\log k - 20N\log\left(\frac{\omega}{\omega_c}\right) \tag{6.3}$$

From Equation (6.3), it is realized that the slope of the filter response decreases at a rate of (20*N)* dB/decade outside the pass band region.

Tsolis [19] set f_c to 12 GHz and the gain at the second harmonic, 20 GHz, was set to -12 dB. From Figure 44, N must be equal to or more than 4 to achieve the required filter response.

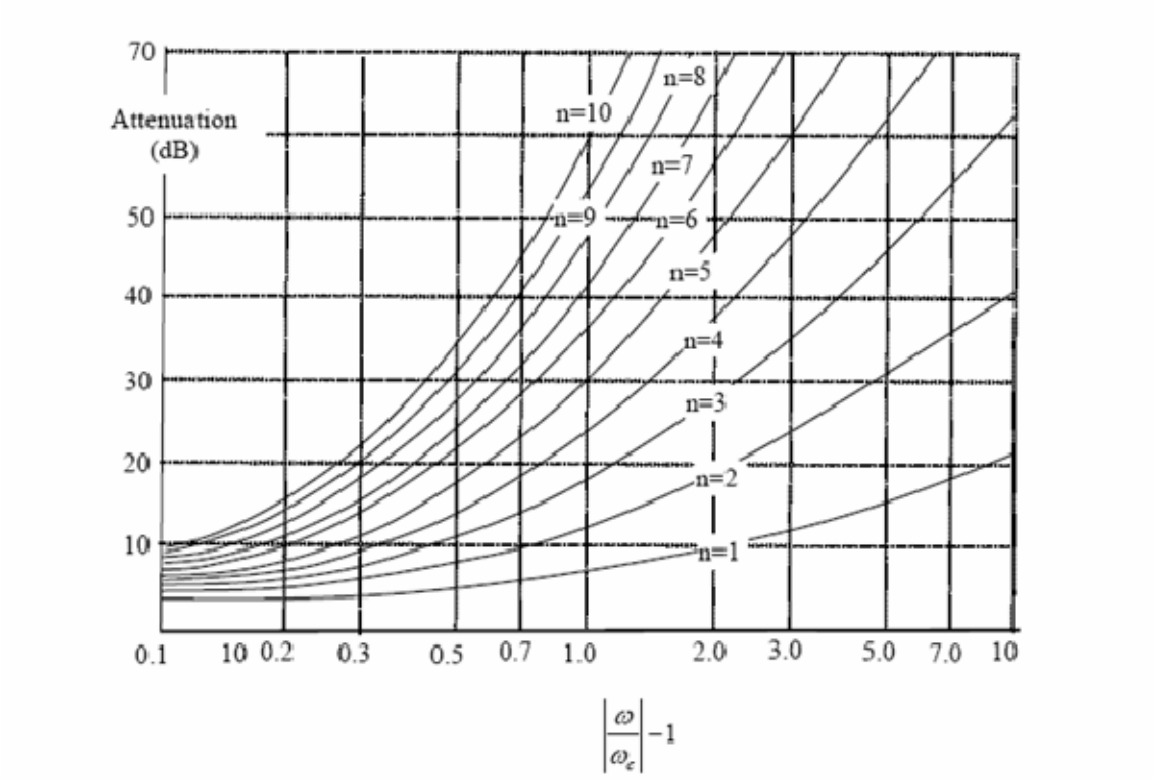

Figure 44. Attenuation versus normalized frequency for maximally flat Butterworth filter prototypes of order n. (From [33])

Step d. Develop the Prototype with a Cutoff Frequency of 1 Hz with Impedance of 1 Ω

The N^{th} order low pass filter is modeled by a ladder network that starts with either a series or shunt element. The two configurations are shown in Figure 45. The low pass prototype filter is normalized to a cutoff frequency of 1 Hz and source impedance of 1 Ω.

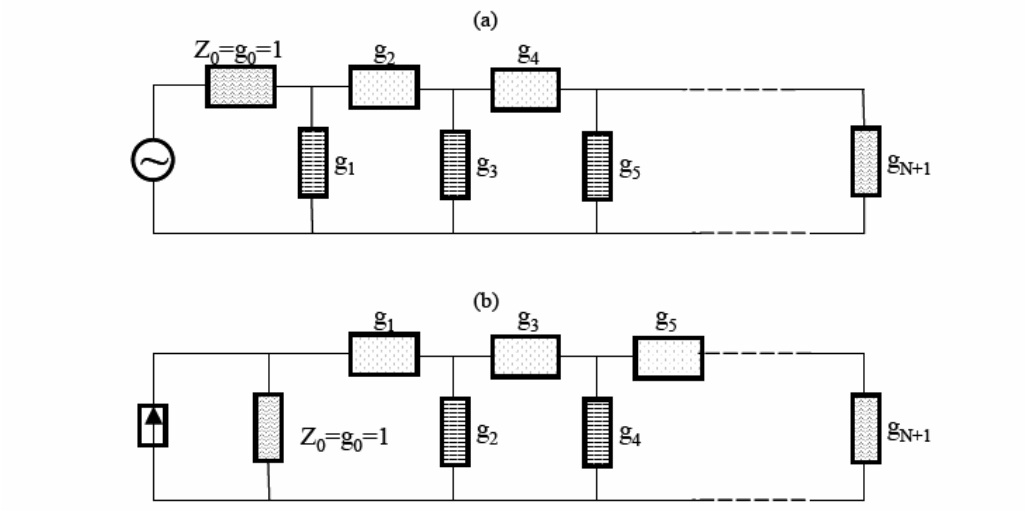

Figure 45. Ladder representation for low pass filter prototype starting with the (a) series element and (b) shunt element (From [35])

Typically the element closest to the generator is denoted as g_0, while the load impedance is g_{N+1}. For low pass filters, the series elements are lumped inductors while the shunt elements are capacitors. The values of g_1 to g_N for an N^{th} order Butterworth filter can be found in Table 13.

N	g_1	g_2	g_3	g_4	g_5	g_6	g_7	g_8
1	2.0000	1.0000						
2	1.4142	1.4142	1.0000					
3	1.0000	2.0000	1.0000	1.0000				
4	0.7654	1.8478	1.8478	0.7654	1.0000			
5	0.6180	1.6180	2.0000	1.6180	0.6180	1.0000		
6	0.5176	1.4142	1.9318	1.9318	1.4142	0.5176	1.0000	
7	0.4450	1.2470	1.8019	2.0000	1.8019	1.2470	0.4450	1.0000

Table 13. Element values for maximally flat (Butterworth) low pass prototype (g_0= 1, ω_c =1) (From [36])

For a fourth order prototype that begins with a series element, the value of each element is shown in Figure 46.

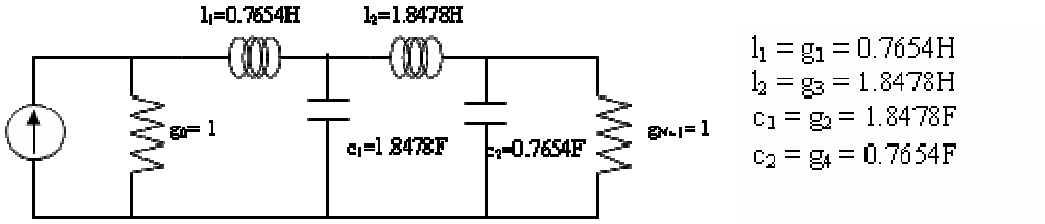

Figure 46. Prototype fourth order low pass filter beginning with series element

Step e. Determine the Values of C and L Needed to Achieve Filter Performance

Since the initial prototype was based on a source and load impedance of 1 Ω, there is a need to conduct a frequency and impedance transformation to achieve the required microstrip dimensions.

Based on the load impedance of R_L and the cutoff frequency ω_c, the prototype values are transformed based on the following equations.

$$R = g_{N+1} R_L \tag{6.4}$$

$$L_i = \frac{I_i R_L}{\omega_c} \tag{6.5}$$

$$C_i = \frac{c_i}{R_L \omega_c} \tag{6.6}$$

For $R_L = 30\ \Omega$ and $\omega_c = 2\pi f_c$ where f_c is set to 12 GHz, this results in the following element values for the fourth order low pass filter:

$$R = 30\ \Omega;\ L_1 = 0.3045\ \text{nH};\ L_2 = 0.7352\ \text{nH};\ C_1 = 0.8169\ \text{pF};\ C_2 = 0.3384\ \text{pF}$$

Step f. Conversion of C and L Values Into Real Microstrip Dimensions, Based on Cutoff Frequency, Dielectric Thickness, and Width of Microstrip Line

In order to calculate the actual microstrip dimensions, the effective dielectric constant and the characteristic impedance for each shunt and series element must be calculated.

Step f1. Effective Dielectric Constant of the Microstrip Line

If the fringing *E*-fields of the microstrip line are fully enclosed by dielectric material, then the effective dielectric constant would be that of the material. However in most cases, one side is air. The fringing *E*-fields in the air contribute to a different effective dielectric constant. The calculation of the effective dielectric constant is given as

$$\varepsilon_e = \frac{\varepsilon_r + 1}{2} + \frac{\varepsilon_r - 1}{2} \frac{1}{\sqrt{1 + 12d/W}} \tag{6.7}$$

where: W is the width of the transmission line,

d is the height of the substrate, and

ε_r is the relative dielectric constant of the substrate.

In line with the previous work [19], the parameters are $\varepsilon_r = 2.33$ and $d = 0.127$ mm.

The implementation of a series or shunt element is through high or low impedance microstrip lines, respectively. For series elements, W is usually less than d to create a high characteristic impedance line of approximately 100 to 150 Ω. For shunt elements, the opposite is true, W is larger than d by 10 or more times, with a characteristic impedance of 10 Ω.

Step f2. Characteristic Impedance for Shunt and Series Element.

The characteristic impedance of a microstrip line is given by [33]

$$Z_0 = \begin{cases} \dfrac{60}{\sqrt{\varepsilon_e}} \ln\left(\dfrac{8d}{W} + \dfrac{W}{4d}\right), & \text{for } W/d \le 1 \\ \dfrac{120\pi}{\sqrt{\varepsilon_e}\left[W/d + 1.393 + 0.667 \ln\left(W/d + 1.444\right)\right]}, & \text{for } W/d \ge 1 \end{cases} \tag{6.8}$$

Based on the previous design, where Z_{cap} = 10 Ω, and Z_{ind} = 100 Ω, W_{cap}/d = 21.26, W_{ind}/d = 0.67.

Therefore using Equations (6.7) and (6.8) the values of ε_{eind}, ε_{ecap}, Z_{ind} and Z_{cap} can be calculated and subsequently used to calculate the actual microstrip dimensions. The lengths of each microstrip stub are calculated in the following equations:

$$l\_L_i = \frac{cL_i}{Z_{ind}\sqrt{\varepsilon_{eind}}} \tag{6.9}$$

$$l\_C_i = \frac{cC_iZ_{cap}}{\sqrt{\varepsilon_{ecap}}} \tag{6.10}$$

with the values of L_i and C_i from Step e, the dimension of each microstrip section were found as,

l_L_1 = 0.6103 mm $\quad$ $Width\_L_1$ = 0.085 mm

l_C_1 = 1.7004 mm $\quad$ $Width\_C_1$ = 2.7 mm

l_L_2 = 1.4734 mm $\quad$ $Width\_L_2$ = 0.085 mm

l_C_2 = 0.7043 mm $\quad$ $Width\_C_2$ = 2.7 mm

To facilitate the dimensions calculation, a program has been written in Matlab and included in Appendix D and E.

B. COMPARISON OF PRE-RECTIFICATION FILTER PERFORMANCE USING MICROWAVE STUDIO

Both the original [19] and new filter designs were simulated in Microwave Studio, with the input and output waveguide port impedances set to 30 Ω.

1. Original Fourth Order Filter

The dimensions of the original fourth order low pass filter are shown in Figure 47. The total length of the filter is 4.688 mm and the maximum width is 2.7 mm. The total area used is 12.65 mm^2.

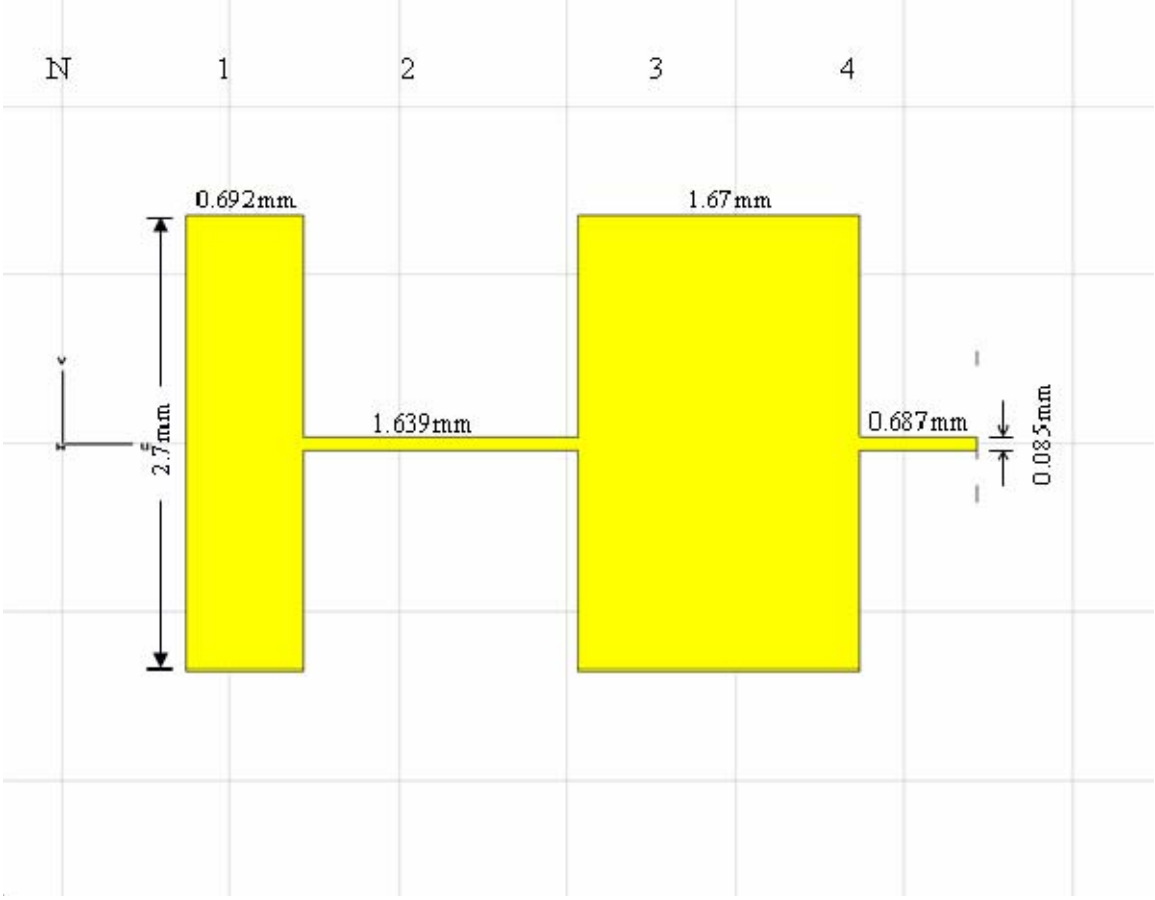

Figure 47. Dimension of the original fourth order low pass filter

The MWS simulator was set to determine the frequency response of the filter from the range of 5 GHz to 25 GHz. The upper limit of the frequency is chosen to determine the filter's response for the second harmonics of 20 GHz.

The *S*-parameters of the original filter are presented in the Figure 48 and at the frequency of 10 GHz, the S_{12} and S_{21} parameters are -2 dB. This means that approximately 63% of the incident wave is transmitting through this filter. This is undesirable as it is critical to transfer as much of the incident power to the subsequent stages of the rectenna element.

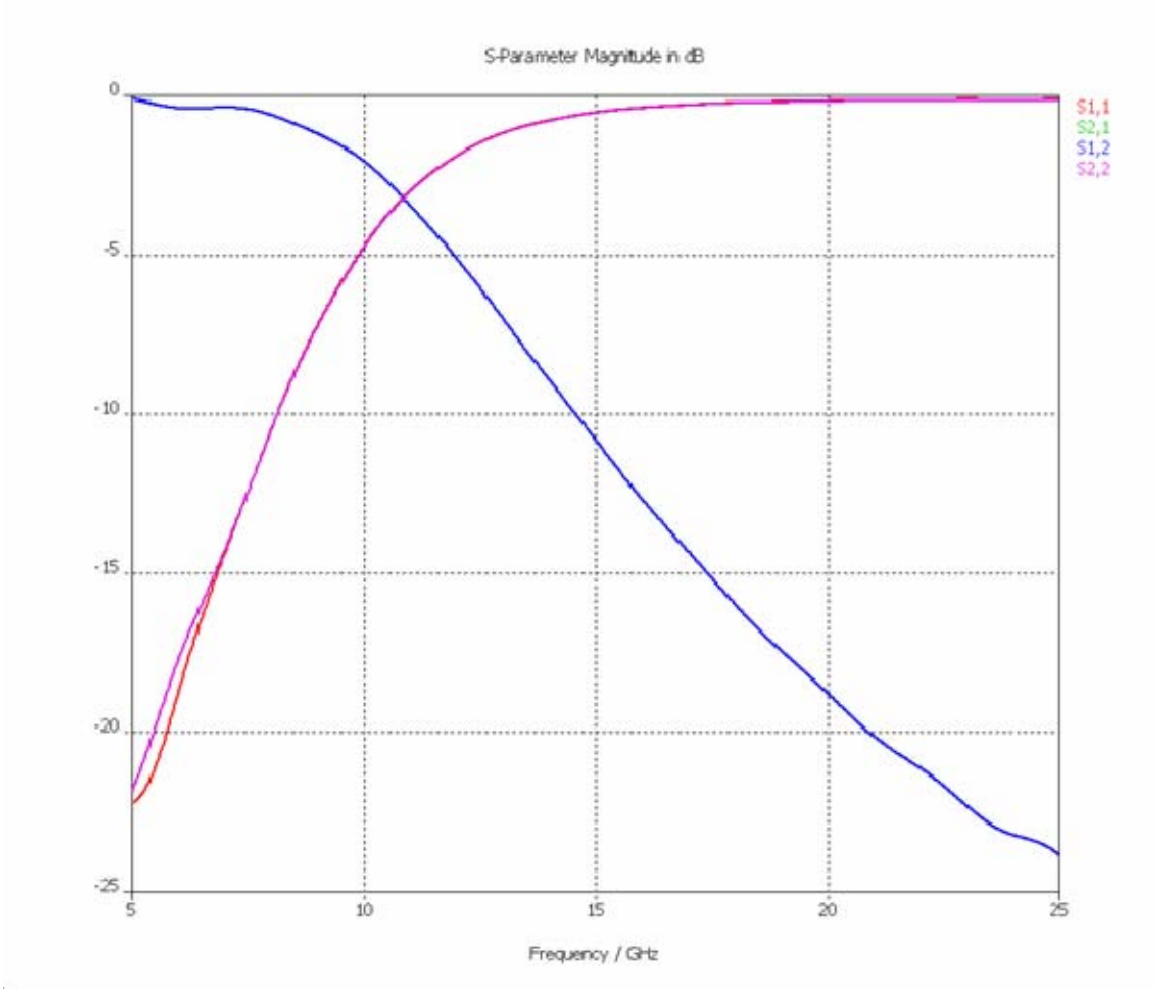

Figure 48. Filter response of original fourth order low pass filter

2. New Fourth Order Filter

Based on the design procedure mentioned in the Section A the new filter with a leading inductive element was simulated in Microwave Studio. The design had a total length of 4.49 mm and with the same width dimension as the original filter, a total area of 12.12 mm^2. The design was shorter by only 0.2 mm, and therefore, from a weight perspective both designs are almost identical.

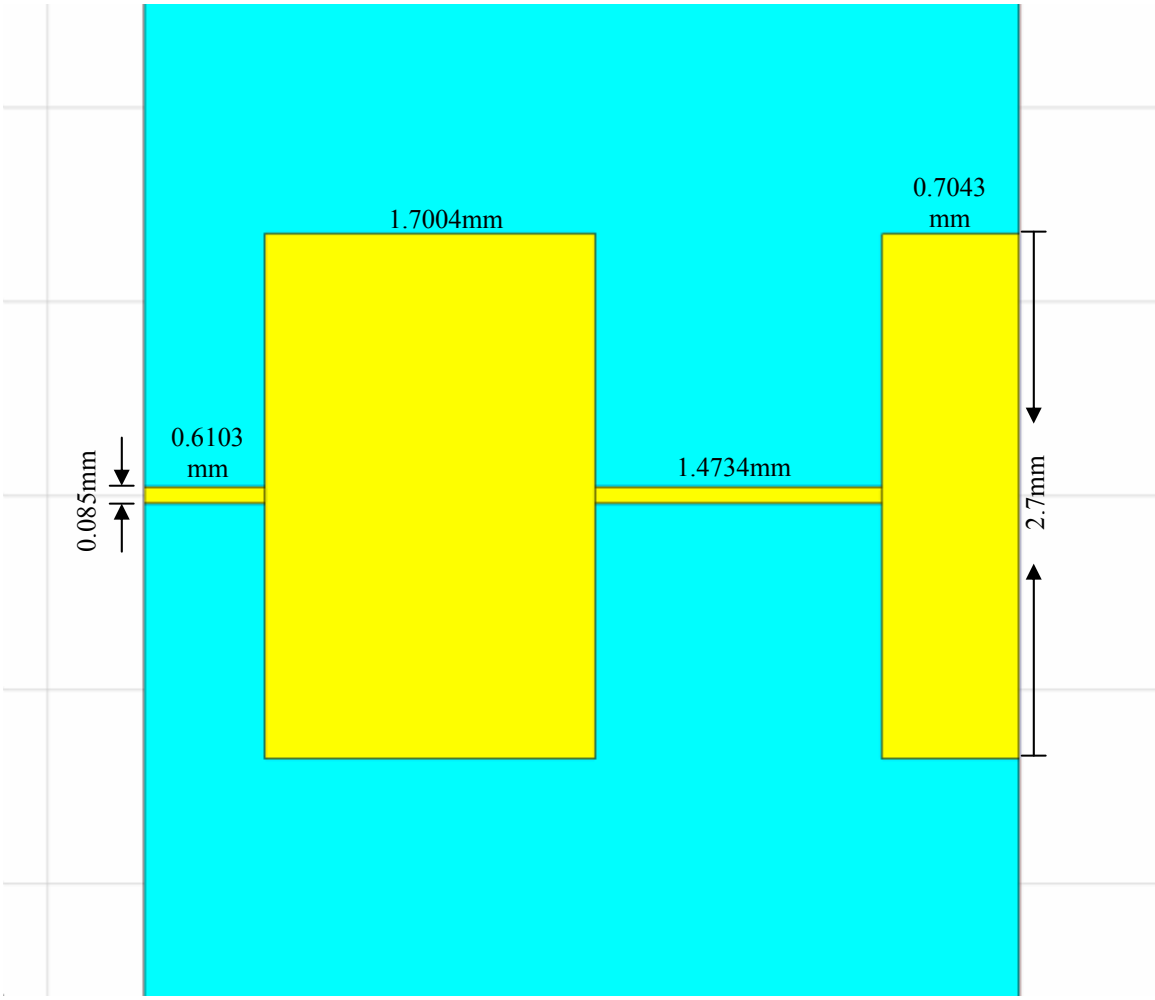

Figure 49. Dimension of new fourth order low pass filter

The performance of the filter is shown in Figure 50. The S_{12} and S_{21} values are -1.45 dB. The use of this filter configuration in place of the original will account for an increase of the transmitted signal by additional 8%, from 63% to 71%. In the pursuit of increasing the efficiency of the filter further, a new higher order filter was subsequently designed and investigated.

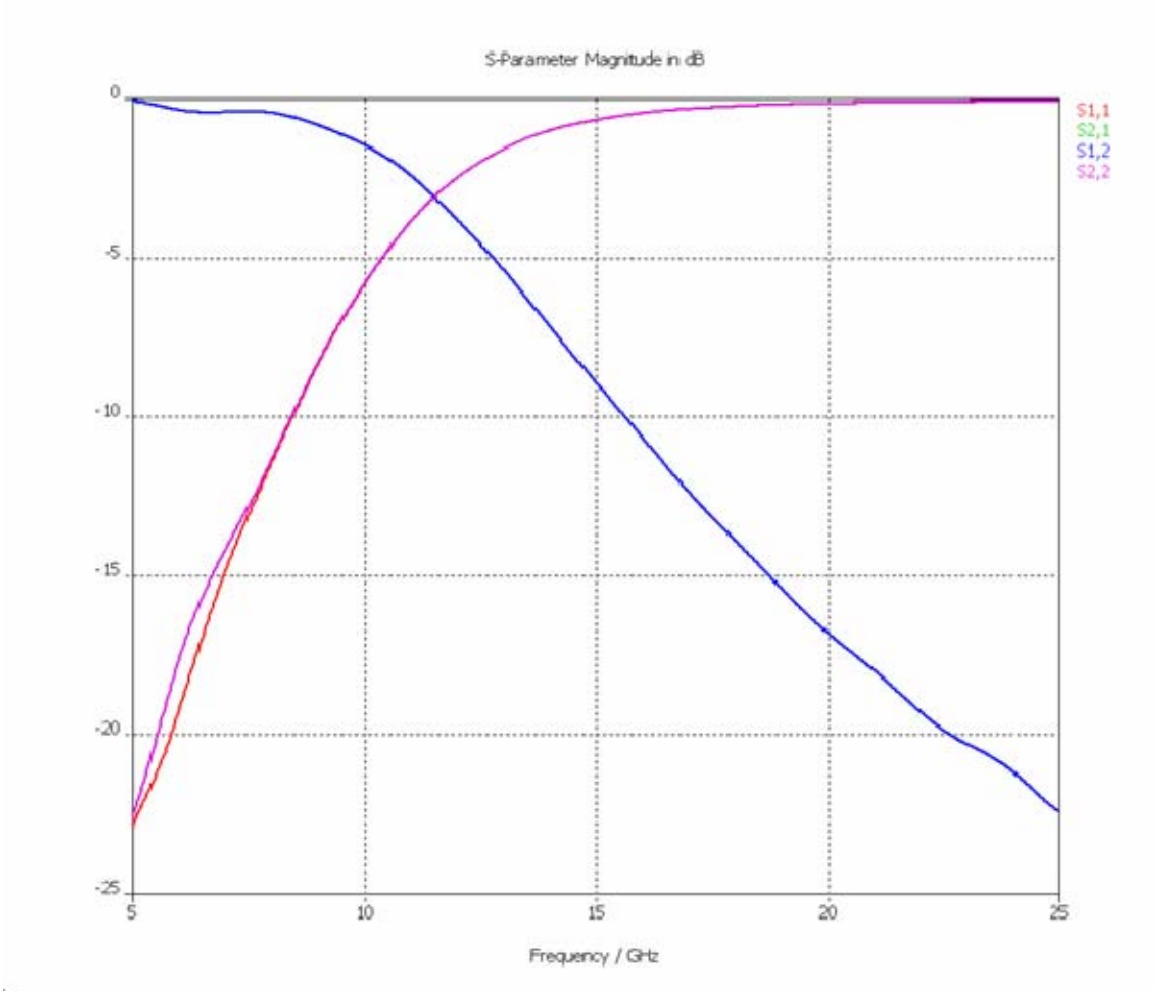

Figure 50. Filter response of new fourth order low pass filter

3. New Sixth Order Filter

In order to allow for a better response at 10 GHz, the cutoff frequency was increase to 14 GHz. In effect this would start the roll off of the frequency response at a higher frequency and decrease the loss at 10 GHz. However, if the order of the filter is left constant, the contributions from harmonics will increase, because the frequency response curve is simply translated upwards in the frequency domain. In order to maintain the requirement of -15 dB at 20 GHz based on Equation (6.1), the order of the filter must be increased to six.

The new sixth order Butterworth filter design is shown in Figure 51. This would result in an overall length of 5.6892 mm, an increase of 25% in weight and length over the original design. The frequency response of the new sixth order filter is shown in the Figure 52.

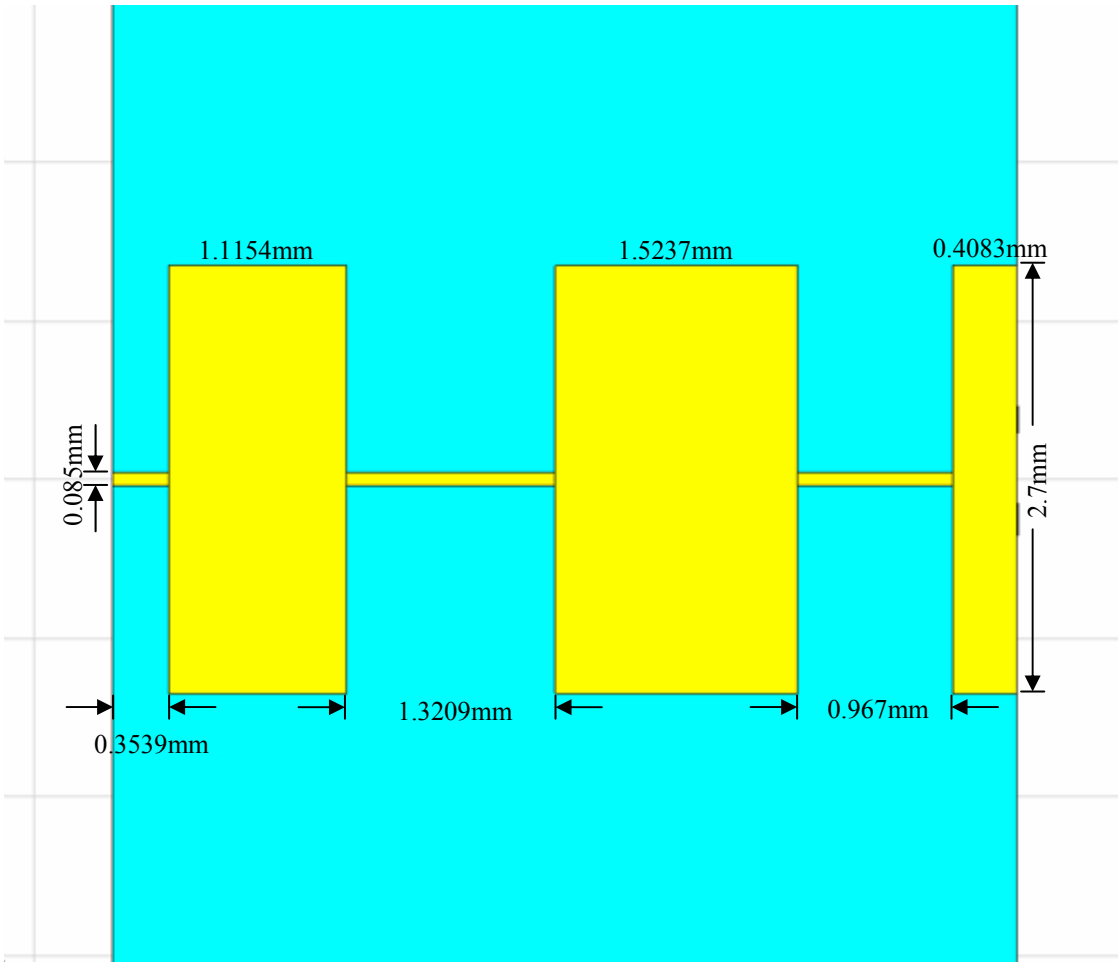

Figure 51. Dimension of new sixth order low pass filter

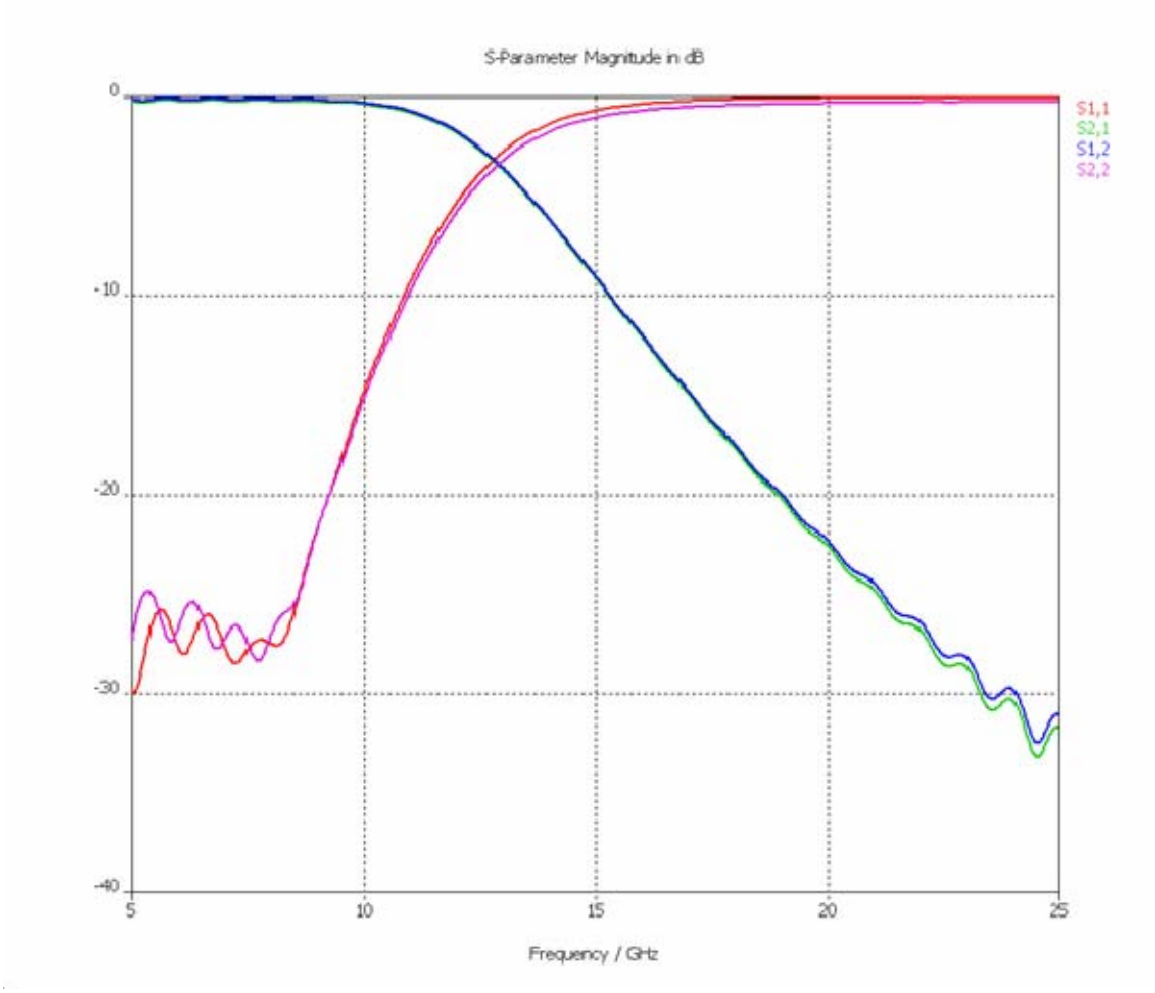

Figure 52. Filter response of new sixth order low pass filter

Now, with the new filter, the S_{12} and S_{21} values are -0.27 dB and -0.35 dB. It has the best performance of 94% transmittance, which is an increase of another 23% over the fourth order filters.

Although the percentage increase of transmittance gain is equal to the percentage increase in weight, the increase in filter order is still required to improve the overall efficiency of the rectenna. The total efficiency of the rectenna can be expressed as the multiplication of the efficiency of each stage of the rectenna

$$\text{Efficiency of Rectenna} = \left[\left(\eta_{antenna}\eta_{pre-recfilter}\right)\eta_{rectification}\right]\eta_{post-rectfilter}$$

Therefore, since the pre-rectification filter is the stage following the receiving antenna, it is important to increase its transmittance in order to maximize the rectenna's overall efficiency.

4. Conclusion for Pre-rectification Filter Performance

The performance of both the original and new fourth order Butterworth filters were investigated and it was determined that their dimensions and performance were very similar.

However, with an efficiency of only 70%, a new filter was designed and evaluated. The new design calls for a higher cutoff frequency and a faster roll off rate. This could only be achieved by a sixth order Butterworth filter.

The transmittance of the sixth order filter increased by 25% relative to the fourth order filter, while its area increased by the same amount. Although the ratio is linear, its impact on the overall rectenna performance outweighs the increase in weight.

C. PERFORMANCE OF POST-RECTIFICATION FILTERS

The incoming rectified microwave signals entering the post-rectification filter will consist of a dc term and harmonics of the original signal. The function of the post-rectification filter is to effectively filter out all these harmonics, which will normally appear as ripples in the output dc signal. In [19], a second-order low pass filter was used. The cutoff frequency was 2 GHz, and was printed on the same substrate as the pre-rectification filter. The dimensions of the original post-rectification microstrip filter are given in the Figure 53.

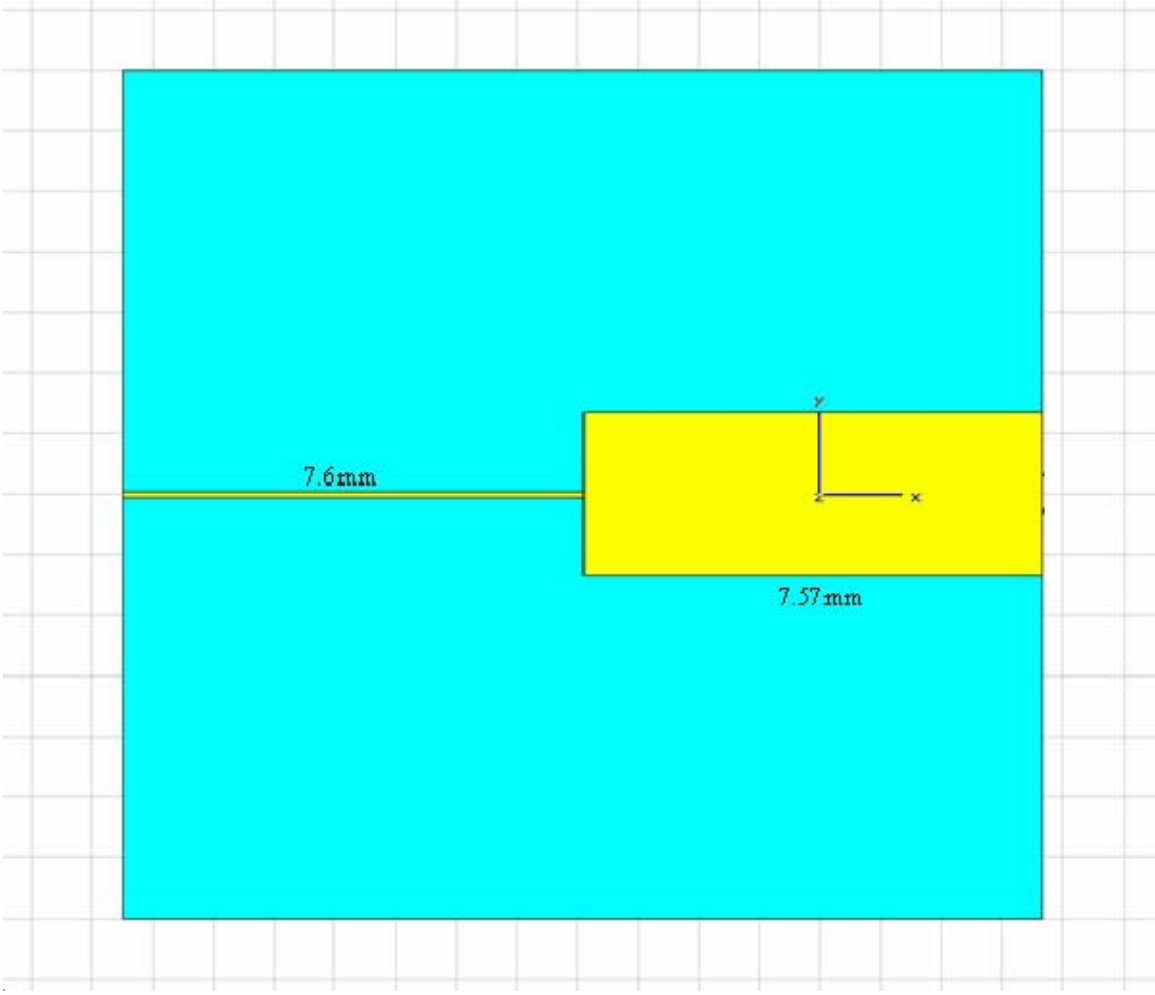

Figure 53. Layout of the original second order post-rectification low pass filter (After [19])

The design was simulated in Microwave Studio and the *S*-parameters were simulated over the frequency range from 0 to 25 GHz. In Figure 54 it is evident that there is a repetitive cycle in the filter response, where the bandwidth of each cycle is approximately 12.5 GHz.

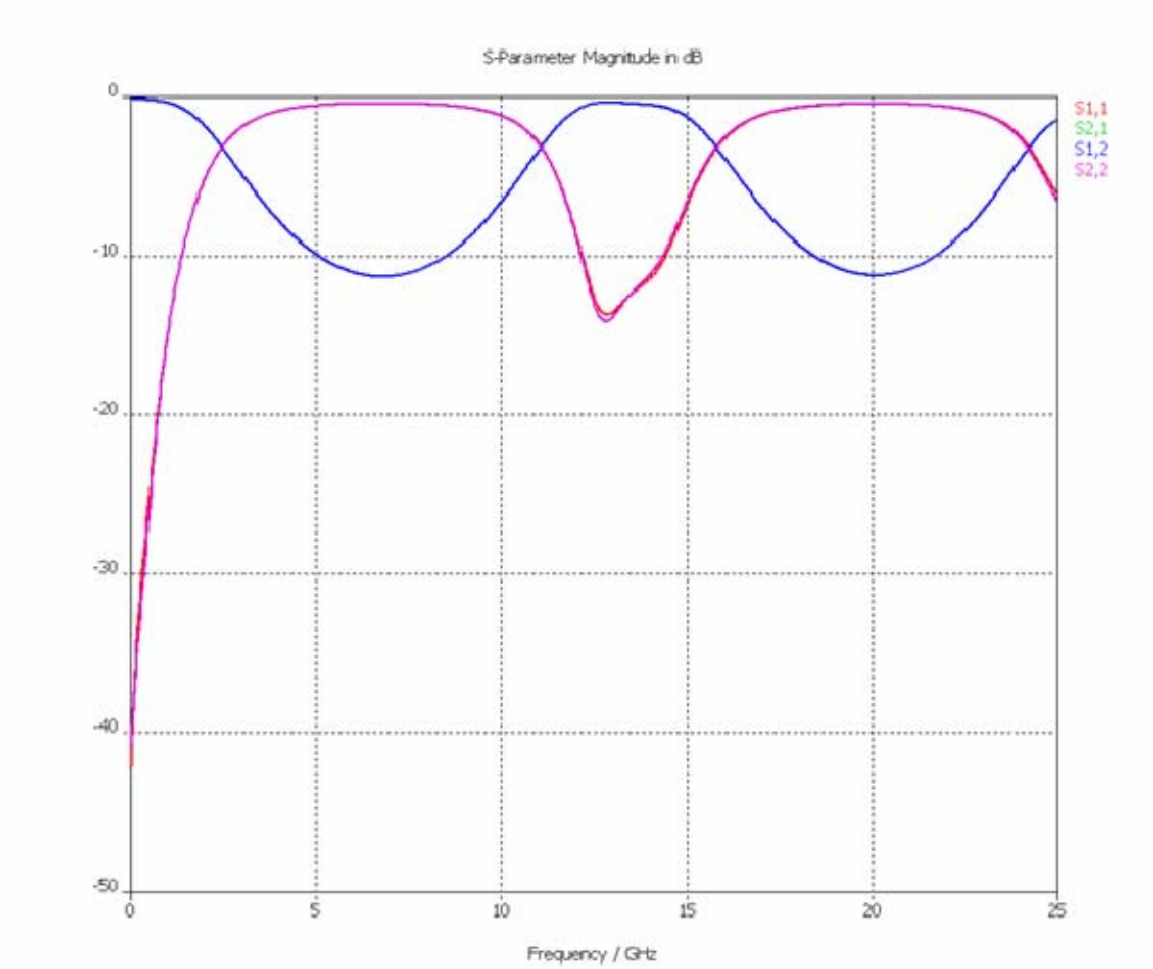

Figure 54. Filter response of original second order post-rectification low pass filter

The implications of this repetitive cycle, which was not highlighted in [19] means that not all higher harmonics are filtered out as initially thought. Although it may be argued that the power contribution from higher order harmonics is small compared to the dc term, they should not contribute much to the degradation in quality of the dc term. The reflection of all higher order harmonics back to the rectifying diode may contribute to better rectenna conversion efficiency.

The second order low pass filter design was re-evaluated based on calculations in the beginning of this chapter and subsequent MWS simulations. The results were similar to [19] with the new design's *S*-parameters varying by only 2%.

Along with the disadvantage of allowing higher order harmonics through, the use of this microstrip filter design tends to take up a lot of space. This design takes up a

length of about 15 mm which is almost 3 times more surface area than used in the sixth order pre-rectification filter. Another implementation of the low pass filter is explored, through the use of an RC circuit. Such a design was implemented in [37], and is shown in Figure 55.

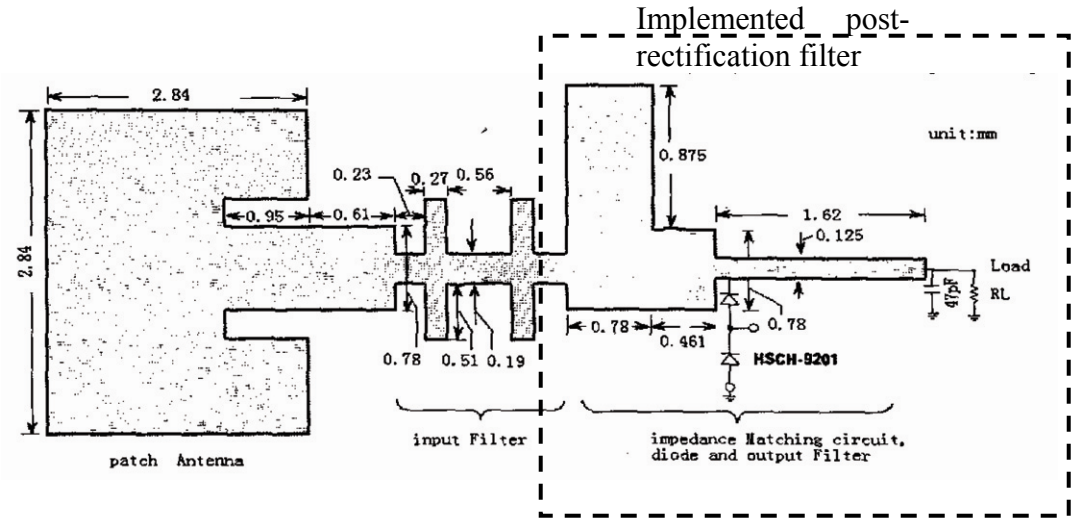

Figure 55. Low pass filter with matching stub (After [37])

1. Single Stub Low Pass Filter with Matching Network

This design [37] calls for the use of a single quarter-wave stub terminated by a 47 pF capacitor. The rf waves approaching the end of the stub will essentially see a short-circuit due to the presence of the capacitor and will be reflected back due to the large impedance mismatch. The dc term only sees the load resistance and will pass. This is essentially the function of the post-rectification filter.

The reflection of the rf waves in the quarter-wave stub creates standing wave, and the location of the peak of the standing wave voltage is where the rectifying diode must be placed. Since the majority of rf power is in the 10 GHz signal, the diode must be placed at a quarter-wave length away at 10 GHz.

The impedance at the diode connection is essentially the diode impedance itself, because it is in parallel with the odd-order harmonic standing wave impedance, which is essentially infinity. Therefore, with this setup, the load resistance has no impact on the impedance seen at the input of the quarter-wave stub. Instead the load resistance only affects the operation of the diode.

From Chapter V, the diode impedance is $45.5 - j13.9\ \Omega$ and thus there is a need to match this impedance to the output of the pre-rectification filter. The matching of the diode's impedance was not considered in [19]. Instead, only the diode's resistance was taken into account, which resulted in larger mismatch losses. The diode's impedance is matched employing a matching network consisting of two microstrip stubs of different characteristic impedance and lengths as shown in Figure 56. Assuming that the characteristic impedance of Z_1 is $50\ \Omega$, the matching network is determined employing a Smith chart in two steps.

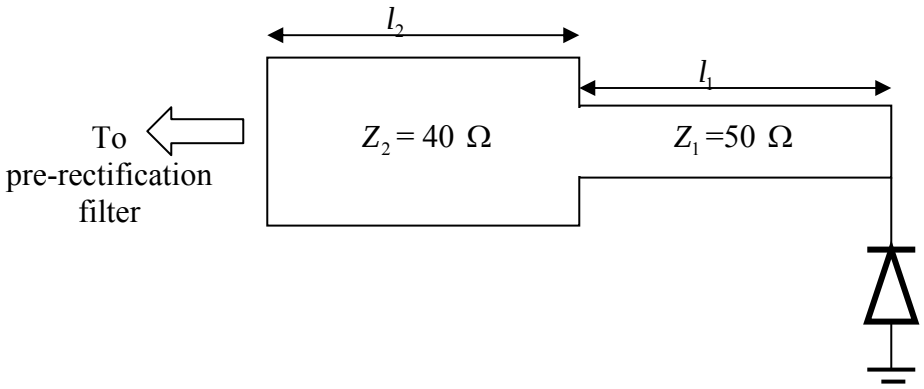

Figure 56. Matching network for diode to pre-rectification filter

a. Determining Z_2 and l_1 of Matching Network

The impedance of the diode ($45.5 - j13.9\ \Omega$) is marked on the Smith chart normalized to $50\ \Omega$ in Figure 57. The VSWR circle of the diode impedance (black circle centered at the origin) is drawn. The value of Z_2 must be chosen such that the VSWR circle of Z_2 and $50\ \Omega$ (blue circle through the origin) cuts the diode VSWR circle. Z_2 was set to $40\ \Omega$. The length l_1 is the distance in the direction towards the generator which is $\left[0.072+(0.5-0.386)\right]\lambda_1 = 0.186\lambda_1$, where λ_1 is the 10 GHz wavelength in the microstrip line of characteristics impedance Z_1, l_1 was calculated as 3.61 mm.

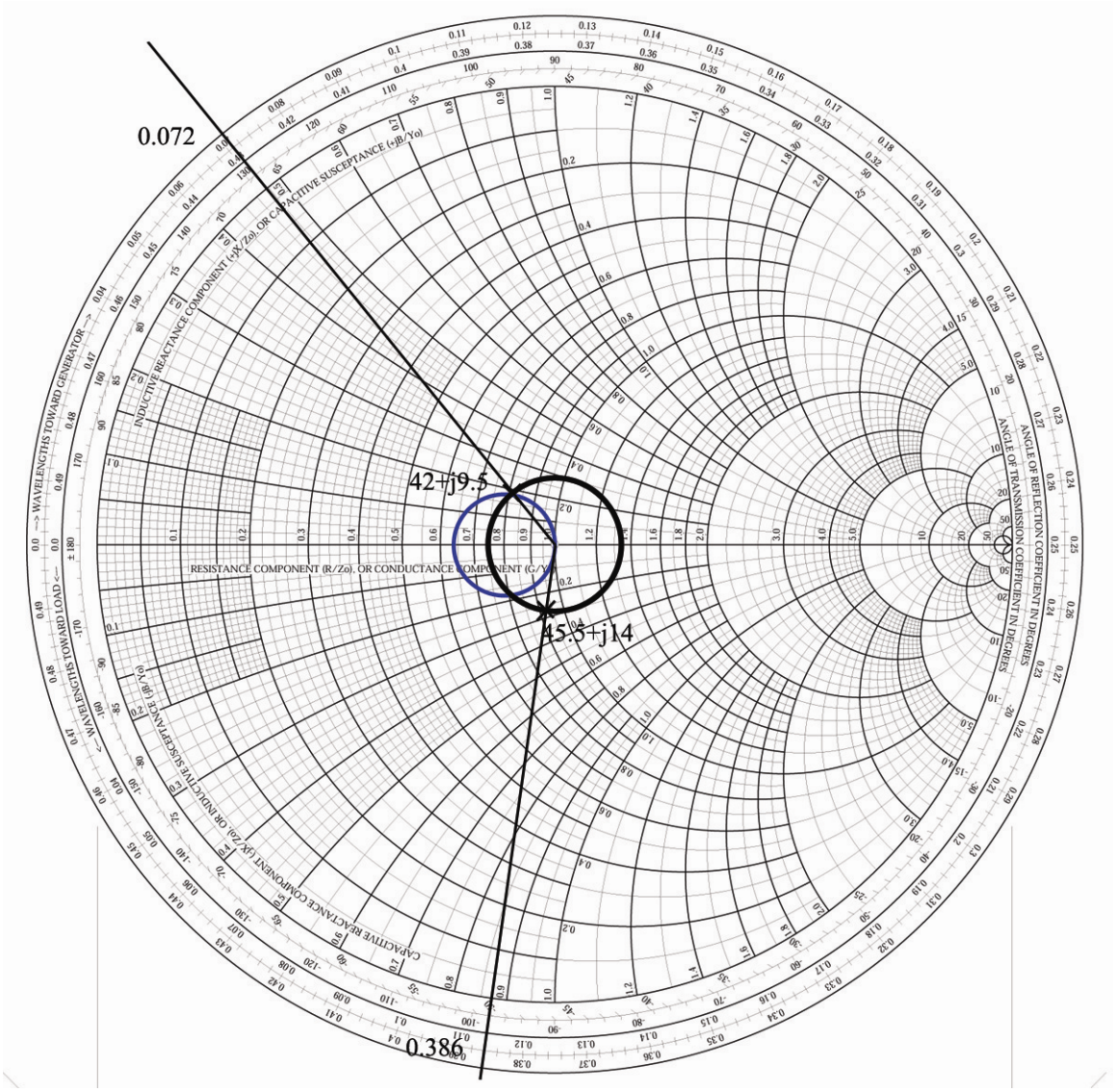

Figure 57. Smith Chart to determine l_1

b. Determining l_2 of Matching Network

Now the impedance seen at the intersection between Z_1 and Z_2 is approximately $42 + j9.5\ \Omega$. The next step is to determine l_2 such that the impedance seen at the intersection of Z_2 and the output of the pre-rectification filter is $50\ \Omega$. The impedance of $42 + j9.5\ \Omega$ is now plotted onto a Smith chart normalized to $40\ \Omega$. The VSWR circle is drawn and the distance towards the generator to achieve $50\ \Omega$ is determined. In Figure 58, the length of l_2 is equal to $(0.25 - 0.152)\lambda = 0.098\lambda$, which is 1.862 mm.

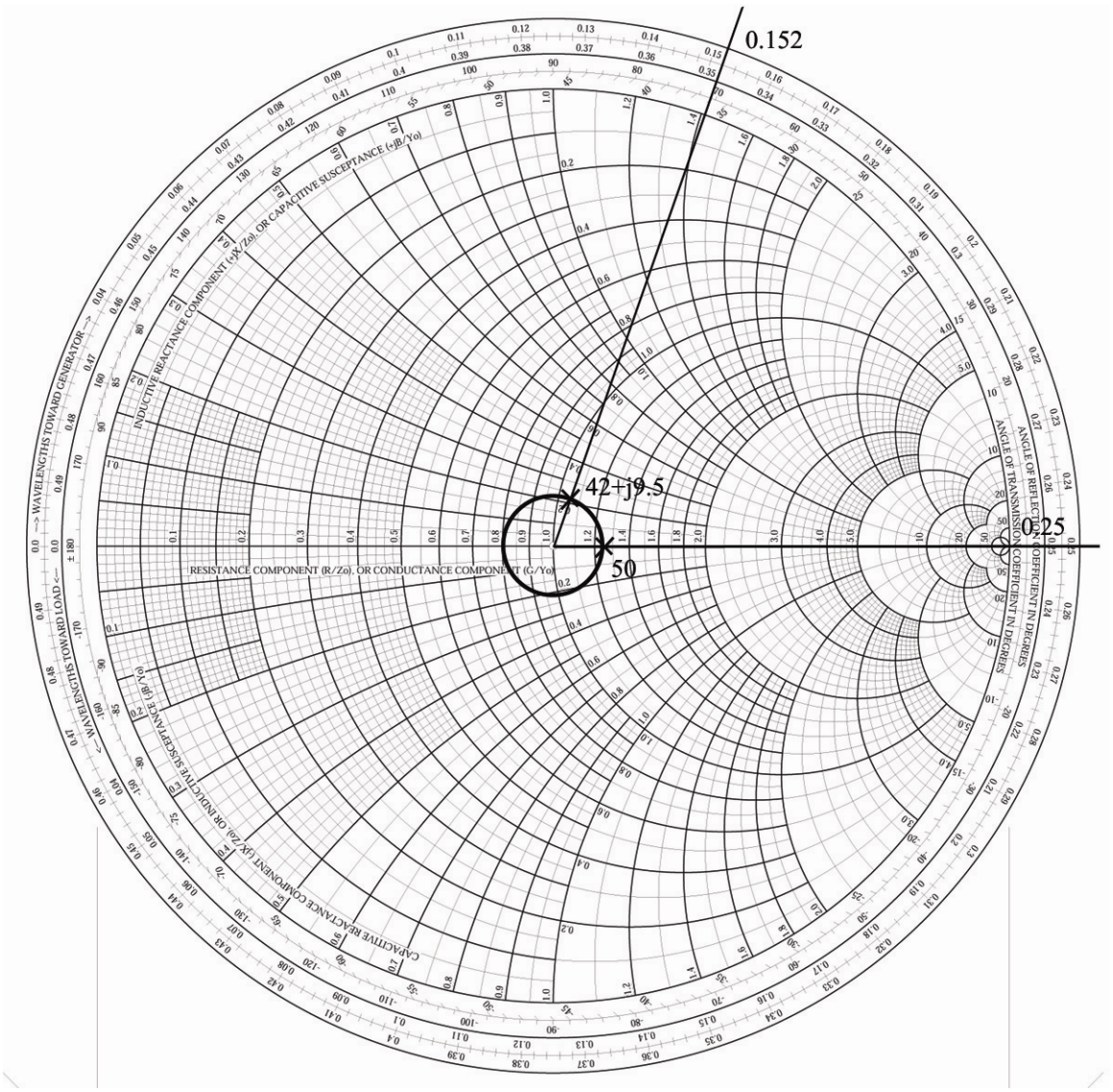

Figure 58. Smith Chart to determine l_2

Therefore, with this matching network, the impedance of the diode is now seen as 50 Ω at the pre-rectification filter. This same impedance matching technique will be used again to match the patch to the input of the pre-rectification filter.

D. MICROSTRIP DISCONTINUITIES

All microstrip paths discussed so far have been implemented with straight lines. However, in order to minimize the footprint of each rectenna, there will be a need to use bends, which are microstrip discontinuities. This section will examine the effects of such bends and how they can be minimized.

The 90° bend can be modeled as a series inductor and capacitor as shown in Figure 59.

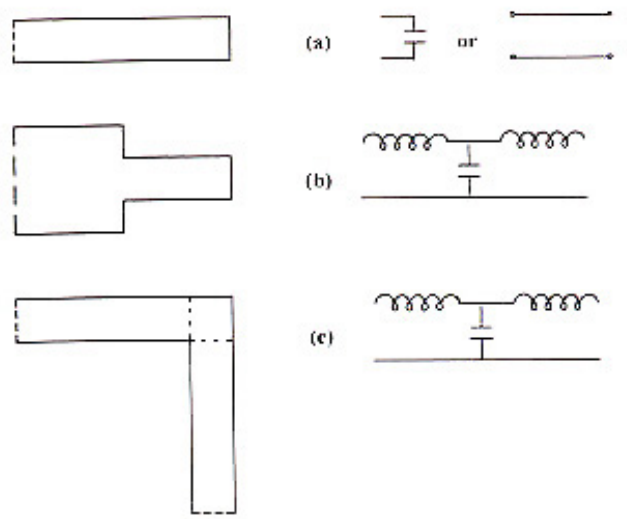

Figure 59. Common microstrip discontinuities and its equivalent circuit.

A MWS simulation was done for a simple 90° bend in a microstrip line with a substrate dielectric constant of 3 and a height of 0.13 mm. Figure 60 displays the S parameters. As frequency increases, the effect of the inductance created by the discontinuity becomes obvious as it reduces the transmittance of the line.

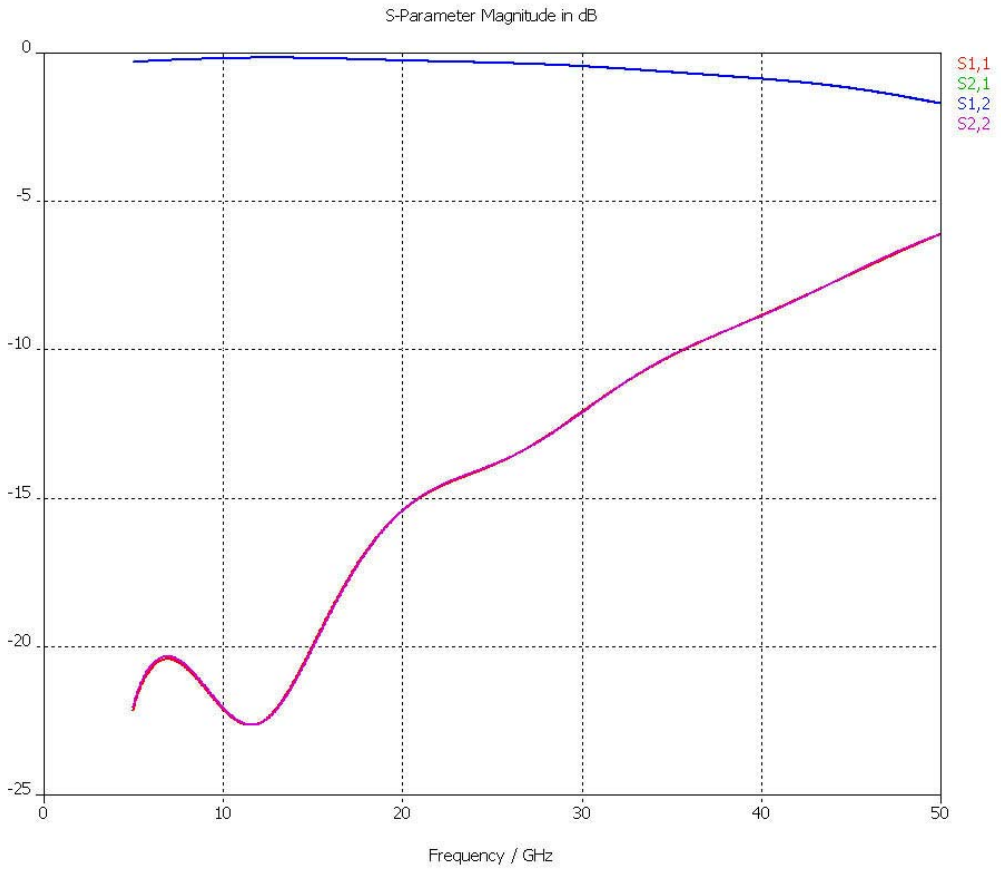

Figure 60. S parameter of 90° bend without chamfering

In order to minimize this inductance a chamfer must be etched out of the 90° bend, and Figure 61 shows how the chamfer is designed to minimize losses. The value of *x* can be calculated from [20]

$$\frac{x}{d} = 0.52 + 0.65e^{-1.35\frac{w}{h}} \tag{6.11}$$

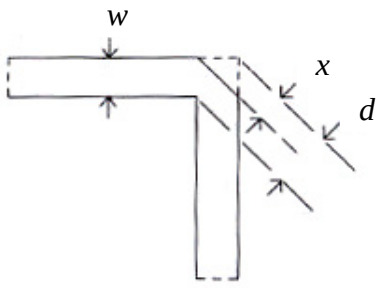

Figure 61. Chamfer of 90° microstrip bend (From [20])

A microstrip line with such a chamfer creates virtually no mismatch to the signal and hence looks as if it is a straight line. A microstrip bend incorporating the chamfer was simulated in MWS and the results of the S parameters (Figure 62) shows the reflection loss and insertion loss at higher frequencies have been significantly reduced.

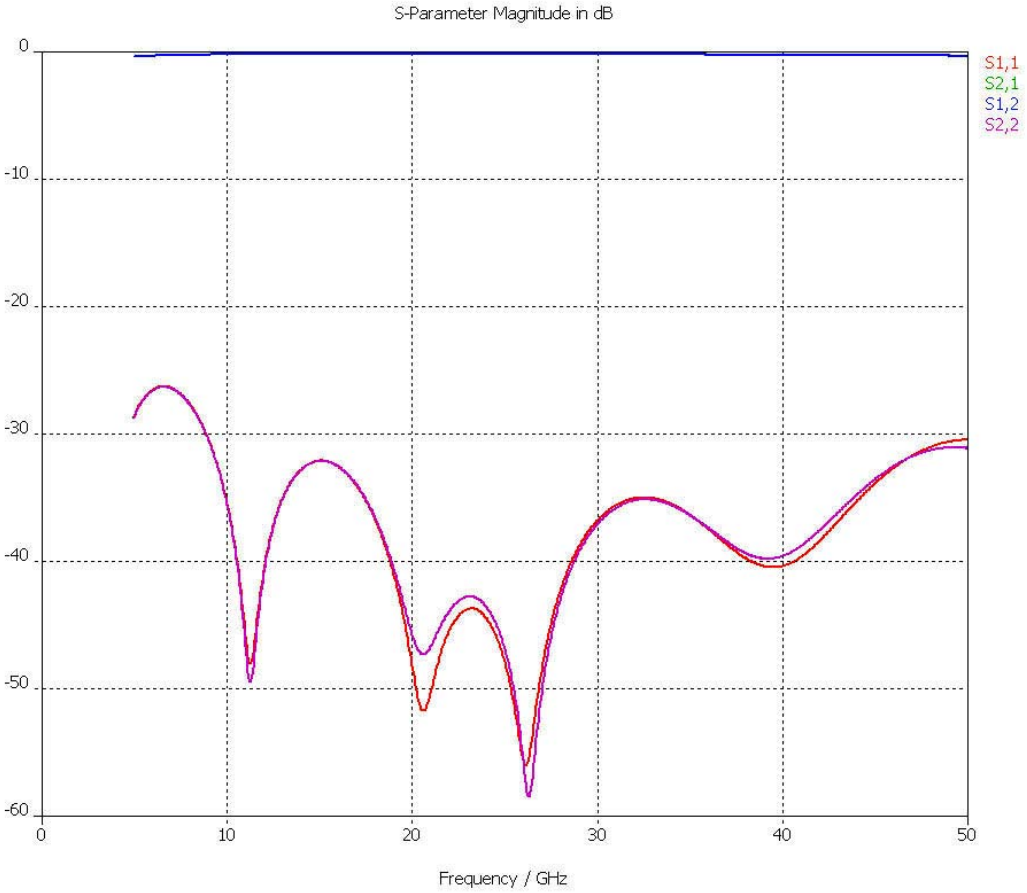

Figure 62. S parameters of 90° bend with chamfering

Finally the chamfered bend is electrically shorter than physical distance along the center line of the microstrip bend. This must be taken into account when line lengths must satisfy phase requirements. The reduction in distance, Δb, is calculated as follows:

$$\Delta b = 0.16D\left[2 - \left(f / f_p\right)^2\right] \tag{6.12}$$

where $f_p = 0.4Z_0 / h$ (mm) and $D = \left(377/\sqrt{\varepsilon_r}\right) h / Z_0$.

E. TUNING THE PROBE FEED

For a simple transition, the probe feed can be connected to the end of a microstrip stub. However for efficient operation, the feed line width must be larger than the dimension of the relief hole in the ground plane and extended beyond the probe such that the standing wave creates E fields that radiate uniformly between the probe and the outside edge of the relief hole. Making the feed line wide enough to completely cover the relief hole aids in creating the desired excitation fields. In Figure 63, the basic and improved transitions are shown.

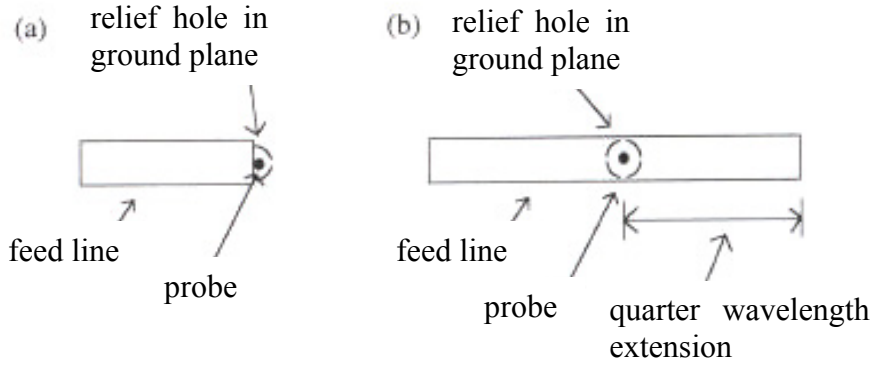

Figure 63. Probe-to-feed line transition (a) basic (b) improved transitions (From [20])

However for high frequency applications, the width of the relief hole may be wider than the width of the microstrip feed line and therefore it is necessary to increase the width of the line and match it accordingly. Figure 64 shows such a situation.

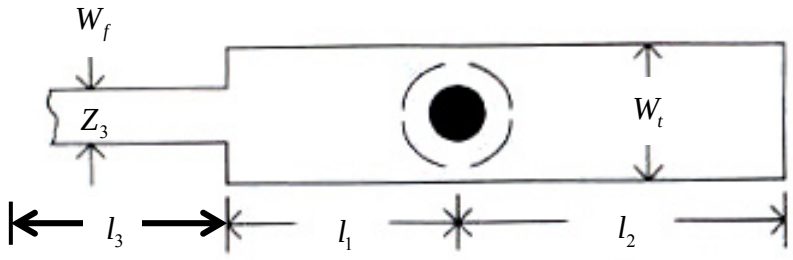

Figure 64. Modified transition for very narrow microstrip feed line width (From [20])

The matching of this probe is done employing similar techniques as those used in the matching network of the post-rectification low pass filter. Assuming the impedance at

the probe is the patch impedance of 50 Ω, and with W_t = 0.55 mm, in order to fully enclose the relief hole, the length l_1 is set to 0.8 mm which is 0.042λ. Now the impedance at the intersection towards the pre-rectification filter is theoretically $37.1 + j19.5$ Ω. However, simulations found the impedance to be $31 + j8.94$ Ω, as shown in Figure 65. The distance l_2 is set to $\lambda/2 = 9.22$ mm.

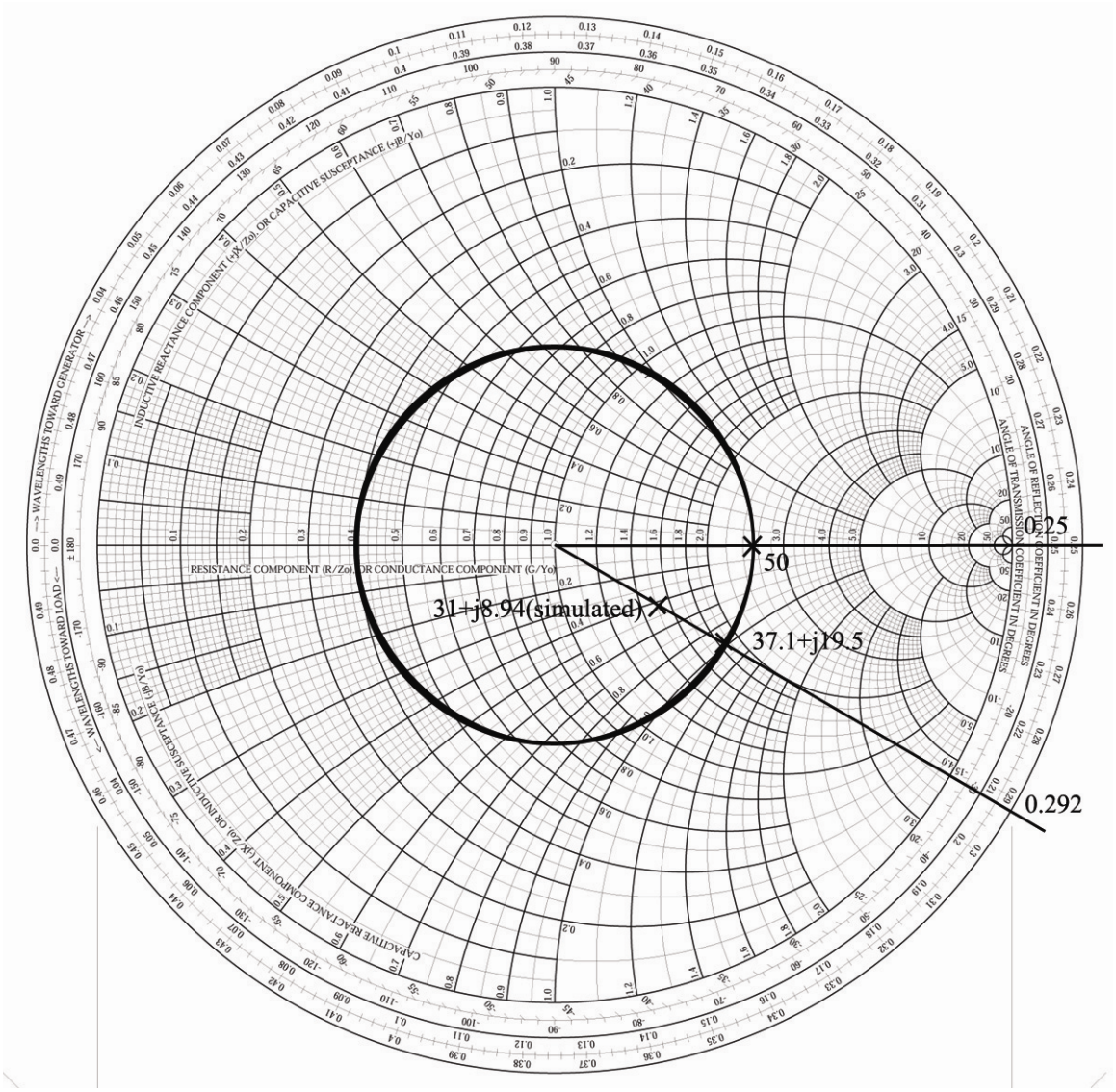

Figure 65. Translation of probe impedance towards pre-rectification filter

Next the width W_f is found by determining the characteristic impedance, Z_3, which is found by plotting the line of equal distance between $50\,\Omega$ and $31 + j8.94$ Ω, and its intersection with the horizontal line (purely resistive impedance). From Figure 66

the impedance required of Z_3 is approximately 36 Ω. With a required impedance of 36 Ω, W_f was calculated as 0.52 mm.

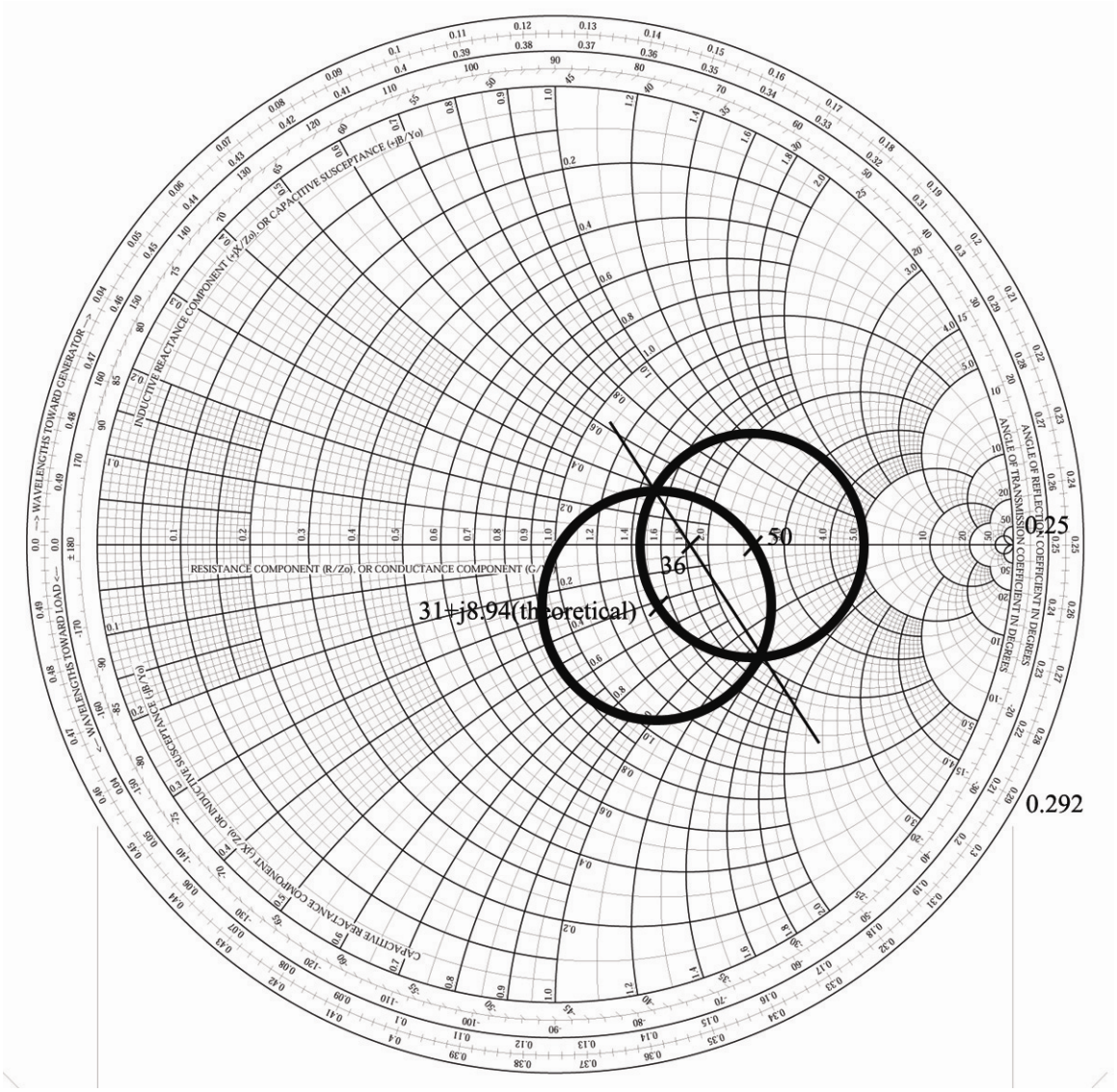

Figure 66. Determining characteristic impedance Z_3

Lastly, the length of the microstrip l_3 is found by plotting the impedance of the $31 + j8.94$ Ω on a Smith chart normalized to 36 Ω, and determining the distance towards the generator to achieve 50 Ω. Subsequently, l_3 was found to be 6.769 mm.

With this matching network, the patch is now matched to the input of the pre-rectification filter.

F. FINAL DESIGN OF RECTENNA

Incorporating all of the improvements into the rectenna system, the complete design of the rectenna was remodeled in MWS, and shown in Figure 67 and Figure 68.

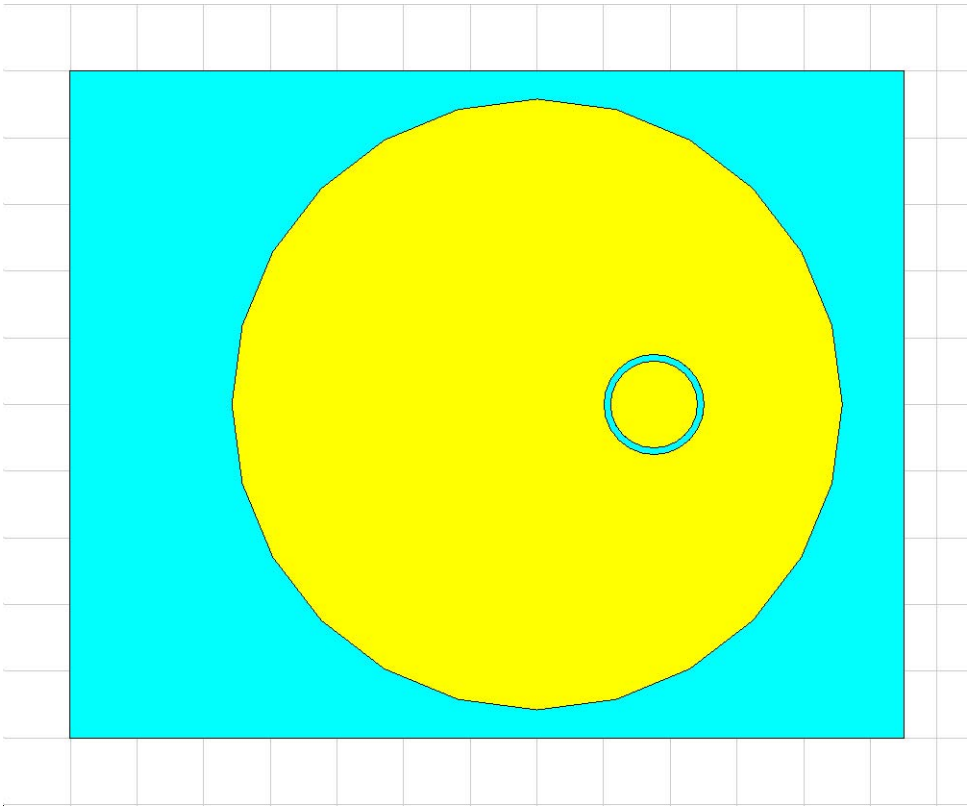

Figure 67. Final design of the rectenna element (Top)

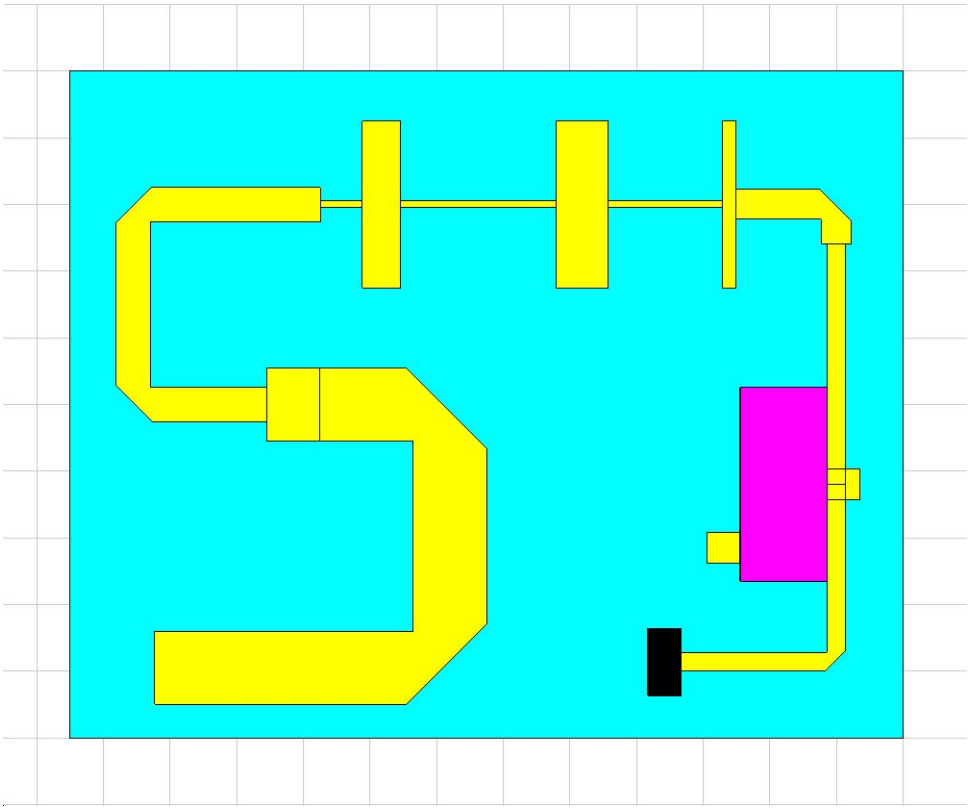

Figure 68. Final design of rectenna element (Bottom)

The final design has dimensions of 12.5 mm by 10 mm by 0.9 mm and has an estimated weight of 0.23 grams excluding the weight of the diode and the chip capacitor. The volume of this rectenna element is approximately 112.5 mm^3 which takes up only 15% of the original design [19], which was 779.7 mm^3. The detailed dimensions of the design are broken out in Appendix F.

THIS PAGE INTENTIONALLY LEFT BLANK

VII. FINDINGS AND RECOMMENDATIONS

A. SUMMARY

The performance of the original circular patch was analyzed and necessary modifications were made to correct the design. Studies were conducted on a corner-fed electromagnetic square patch and a inset-fed rectangular patch to determine their tolerances to variations in feed location. Subsequent findings resulted in the design of a capacitive probe circular patch.

The operation of the Schottky diode was re-evaluated using techniques from [31, 32] and the effect of conversion efficiency and diode impedance with changes in load resistance was determined. The filter performances were evaluated and suggestions were made to increase the efficiency of the rectenna. Lastly, the effect of microstrip discontinuities, required impedance matching, and tuning of the probe feed was covered.

B. CONCLUSIONS

The design of a rectenna requires numerous considerations that need to be understood in order to attain the highest possible conversion efficiency. This thesis covered the areas of concern related to each of the four subsystems involved in a rectenna element.

The original patch antenna design had a very narrow bandwidth that significantly contributed to stringent manufacturing requirements of the patch. The need for an isolating ground plane was confirmed and the use of the probe feed was justified, although a new capacitive probe circular patch was also designed and implemented.

The performance of the Schottky diode was studied, and a trade-off between attaining maximum conversion efficiency versus operational requirements was presented. The impedance of approximately 50 Ω was found to be suited for the intended operational application and a maximum theoretical conversion was computed at 60%. This means that the overall conversion efficiency of the rectenna is limited mainly by the conversion efficiency of the Schottky diode.

The filtering stages of the rectenna were studied. A sixth order pre-rectification Butterworth filter was suggested to reduce losses. The post-rectification filter was

simplified to a simple quarter-wave stub, shorted with a 47 pF capacitor which created the required voltage maximum at the connection of the Schottky diode.

The matter of microstrip discontinuities was discussed, along with a proposed solution for matching of impedance utilizing the technique of two stubs with different characteristic impedances. The connection of the probe feed for high frequency applications was highlighted and lastly, the accumulation of all of the findings of this thesis resulted in a design that employs an area of only 15% of the original design. The final system specifications are summarized in Table 14.

Final system specification		
Parameters	**Unit**	**Value**
Size	mm	10x12.5x0.9
Estimated Weight	g	< 1
Estimated Conversion Efficiency	%	50
Bandwidth ($S_{11} = -12$ dB)	%	2
Dielectric constant (Top)		3
Dielectric height (Top)	mm	0.75
Dielectric constant (Bottom)		3
Dielectric height (Bottom)	mm	0.13
Copper Track height	um	17
Probe feed diameter	mm	0.125
Ground plate relief hole radius	mm	0.55
Schottky diode		HSMS-8101
Chip capacitor		Vishay Part No. VJ0402A470JXACW1BC

Table 14. Final system specification of rectenna

C. RECOMMENDATIONS

It is unfortunate that no physical implementation of the design was constructed to validate the findings from Microwave Studio and it is recommended that the rectenna be built to determine the rectenna's fabrication robustness and conversion efficiency.

Assuming minimal mismatch losses in the rectenna design, the conversion efficiency of the diode is limited primarily by the rectifying diode. As such recommendations towards determining ways of increasing the conversion efficiency of the diode other than through the change of load resistance is beneficial.

In reality, the load resistance to the rectenna does vary and this variation will cause issues of mismatches and changes in operational power levels. Therefore a study on making the rectenna adaptable to these load variations will be a good next step.

The method of using thicker substrates may be incorporated with other techniques to increase the bandwidth of the patch. For example, the use of a U slot patch antenna that employs the merging of two resonant frequencies to create an overall wider bandwidth.

Finally, the conversion performance of an array of such rectennas could be analyzed. Figure 69 proposes the rectenna array configuration for series connections to achieve necessary current.

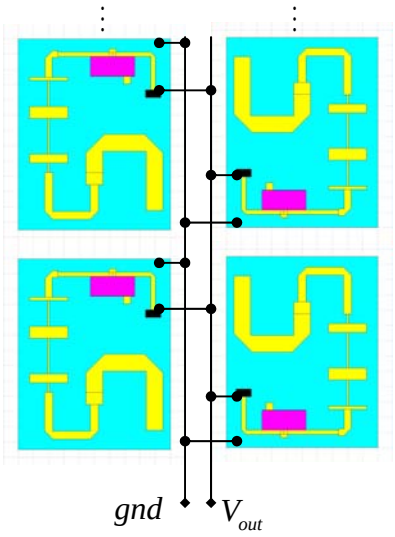

Figure 69. Rectennas connected in series

To increase V_{out}, the series array configuration are connected in parallel as shown in Figure 70.

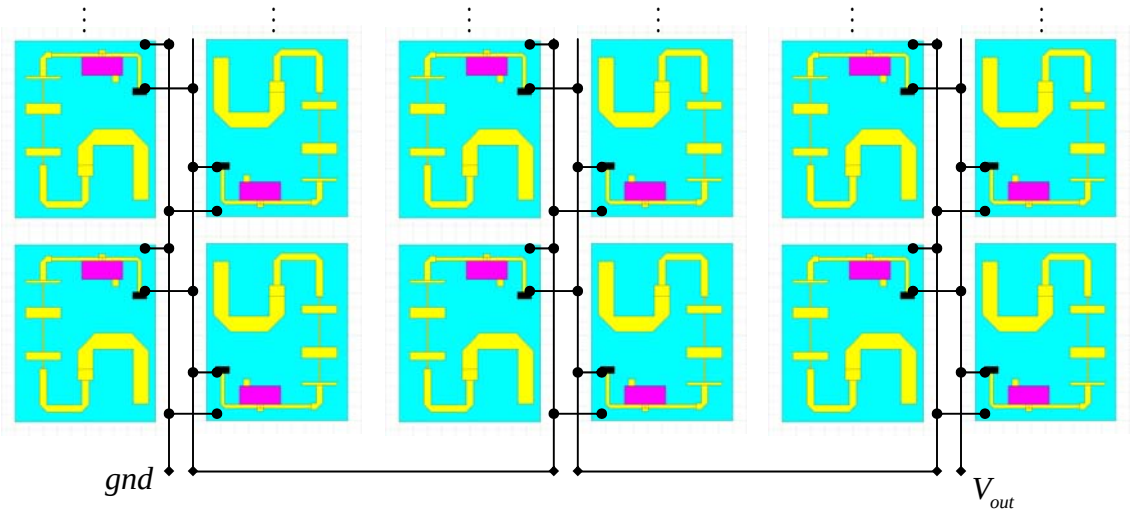

Figure 70. Rectennas connected in series and parallel

APPENDIX A

This appendix contains a Matlab program that employs the Ritz-Galerkin technique to calculate the expected output dc voltage of a rectifying diode with respect to input rf power

```
%Employing the Ritz-Galerkin technique to calculate Vo vs Pinc of a diode

clear all
close all

%t = input('Please input temperature in K = ');
%n = input('Please input diode ideality factor, n = ');
%Io = input('Please input bias current(A) = ');
%Is = input('Please input Is, Saturation current(A) = ');
%RL = input('Please input Load Resistor Value (ohm) = ');
%RG = input('Please input Generator Resistor Value (ohm) = ');
%RS = input('Please input Diode Series Resistance (ohm) = ');

t = 300;                    %operation temperature in Kelvin
n = 1.12;                   %diode ideality factor
Io = 0.0;                   %diode bias current (zero)
Is = 4.6e-8;                %Saturation current
RL = 50;                    %Load resistance
RG = 50;                    %Generator resistance
RS = 6;                     %Series resistance

%finding value of zeroth order of first kind
Pinc(1:10) = 10e-6:10e-6:100e-6;        %setting input power FROM 0.01mW to 0.1mW, -20dbm
                                        %to -10dbm
Pinc(11:20) = 100e-6:100e-6:1e-3;       %setting input power FROM 0.1mW to 1mW, -10dbm to
                                        %0dbm
Pinc(21:30) = 1e-3:1e-3:10e-3;          %setting input power FROM 1mW to 10mW, 0dbm to
                                        %10dbm
Pinc(31:40) = 10e-3:10e-3:100e-3;       %setting input power FROM 10mW to 100mW, 10dbm
                                        %to 20dbm

alpha = 38.5*300/t;
X = alpha*(sqrt(8*RG.*Pinc))/n;
temp = BESSELI(0.0,X);                  %Modified Bessel function of the first kind, zeroth order

%Determining value of Vo for given Pinc
Vo = zeros(1,40);
for j=1:1:40,
   difference = inf;
   for i = 0:1e-3:10,                   %run for Vo values from 0 to 5 volts in steps of 1mV, to find
                                        %the closest match to the LHS of the equation
      temp2 = (1.0 + (Io/Is) + (i/(RL*Is)))*exp((1.0 + ((RG+RS)/RL))*(alpha*i/n) + (alpha*RS*Io/n));
      difference_temp = abs(temp(j)-temp2);
```

```
      if difference_temp < difference,        %if difference is smaller than previously stored
         difference = difference_temp;        %take note of difference
         Vo(j) = i;                           %store value of Vo
      end
   end
end


%Plots Vo to Pinc in log scale
semilogy(10*log10(Pinc*1000), Vo);
xlabel('Input Power (dbm)');
ylabel('Vo (V)');

%Plots Output Power Vs Input Power
Pout = (Vo.^2)./RL;                        %Pout is determined as a function of Vo and RL
figure
hold
%plots Pin Vs Pout
plot(10*log10(Pinc*1000), 10*log10(Pout*1000), 'b');
%plots for Pout = Pin, i.e. 100% conversion
plot(10*log10(Pinc*1000),10*log10(Pinc*1000), 'r');
hold
xlabel('Input Power (dbm)');
ylabel('Output Power (dbm)');
```

APPENDIX B

This appendix contains a Matlab program that employs the technique used by Yoo and Chang to calculate the diode conversion efficiency with respect to input rf power and the diode impedance with respect to output dc voltage.

```
%determing diode performance as in paperS by Yoo and Chang.
%Plots the effect of diode impedance with Output voltage
%Plots the efficency of diode with respect to Pin
%Plots both Pin and Pout with respect to Vo

clear all
close all

RL = 50;                                %Load resistor
RS = 6;                                 %Series Resistance
Vbr = 7;                                %Diode Breakdown Voltage
Cjo = 0.18e-12;                         %zero bias capacitance
Is = 4.6e-8;                            %diode saturation current
n = 1.09;                               %diode ideality factor
f = 10e9;                               %operating frequency

V0 = 0.1:0.1:Vbr/1.9;                   %Range of Vo from 0.1 to Vbr/1.9 Volts


Vf = n*25.852e-3*log((V0./(Is*RL))+1);  %calculate diode forward voltage which is a function of
                                        %forward current, which is dependent on Pout

r = RS/RL;
Pout = (V0).^2/RL;                      %Output power by diode, a function of RL and VO

%Determine value of degree_off
temp = pi*RS./(RL*(1+Vf./V0));

degree_off = zeros(1,length(V0));
for j=1:length(V0),

   difference = inf;
   for k = 0 : 0.0001 :pi/2.1,
      temp2 = abs(temp(j) - (tan(k)-k));
      if temp2 < difference
         difference = temp2;
         degree_off(j) = k;             %degree_off is saved when difference is smallest
      else
         break                          %breaks out of for loop when lowest difference found
      end
   end
end
```

```
%Determine efficiency of diode
Cj = Cjo*((Vf./(Vf+V0)).^0.5);
w = 2*pi*f;

A = RL/(pi*RS)*((1+Vf./V0).^2).*( (degree_off .* ( 1 + 1./(2.*(cos(degree_off).^2)))-
3./2.*tan(degree_off));
B = RS*RL*((Cj*w).^2)/(2*pi) .* (1 + Vf./V0) .* ((pi-degree_off)./(cos(degree_off).^2) +
tan(degree_off));
C = RL/(pi*RS) * (1 + Vf./V0) .* (Vf./V0) .* (tan(degree_off) - degree_off);

diode_eff = 1 ./ (1 + A + B + C);                %diode efficiency is found

Zd = pi*RS./(cos(degree_off).*(degree_off./cos(degree_off) - sin(degree_off)) + i.*(w*RS.*Cj.*(((pi-
degree_off)./cos(degree_off)) + sin(degree_off))));
%determines diode impedance at operating frequency

Pin = Pout./diode_eff;                           %determines Pin from Pout and calculated efficiency

figure(1);                                       %Plots impedance with change in Vout, is proportional
hold                                             %to Pout^0.5
plot(0.1:0.1:Vbr/1.9, real(Zd),'r');
plot(0.1:0.1:Vbr/1.9, imag(Zd),'b');
hold
xlabel('Vout (V)'); ylabel('Zdiode');

figure(2);  %Plots diode efficency vs Pin
plot(Pin.*1000, diode_eff*100);
xlabel('Pin (mW)'); ylabel('diode efficiency (%)');

figure(3);  %Plots diode efficency vs Vo
plot(V0, diode_eff*100);
xlabel('Vout (V)'); ylabel('diode efficiency (%)');


figure(4)   %Plots Power vs V0
hold
plot(Pin.*1000, V0);
plot(Pout*1000, V0);
xlabel('Power (mW)'); ylabel('Output voltage (V)');
hold
```

APPENDIX C

This appendix contains a Matlab program that employs the technique used by Yoo and Chang to calculate the diode conversion efficiency with respect to changes in load resistance, R_L . An assumption is made that the diode is operating at the maximum power level.

```
%Determining diode maximum efficiency performance with respect to changes in
%RL as in paper by Yoo and Chang.
clear all
close all

RL = 10:20:10000;                       %Value of load resistor
RS = 6;                                 %Series Resistance
Vbr = 7;                                %Reverse Breakdown Voltage
Cjo = 0.18e-12;                         %Zero Bias Capacitance
Is = 4.6e-8;                            %diode saturation current
n = 1.09;                               %ideality factor
V0 = Vbr/2;                             %Set value of V0 at maximum power rating, divided by 2
                                        %is used, 2.2 maybe used too

Vf = n*25.852e-3*log((V0./(Is.*RL))+1); %note Vf is a function of forward current, which is
                                        %dependent on Pout

r = RS./RL;
Pout = V0^2./RL;                        %Expected output power by diode

%Determine value of angle_off for different RL values
temp = pi*RS./(RL.*(1+Vf/V0));

degree_off = zeros(1,length(RL));

for j=1:length(RL),

   difference = inf;
   for k = 0 : 0.0001 :pi/2.1,
      temp2 = abs(temp(j) - (tan(k)-k));
      if temp2 < difference
         difference = temp2;
         degree_off(j) = k;             %degree_off is saved
      else
         break
      end
   end
end

%Determine efficiency of diode
Cj = Cjo*((Vf./(Vf+V0)).^0.5);
w = 2*pi*10e9;
```

```
A = RL./(pi*RS).*((1+Vf./V0).^2).*( (degree_off .* ( 1 + 1./(2.*(cos(degree_off).^2)))-
3./2.*tan(degree_off));
B = RS*RL.*((Cj*w).^2)/(2*pi) .* (1 + Vf./V0) .* ((pi-degree_off)./(cos(degree_off).^2) +
tan(degree_off));
C = RL./(pi.*RS) .* (1 + Vf./V0) .* (Vf./V0) .* (tan(degree_off) - degree_off);

diode_eff = 1 ./ (1 + A + B + C);

Zd = pi*RS./(cos(degree_off).*(degree_off./cos(degree_off) - sin(degree_off)) + i.*(w*RS.*Cj.*(((pi-
degree_off)./cos(degree_off)) + sin(degree_off))));

Pin = Pout./diode_eff;

figure(1);                                  %plot max efficiency vs RL for maximum power level
plot(10:20:10000, diode_eff,'r');
xlabel('RL (ohm)'); ylabel('diode efficiency');

figure(2);                                  %plot number of rectenna elements required vs RL
plot(10:20:10000, 1.2./Pout,'r');
xlabel('RL (ohm)'); ylabel('No. of diode elements to achieve 1.2W');
```

APPENDIX D

This appendix contains a Matlab program that calculates the length and width of each microstrip stub in a low pass Butterworth filter, with a leading capacitor element.

```
%Program to calculate length and width of microstrip Low Pass Filter (Butterworth)
%note this uses a leading capacitor followed by alternating inductor and capacitor
%Output are C_length_mm and L_length_mm
clear

%Input parameters and number of stages for filter
N = input('Please input number of N stages (1-6) = ');
Fc = input('Please input cutoff frequency (GHz) = ');
Z0 = input('Please input Loading Impedance (Ohm) = ');

Er = input('Please input Er of substrate material = ');
d = input('Please input thickness height of substrate material (mm)= ');

%Calculated values
Fc = Fc * 1e9;
Wc = 2*pi*Fc;

%creating and determining the g factors
if N == 1
   g = 2.0;
elseif N == 2
   g(1)=1.4142; g(2)=1.4142;
elseif N == 3
   g(1)=1.0; g(2)=2.0; g(3)=1.0;
elseif N ==4
   g(1)=0.7654; g(2)=1.8478; g(3)=1.8478; g(4)=0.7654;
elseif N ==5
   g(1)=0.618; g(2)=1.618; g(3)=2.0; g(4)=1.618; g(5)=0.618;
elseif N == 6
   g(1)=0.5176; g(2)=1.4142; g(3)=1.9318; g(4)=1.9318; g(5)=1.4142; g(6)=0.5176;
end

%now calculating the L & C values; Starting with Inductive load followed by
%capacitive
for I = 1:N,
   if mod(I,2) == 1                          %odd function, i.e Capacitor C
      C(floor(I/2)+1) = g(I)/(Z0*Wc);
   else                                      %even function, i.e inductor L
      L(I/2) = g(I)*Z0/Wc;
   end
end

%Next stage is to determine the width and length of the respective
%capacitive and inductors parts;
```

```
Wdratiohigh = input ('Please input the expected Width to Height Ratio for High Impedance (0.2 to 1) = ');
%capcitor
Wdratiolow = input ('Please input the expected Width to Height Ratio for low Impedance (8 to 10) = ');
%inductor

Width_high = Wdratiohigh * d;                %actual width of capacitive stub
Width_low =  Wdratiolow *d;                  %actual width of inductive stub
Ee_high = (Er+1.0)/2.0 + (Er-1.0)/(2.0*(sqrt(1.0+(12.0/Wdratiohigh))));
Ee_low  = (Er+1.0)/2.0 + (Er-1.0)/(2.0*(sqrt(1.0+(12.0/Wdratiolow))));

Z_high  = 60.0*log(8.0/Wdratiohigh + Wdratiohigh/4.0)/sqrt(Ee_high);                % for W/H < 1.0
Z_low   = 120.0*pi/(sqrt(Ee_low)*(Wdratiolow + 1.393 + 0.667*log(Wdratiolow + 1.444)));
                                                                                   % for W/H > 1.0
%now calculating the actual length of the L & C stubs.
for I = 1:N,
   if mod(I,2) == 1    %odd function, i.e Capacitor C
      C_length_mm(floor(I/2)+1) = 3e11*C(floor(I/2)+1)*Z_low/sqrt(Ee_low);
   else              %even function, i.e inductor L
      L_length_mm(I/2) = 3e11*L(I/2)/(Z_high*sqrt(Ee_high));
   end
end
```

APPENDIX E

This appendix contains a Matlab program that calculates the length and width of each microstrip stub in a low pass Butterworth filter, with a leading inductor element.

```
%Program to calculate length and width of microstrip Low Pass Filter (Butterworth)
%note this uses a leading inductor followed by alternating capacitors and inductors
%Output are L_length_mm and C_length_mm
clear

%Input parameteres and number of stages for filter
N = input('Please input number of N stages (1-6) = ');
Fc = input('Please input cutoff frew (GHz) = ');
Z0 = input('Please input Loading Impedance (Ohm) = ');

Er = input('Please input Er of substrate material = ');
Er_enclosed = input('Is the microstrip line enclosed in dielectric material (N=0, Y=1) = ');
d = input('Please input thickness height of substrate material(mm) = ');


%Calculated values
Fc = Fc * 1e9;
Wc = 2*pi*Fc;


%creating and determining the g factors
if N == 1
   g = 2.0;
elseif N == 2
   g(1)=1.4142; g(2)=1.4142;
elseif N == 3
   g(1)=1.0; g(2)=2.0; g(3)=1.0;
elseif N ==4
   g(1)=0.7654; g(2)=1.8478; g(3)=1.8478; g(4)=0.7654;
elseif N ==5
   g(1)=0.618; g(2)=1.618; g(3)=2.0; g(4)=1.618; g(5)=0.618;
elseif N == 6
   g(1)=0.5176; g(2)=1.4142; g(3)=1.9318; g(4)=1.9318; g(5)=1.4142; g(6)=0.5176;
end

%now calculating the L & C values; Starting with Inductive load followed by
%capacitive
for I = 1:N,
   if mod(I,2) == 1                          %odd function, i.e inductor L
      L(floor(I/2)+1) = g(I)*Z0/Wc;
   Else                                      %even function, i.e Capacitor C
      C(I/2) = g(I)/(Z0*Wc);
   end
end

%Next stage is to determine the width and length of the respective
```

```
%capacitive and inductors parts;

Wdratiohigh = input ('Please input the expected Width to Height Ratio for High Impedance (0.2 to 1) = ');
%capcitor
Wdratiolow = input ('Please input the expected Width to Height Ratio for low Impedance (8 to 10) = ');
%inductor

Width_high = Wdratiohigh * d;                %actual width of capacitive stub
Width_low =  Wdratiolow *d;                  %actual width of inductive stub
if Er_enclosed == 0
  Ee_high = (Er+1.0)/2.0 + (Er-1.0)/(2.0*(sqrt(1.0+(12.0/Wdratiohigh))));
  Ee_low  = (Er+1.0)/2.0 + (Er-1.0)/(2.0*(sqrt(1.0+(12.0/Wdratiolow))));
else
  Ee_high = Er;
  Ee_low = Er;
end

Z_high  = 60.0*log(8.0/Wdratiohigh + Wdratiohigh/4.0)/sqrt(Ee_high);                % for W/H < 1.0
Z_low   = 120.0*pi/(sqrt(Ee_low)*(Wdratiolow + 1.393 + 0.667*log(Wdratiolow + 1.444)));
                                                                                   % for W/H > 1.0

%now calculating the actual length of the L & C stubs.
for I = 1:N,
   if mod(I,2) == 1                          %odd function, i.e inductor L
      L_length_mm(floor(I/2)+1) = 3e11*L(floor(I/2)+1)/(Z_high*sqrt(Ee_high));
   Else                                      %even function, i.e Capacitor C
      C_length_mm(I/2) = 3e11*C(I/2)*Z_low/sqrt(Ee_low);
   end
end
```

APPENDIX F

This appendix shows the final rectenna design with dimensional details. Figure 71 shows the details for the top section of the rectenna, with a substrate dielectric constant of $\varepsilon_r = 3$, dielectric height of 0.75 mm, and $1/2$ oz copper thickness.

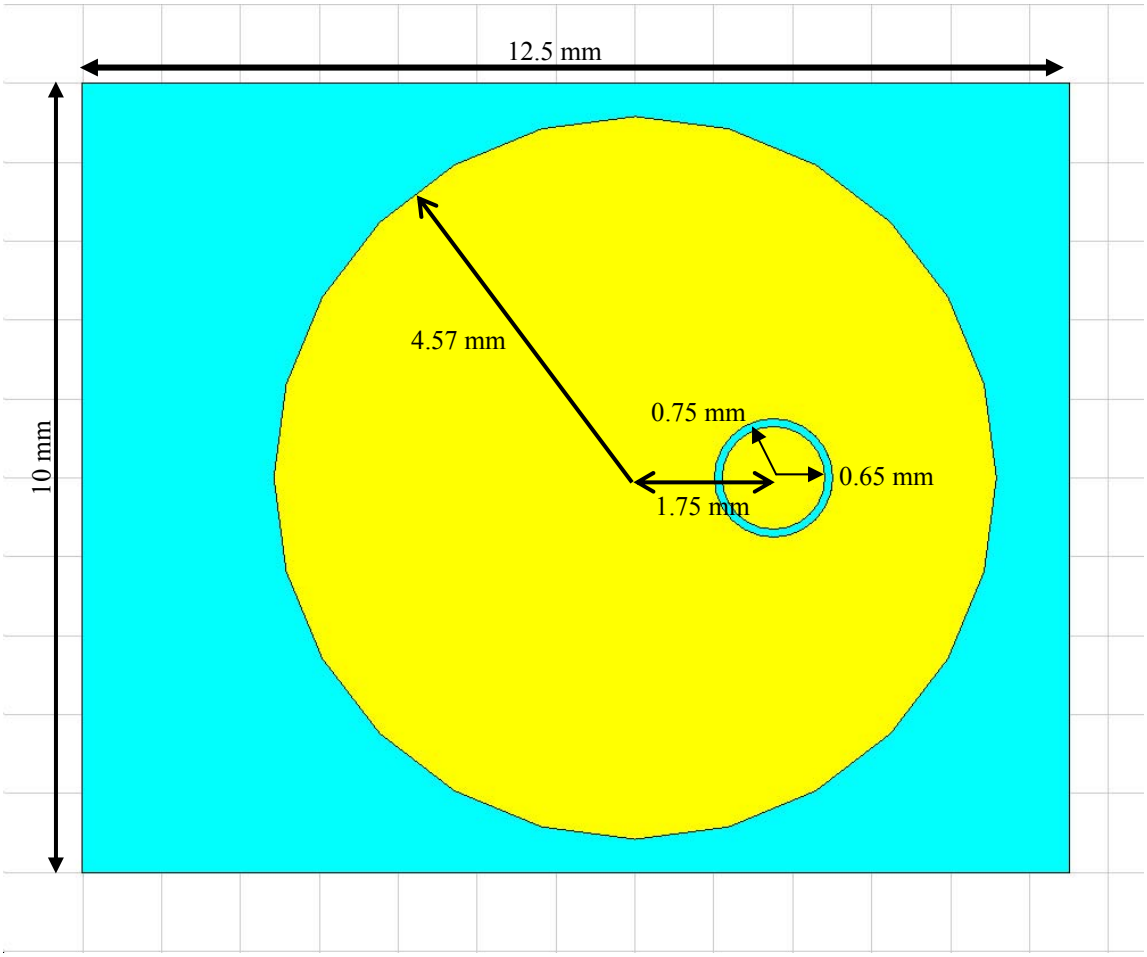

Figure 71. Final design of the rectenna element with dimensional details (Top)

Figure 72 shows the dimensional detail of the bottom side of the rectenna, where the substrate has a dielectric constant of ε_r = 3, substrate height of 0.13 mm and 1/2 oz copper thickness.

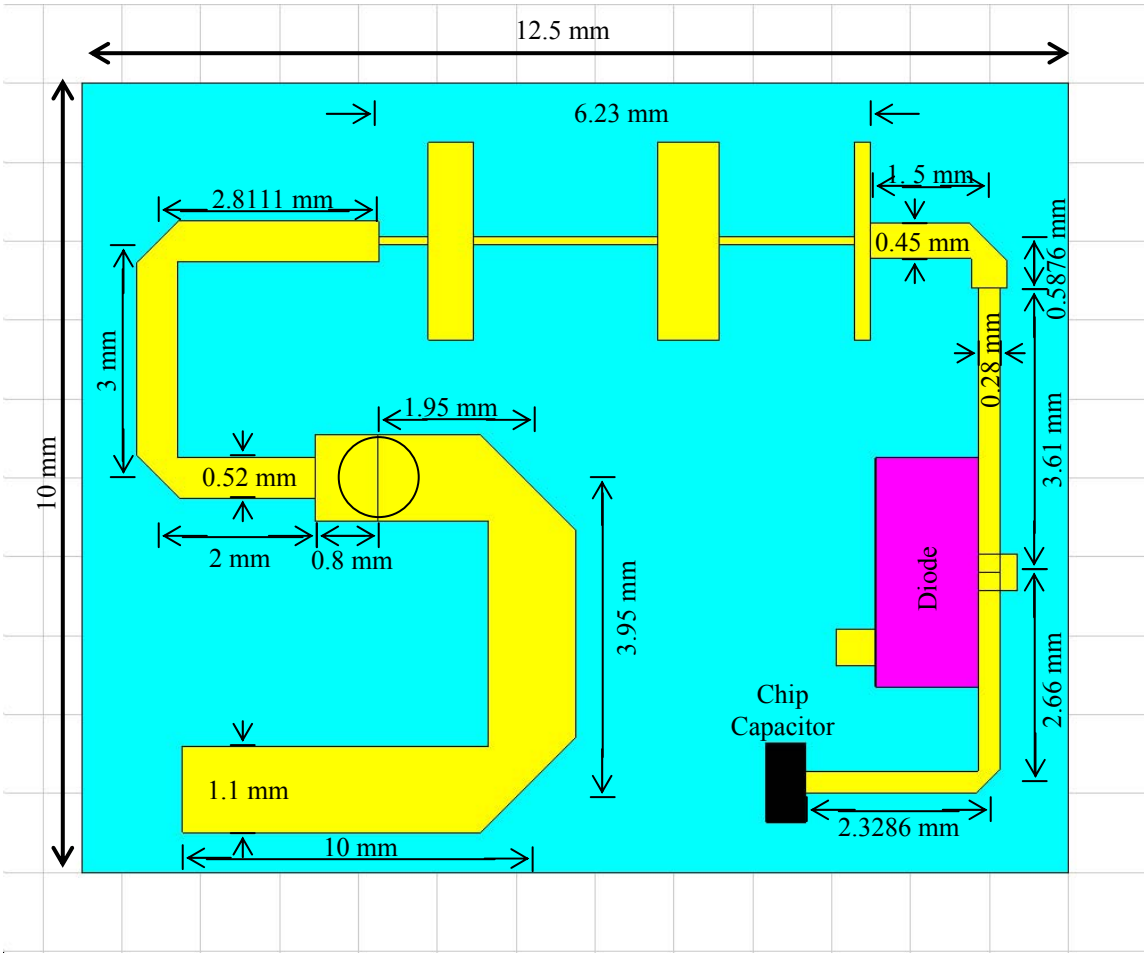

Figure 72. Final design of rectenna element with dimensional detail (Bottom)

LIST OF REFERENCES

[1] William C. Brown, "The History of Power Transmission by Radio Waves," *IEEE Transactions of Microwave Theory and Techniques*, Vol MTT-32. No. 9, September 1984.

[2] H. Hertz, *Dictionary of Scientific Biography*, vol. VI. New York: Scribner, pp. 340-349.

[3] J. J. O'Neill, *Prodigal Genius – the Life of Nikola Tesla*, New York: Washburn, 1944.

[4] M. Cheney, *Tesla, Man Out of Time*, Englewood Cliffs, NJ: Prentice-Hall, 1981.

[5] G. Goubau and F. Schwering "On the guided propagation of electromagnetic wave beams," *IRE Transactions on Antenna Propagation*, vol. AP-9, pp. 248-256, May 1961.

[6] W. C. Brown, "Description and operating characteristics of the platinotron – A new microwave tub device," *Proc. IRE*, vol. 45, no. 9, pp. 1209-1222, Sept. 1957.

[7] "The amplitron, a super power microwave generator," *Electron. Prog.*, vol. 5, no. 1, pp. 1-5, July 1960.

[8] James O. McSpadden, Taewhan Yoo, and Kai Chang, "Theoretical and Experimental Investigation of a Rectenna Element for Microwave Power Transmission," *IEEE Transactions on Microwave Theory and Techniques*, Vol. 40, No. 12, Dec 1992.

[9] Naoki Shinohara and Hiroshi Matsumoto, "Experimental Study of Large Rectenna Array for Microwave Energy Transmission," *IEEE Transaction on Microwave Theory and Techniques*, Vol. 46, No. 3, March 1998.

[10] Dong-Gi Youn, Yang-Ha Park, Kwan-Ho Kim and Young-Chul Rhee, "A Study on the Fundamental Transmission Experiment for Wireless Power Transmission System," 1999 *IEEE TENCON*.

[11] Joseph A. Hagerty, Florian B. Helmbrecht, William H. McCaplin, Regan Zane and Zoya B. Popovic, "Recycling Ambient Microwave Energy With Broad-Band Rectenna Arrays," *IEEE Transactions on Microwave Theory and Techniques*, Vol. 52, No. 3, March 2004.

[12] James C. Lin, "Space Solar-Power Stations, Wireless Power Transmission, and Biological Implications," *IEEE Microwave Magazine*, Mar 2002.

[13] James O. McSpadden, John C. Mankins, "Space Solar Power Programs and Microwave Wireless Power Transmission Technology," *IEEE Microwave Magazine*, Dec 2002.

[14] Texas Space Grant Consortium "Commercial Power from Space," www.tsgc.utexas.edu/tadp/1996/general/power.pdf, June 2005.

[15] Joseph J. Schlesak, Adrian Alden and Tom Ohno, "A Microwave Powered High Altitude Platform," *IEEE MTT-S Digest*, 1988.

[16] Peter Siegel, Harish Manohara, "Nanoconverters for powering nanodevices," http://www.findarticles.com/p/articles/mi_qa3957/is_200303 /ai_n9233377, June 2005.

[17] William B. Scott and David A. Fulghum, "'Black' Snooper UAVs," *Aviation Week and Space Technology*, Oct 3, 2005.

[18] Robert L. Vitale, "Design and Prototype Development of a Wireless Power Transmission System for a Micro Air Vehicle (MAV)," Naval Postgraduate School, June 1999.

[19] George Tsolis, "Theoretical and experimental study of micro air vehicle powered by RF Signal at 10 GHz," Naval Postgraduate School, Dec 2003.

[20] Robert A. Sainati, *CAD of Microstrip Antennas for Wireless Applications*, Artech House, 1996, ISBN 0-89006-562-4.

[21] Constantine A. Balanis, *Antenna Theory – Analysis and Design*, 2nd Edition, John Wiley and Sons, Inc, 1997, ISBN 0-471-59268-4.

[22] Mayhew-Ridgers, "Wideband Probe-Fed Microstrip Patch Antennas and Modelling Techniques," upetd.up.ac.za/thesis/available/etd-09162004-083016/unrestricted/02chapter2.pdf, June 2005.

[23] The Nan Chang and Yu Chen Wei, "Proximity-Coupled Microstrip Reflectarray," *IEEE Transactions on Antennas and Propagation*, Vol. 52, No. 2, February 2004.

[24] Wadell, Brian C, *Transmission Line Design Handbook*, Artech House 1991.

[25] IPC-2141, "Controlled Impedance Circuit Boards and High-Speed Logic Design," April 1996.

[26] Andrew J. Burkhardt, Christopher S. Gregg and J. Alan Staniforth, "Calculation of PCB Track Impedance", http://www.polarinstruments.com/support/cits/IPC1999.pdf, June 2005.

[27] Microstrip Transmission Line Characteristic Impedance Calculator, http://chemandy.com/calculators/microstrip_transmission_line_calculator_Hartley27.htm , July 2005.

[28] Agilent HSMS-8101, 8202, 8207, 8209 Surface Mount Microwave Schottky Mixer Diodes Data Sheet

[29] Hewlett-Packard Application Note 1088, "Designing the Virtual Battery."

[30] Robert G. Harrison, Xavier de Prolozec, "Nonsquarelaw Behavior of Diode Detectors Analyzed by the Ritz-Galerkin Method," *IEEE Transactions on Microwave Theory and Techniques*, Vol. 42, No. 5, May 1994.

[31] James O. McSpadden, Lu Fan and Kai Chang, "Design and Experiments of a High-Conversion-Efficiency 5.8-GHz Rectenna," *IEEE Transaction on Microwave Theory and Techniques*, Vol. 46, No. 12, Dec 1998.

[32] Tae-Whan Yoo and Kai Chang, "Theoretical and Experimental Development of 10 and 35 GHz Rectennas," *IEEE Transactions on Microwave Theory and Techniques*, Vol. 40, No. 6, June 1992.

[33] David M. Pozar, *Microwave Engineering*, John Wiley and Sons, Inc., New York, 1998.

[34] R. Collin, *Foundations of Microwave Engineering*, McGraw Hill, 1966

[35] Zoya Popvic and Dejan Filipovic, "CAD of Microwave Circuits," http://ece-www.colorado.edu/~ecen5104/ECEN5104-Lecture4.pdf, Jul 2005.

[36] G.L. Matthaei, L. Young and E.M.T. Jones, *Microwave filters, impedance-matching networks, and coupling structures*, Artech House, 1980.

[37] Deng Hong Lei, Kong Li, "A Novel High-Efficiency Rectenna for 35 GHz Wireless Power Transmission," *4th international Conference on Microwave and Milimeter Wave Technology Proceedings*, 2004.

INITIAL DISTRIBUTION LIST

1. Defense Technical Information Center
   Ft. Belvoir, Virginia

2. Dudley Knox Library
   Naval Postgraduate School
   Monterey, California

3. Professor James H. Lucombe
   Code PH
   Naval Postgraduate School
   Monterey, California

4. Professor David C. Jenn
   Department of Electrical and Computer Engineering
   Code EC/Jn
   Naval Postgraduate School
   Monterey, California

5. Professor Richard Harkins
   Code PH/Hr
   Naval Postgraduate School
   Monterey, California

6. James King
   Office of Naval Research
   Arlington, Virginia

7. Professor Yeo Tat Soon
   Dir, Temasek Defence Science Institute
   National University of Singapore
   Singapore

8. Professor Michael Melich
   Wayne E. Meyer Institute of Systems Engineering
   Monterey, California

9. Professor Rodney Johnson
   Wayne E. Meyer Institute of Systems Engineering
   Monterey, California

10. Yeo Siew Yam
    Defence Science Technology Agency
    Singapore

11. Lee Meng Mark Tan
Ministry of Defence
Singapore